THE UNIVERSITY
of EDINBURGH

Global scale modelling of ozone deposition processes and interaction between surface ozone and climate change

Federico Centoni

A thesis presented for the degree
of Doctor of Philosophy

The University of Edinburgh
2017

Declaration

I declare that this thesis work has been composed by myself and has not been submitted for any other professional qualification or previous degree.

Chapter 3 includes experimental data sets which were collected by other groups for comparison with the model outputs from my research.
I confirm that appropriate credit has been given to their works within the thesis where reference was provided.

Federico Centoni
February, 2017

Lay summary

Ozone is considered a critical air pollutant and is strongly influenced by removal processes (dry deposition) to the biosphere and other surfaces. Deposition processes are very sensitive to temperature and relative humidity at the surface and are expected to respond to global climate change, with implications for both air quality (i.e. human health) and ecosystem services (i.e. crop yields). In this PhD study, a modelling framework (UKCA) was used to simulate ozone deposition processes globally. A thorough investigation of the scheme representing these processes within UKCA constituted the first part of the study. Some errors within this scheme were identified and corrected. These model amendments led to a large increase of surface ozone concentration simulated over land in the Northern Hemisphere (NH) with values up to +50% higher on annual average. The model corrections led also to a decrease (-13%) of the total annual amount of ozone deposited ozone globally, which brings UKCA more in line with other model estimates.

Many studies have shown that the ozone absorption by vegetation occurring through the pores on the leaves (or stomata), which causes damages to plants, typically accounts for 40-60% of total deposition on average and the other part which occurs through other pathways is not constant. An alternative and more dynamic representation of the ozone deposition was implemented in the model to explore the sensitivity of simulated surface ozone concentration and ozone deposition. This alternative representation of the ozone deposition led to an increase of modelled ozone deposition rate by to +40% over boreal forests and to a decrease of that rate by up to -30% over tropical regions on annual average. This study showed that the fraction of ozone deposition not occurring through stomata (and not damaging vegetation plants) varies both in space and in time.

Secondly, to assess the representativeness of the model simulations, the performance of the model was compared against measurements. Overall, this analysis revealed that the model is capable of reproducing the diurnal variations of the ozone deposition to vegetated surfaces and to capture the spatial and temporal differences of the observed surface ozone concentration throughout the globe.

However, some uncertainties were found within the model.

Finally, a climate simulation for the RCP 8.5 scenario (predicting a large increase of the surface temperature by up to +10 ^{o}C) was used to quantify the influence of future changes in surface ozone. This study showed that the ozone removal rate from the atmosphere over lands reduces from 2000 to 2100, and most strongly over vegetated areas. Climate change led to an increase of surface over land by up to ~20%. This study also demonstrated that changes to ozone deposition due to climate change might have implications on the future air quality.

Abstract

Atmospheric concentrations of surface ozone (O_3) are strongly affected by deposition to the biosphere. Deposition processes are very sensitive to turbulence, temperature, relative humidity and soil moisture deficit and are expected to respond to global climate change, with implications for both air quality (e.g. human health) and ecosystem services (e.g. crop yields). In this PhD study, the global chemistry aerosol model UKCA (United Kingdom Chemistry Aerosol model) dry deposition scheme was thoroughly investigated. Some errors in the existing implementation of the current UKCA stomatal resistance and in-canopy aerodynamic resistance terms for O_3 and NO_w (NO_2, PAN, PPAN, MPAN) were identified and corrected (WES scheme). These model corrections led to a decrease of the total annual dry deposition of -150 $Tg(O_3)$ yr^{-1} (-13%) which brings UKCA more in line with multi-model inter-comparison estimates. This was associated with a large increase of surface O_3 concentration over land in the Northern Hemisphere (NH) with values up to 12 ppb (+50%) higher on annual average.

Many studies have shown that O_3 stomatal uptake by vegetation, which is the pathway leading to damage, accounts for 40-60% of total deposition on average. The remaining non-stomatal deposition flux is to external foliar surfaces, and soil. A more mechanistic non-stomatal dry deposition approach along with a scheme to simulate the effect of moisture on foliar surfaces on the stomatal transport (ZHG scheme) was introduced in UKCA to study the relative contributions of O_3 flux occurring to stomatal and non-stomatal pathways at the global scale, and to explore the sensitivity of simulated surface O_3 and O_3 deposition flux. The ZHG scheme, led to significant changes in the O_3 dry deposition velocity (V_d) (+40% in the North Hemisphere over boreal forests and -30% over tropical regions on annual average). The results of this study show that the ZHG scheme significantly changes the partitioning between stomatal and non-stomatal O_3 flux. The non-stomatal fraction increased throughout the year and considerably during the cooler season and in spring (with maxima values by up to 60% for C3 grass and by up to 70% for needle leaf trees).

The performance of both UKCA dry deposition schemes were compared with measurements, focussing on the diurnal and seasonal variations of the dry deposition velocity terms and the partitioning of O_3 fluxes between stomatal and non-stomatal sinks. Overall, both UKCA dry deposition schemes capture the diurnal variations of V_d reasonably well. However, this study highlighted difficulties in comparing large grid (~280 x 390 km at mid-latitudes) averaged modelled values with site and vegetation specific characteristics of the measured exchange processes (~1 km^2) and the driving meteorological variables. These differences in scale are a large source of uncertainty in the comparison of measured and modelled O_3 V_d. Off-line simulation tests conducted on the non-stomatal deposition component with the ZHG scheme demonstrated the importance of modelling some key environmental and meteorological factors accurately (e.g. relative humidity, friction velocity, leaf area index). This was found to be crucial in order to improve O_3 V_d model performance as well as improving the representation of specific vegetation properties.

A comparison of the modelled global surface O_3 concentration against observations both in the NH and SH revealed that the model performs well in the NH using both schemes, capturing the observed surface O_3 cycle and the absolute values. The ZHG scheme led to a reduction of the annual bias (up to -13.5% on average) in the NH monitoring sites considered for this study. This is associated with a decrease in O_3 deposition simulated with ZHG (as much as of -20% on annual average). By contrast, the seasonal cycle and absolute values of the observed surface O_3 are not well reproduced by the model across the SH monitoring sites used in this study and a larger bias was found using the ZHG scheme (60% on average) compared to WES scheme (47% on average), as a consequence of an increase in O_3 deposition (as much as of +20% on annual average) calculated with ZHG.

A future climate integration for the 2090s using RCP 8.5 scenario was used to investigate the response of UKCA modelled O_3 to climate change. The effect of climate change (by altering only the GHG concentrations predicted with RCP 8.5) on the dry deposition sink of O_3 was addressed contrasting the two non-stomatal deposition parameterizations, and ignoring the changes in land-use and anthropogenic emissions. The study showed that O_3 V_d over land declines from 2000 to 2100, and most strongly over vegetated areas (up to -24% over S. America, -17%

over N. America and -10% over Europe). Climate change led to an increase of surface O_3 concentration over land (by up to 20%). Whilst the two schemes behave similarly, and an increase in turbulence has been identified as the main driver, the decrease in land V_d is generally stronger in ZHG. This effect is more important over N. America and Eurasia where ZHG exhibits larger differences in deposition compared to WES as a result of changing climate. The increase in surface O_3 over Arctic and Antarctic regions shows the effect that changes in O_3 deposition might have on the long-range transport of O_3.

Finally, the influence of climate change on the partitioning of the O_3 deposition flux was examined. This analysis revealed that more O_3 is predicted to deposit through stomatal pathways with ZHG over N. America, C. Europe and E. Asia (up to +30%) compared to WES as a result of changing climate.

Given that ZHG scheme captures the influence of meteorology and changing climate on surface O_3 better than WES, it was concluded that modelled surface O_3 using ZHG scheme showed a larger sensitivity to a changing climate than WES. These results imply potentially important effects of climate change on tropospheric O_3, degrading air quality through the later decades of this century.

Acknowledgements

I would like to thank all the people who helped me and supported me during my studies and during the writing process of this thesis. First of all, all my supervisors Prof. David Stevenson, Prof. David Fowler and Dr. Eiko Nemitz for giving me the opportunity to work on this project, which I always felt very privileged to be part of, and for their invaluable suggestions and comments on this thesis. I would particularly like to acknowledge David Stevenson's and Eiko Nemitz's positive and pragmatic attitudes, especially in the most delicate phases of my PhD and for making always time for me. Thankyou also to David Fowler for his precious feedbacks on my work and for making every situation brighter and scientifically appealing.

Many thanks to the Met Office and to Dr. Gerd Folberth for his useful advices on the UKCA model code, for offering comprehensive explanations of the model parameter interactions and for suggesting a sensible solution for the stomatal conductance error which was found and corrected in the first part of this project. Thankyou also to Dr. Luke Abraham for his invaluable support and for giving understandable clarifications of complex aspects of the UKCA model.
Many thanks to both my examiners Dr. Lisa Emberson and Dr. Mathew Heal for taking time to read my thesis and make helpful suggestions.

I would particularly like to acknowledge all the data Owners considered in this thesis for sharing their data. Many thanks to Dr. Silvano Fares and to Dr. Flavia Savi for sharing useful information and pre-processed data regarding the Castelporziano monitoring site.

I would especially like to acknowledge the EU PEGASOS project for making this project possible. As a strong computational project, I would also like to acknowledge the Centre for Ecology and Hydrology, and the University of Edinburgh for their technical support and facilities, without which none of this work could have been achieved.

Many thanks to all the MacAque modelling group members for all the useful discussions and different perspectives about my work throughout all the stages of this project.

Finally, I owe a debt of gratitude to my partner of life, Chiara Montani, who no doubts positively influenced me during this challenging journey and for being always encouraging. Many thanks to my father, Sergio Centoni, who also gave me unconditional support.

List of Figures

List of Tables

Glossary

ACCENT	–	Atmospheric Composition Change: the European Network of excellence
ACCMIP	–	Atmospheric Chemistry and Climate Model Inter-comparison Project
AOTX	–	Vegetation ozone damage approach based on the accumulated exposure over threshold of X ppb
$AF_{st}Y$	–	Vegetation ozone damage metrics based on accumulated stomatal flux above a thresholds *Y*
A_l	–	Modelled net leaf photosynthesis rate
A_p	–	Non-moisture stressed net photosynthesis rate
AURAMS	–	A Unified Regional Air quality Modelling System
BL	–	UKCA and MOSES broadleaf forest vegetation type
BL_h	–	Modelled boundary layer height
BVOCs	–	Biogenic volatile organic compounds
C3	–	UKCA and MOSES C3 temperate grass vegetation type
C4	–	UKCA and MOSES C4 tropical grass vegetation type
CAMx	–	Comprehensive Air Quality Model with Extensions photochemical grid model
$C_{CO2\,i}$	–	CO_2 partial pressure within the plant leaf
$C_{CO2\,l}$	–	External Leaf CO_2 partial pressure
C_{d0}	–	Cuticular resistance lookup table resistance value in dry conditions for vegetated surfaces
C_g	–	UKCA modelled depositing gas concentration
CFCs	–	Chlorofluorocarbons
CH_4	–	Methane
C_{O3}	–	Modelled ozone concentration

CTM	–	Chemical transport model
CWC	–	Modelled canopy water content
C_{w0}	–	Cuticular resistance lookup table resistance value in wet conditions for vegetated surfaces
D_c	–	Leaf surface parameter controlling the response of stomata to humidity deficit
D_l	–	Leaf surface humidity deficit
DO_3SE	–	Deposition of O_3 for Stomatal Exchange model
ECMWF ERA-40	–	Meteorological re-analysis data used to nudge UKCA model
EMEP	–	European Monitoring and Evaluation Programme model
F_0	–	Calibration parameter associated with stomatal opening
F_d	–	Dry deposition flux in UKCA model
F_{O3}	–	Dry deposition flux of ozone in UKCA model
g	–	Gravitational constant
g_c	–	Canopy stomatal resistance for water vapour
g_l	–	Modelled stomatal conductance to water vapour at the leaf level
G_{cut}	–	Cuticular conductance
GHGs	–	Greenhouse gases
$G_{inc.+s.}$	–	In-canopy aerodynamic+soil conductance
G_{ns}	–	Non-stomatal conductance for ozone
G_{ns}/G_c	–	Ratio between the ozone non-stomatal conductance and the canopy conductance
G_s	–	Stomatal conductance for ozone
G_s/G_c	–	Ratio between the ozone stomatal conductance and the canopy conductance
H	–	Sensible heat flux

HadGEM2-CC	−	Coupled atmosphere ocean UM model
HadISST	−	Sea Ice fields obtained from observational data sets
h_{BL}	−	Height of the highest model level contained within the boundary layer
h_c	−	Canopy vegetation height
HCFCs	−	Hydrochlorofluorocarbons
IPCC	−	Intergovernmental Panel On Climate Change
I_s	−	Net short-wave solar radiation
k	−	Von Kármán constant
L	−	Monin-Obukhov length
LAI	−	Leaf Area Index
LE	−	Latent heat flux
MAE	−	Mean Absolute Error (Model performance metrics)
MIM	−	Mainz Isoprene Mechanism adopted in UKCA model
MOSES 2.2	−	The Met Office Surface Exchange Scheme v2.2
MRB	−	Mean Relative Bias (Model performance metrics)
NL	−	UKCA and MOSES needleleaf forest vegetation type
O_3	−	ozone
P	−	Atmospheric pressure
PANs	−	Peroxyacetyl nitrates
Pr	−	Prandtl number
q	−	Specific humidity
R	−	Universal gas constant
R_a	−	Aerodynamic resistance

R_{ac}	–	In-canopy aerodynamic resistance
R_{ac0}	–	In-canopy aerodynamic lookup table resistance value (ZHG scheme) for vegetated surfaces
R_b	–	Quasi laminar boundary layer resistance
R_c	–	Canopy resistance
RCP 8.5	–	Representative Concentration Pathway 8.5
R_{cut}	–	Cuticular resistance
$R_{cut}(O_3)$		Constant for cuticular resistance for ozone (WES scheme)
RH	–	Relative humidity
R_s	–	Stomatal resistance for ozone
R_{soil}	–	Soil resistance
Sc	–	Schmidt number
SIC	–	Sea-ice concentrations
SMC	–	Soil moisture content at the root zone
SST	–	Sea surface temperatures
STE	–	Stratosphere-troposphere exchange
Surfatm-O_3	–	Surface Atmosphere ozone model
T	–	Atmospheric temperature
TF HTAP	–	Task Force on Hemispheric Transport of Air Pollution
T_l	–	Plant leaf temperature
TropIsop	–	UKCA Tropospheric chemistry scheme with Isoprene oxidation
T_s	–	Surface temperature
u	–	Zonal component of wind
u_*	–	Friction velocity

UN-ECE	–	United Nations Economic Commissions for Europe
UKCA	–	United Kingdom Chemistry Aerosol model
UM	–	UK Met Office's Unified Model
VPD	–	Vapour pressure deficit
W_{bk}	–	Modelled fraction of stomata blocked by a thin water film under wet conditions (ZHG scheme)
WES	–	Revised UKCA dry deposition scheme based on a simplified version of Wesely (1989)
z'	–	Roughness height for the exchange of the trace gas and sensible heat
z_0	–	Roughness length
z_{0w}	–	Modelled roughness length over the oceans
ZHG	–	Alternative UKCA dry deposition scheme based on a simplified version of Zhang et al. (2003)
α_m	–	Minimum canopy capacity
β	–	Modelled vegetation type soil moisture stress factor
Γ_g	–	Model grid surface type fraction
ε_{sm}	–	Modelled soil moisture ratio
η_c	–	Modelled canopy water content in fraction of area
θ_c	–	Modelled soil moisture concentrations at critical point
θ_s	–	Modelled volumetric soil moisture concentration as fraction of saturation
θ_w	–	Modelled soil moisture concentrations at wilting point
μ_c	–	the capacity of the canopy to hold water through the interception of rainfall
v	–	kinematic viscosity of air
ρ_m	–	Minimum canopy capacity

σ	–	Diffusion correction factors for O_3, NO_2 and PANs
τ_m	–	UKCA time step
Φ_m	–	Businger function for momentum
Ψ_w	–	Modelled average canopy water content
ω	–	rate of change of vegetation roughness with height
Ω	–	Model grid-box volume
χ_d	–	Modelled grid dry deposition loss rate of the deposited gas

Contents

Chapter 1

Motivation and background

1.1 Motivation

Atmospheric concentrations of ozone (O_3) are strongly affected by deposition processes to the biosphere. Dry deposition to terrestrial surfaces is the most important removal process of O_3 in the boundary layer, regulating the lifetime and concentrations at the surface (Royal Society, 2008).

To date, a mechanistic representation of O_3 dry deposition processes within global climate-chemistry models (GCMs) remains challenging, owing to difficulties in simulating the large spatial and temporal variability and complexity of O_3 dry deposition processes which depend on meteorological factors, vegetation specific characteristics of the surfaces as well as the rapid in-canopy O_3 chemistry reactions (Fowler et al., 2009; Wu et al., 2011).

Different treatments of dry deposition within GCMs constitute a source of variability in inter-model surface O_3 predictions (Wild, 2007; Fiore et al., 2009). Differences between modelled and observed O_3 dry deposition fluxes are mainly driven by the modelled deposition rates rather than by surface O_3 (Hardacre et al., 2015). By its nature, a GCM is a simplification of the real world, but if the outputs are used to

support decisions for climate policies aimed at limiting O_3 damage, it is essential to assess the modelled dry deposition and surface O_3 performance and to test their sensitivities to different deposition approaches.

Deposition processes are very sensitive to surface temperature and relative humidity and soil moisture deficit and are expected to respond to global climate change, with implications for both air quality (e.g. human health) and ecosystem services (e.g. crop yields) (Fowler et al., 2009). However, the level of confidence of model predictions, regarding the effects of climate change on O_3 dry deposition, is considered to be low (Fiore et al., 2012). Employing a sophisticated global chemistry aerosol model allows the interactions between atmosphere and biosphere exchange of O_3 to be studied, and the sensitivities of O_3 predictions to climate change using different deposition schemes to be explored. Such a study tests and improves the current understanding of O_3 dry deposition processes at the global scale, and highlights phenomena and uncertainties which may have potential implications both for present day and future O_3 air quality and climate.

This chapter presents an overview of the theory of atmosphere-biosphere exchange of tropospheric O_3 and the interactions between climate and O_3, with particular regards to the current understanding of O_3 dry deposition processes and modelling approaches. Particular emphasis is also placed on the challenges existing in modelling the effect of climate change on surface O_3 and O_3 deposition, highlighting source of uncertainties and gaps of knowledge.

1.2 Tropospheric Ozone

O_3 is a natural atmospheric component which is found both in the stratosphere and in the troposphere (Royal Society 2008). Stratospheric O_3, which is produced as a result of the photolysis of molecular oxygen, forms a protective layer against the UV radiation from the Sun (Royal Society 2008). By contrast, throughout the troposphere and at the surface, O_3 is considered a secondary short-lived air pollutant (Monks et al., 2015) and the third most important greenhouse gas (IPCC, 2013; Stevenson et al, 2013, 2006). Tropospheric O_3 is created in the presence of sunlight as a result of

chemical reactions between nitrogen oxides (NO_x), volatile organic compounds (VOCs), methane (CH_4) and carbon monoxide (CO) and many other pollutants (Crutzen 1974; Liu et al., 1980; Atkinson 2000). Owing to the dependence of O_3 formation on photochemical reactions, the highest concentrations of O_3 are usually observed during spring and summer whereas the lowest levels generally occur in autumn (Cooper et al., 2014).

In the presence of NO_x and VOCs, the key chemical processes leading to tropospheric O_3 formation are the following (Von Schneidemesser et al., 2015; Monks et al., 2015; Sillman et al., 1999) as described in reactions 1-6:

$$VOC + OH \xrightarrow{O_2} RO_2 + H_2O \quad (1)$$

$$CO + OH \xrightarrow{O_2} HO_2 + CO_2 \quad (2)$$

$$RO_2 + NO \xrightarrow{O_2} \text{secondary VOC} + HO_2 + NO_2 \quad (3)$$

$$HO_2 + NO \rightarrow OH + NO_2 \quad (4)$$

$$NO_2 + h\nu \rightarrow NO + O \quad (5)$$

$$O + O_2 + M \rightarrow O_3 + M \quad (6)$$

Peroxy radicals (HO_2) are produced through oxidation of VOCs by OH, O_3 or nitrate radical (NO_3); these lead to O_3 accumulation in the atmosphere by displacing O_3 in the oxidizing reaction of NO to NO_2 (Atkinson 2000; Von Schneidemesser et al., 2015).

Different chemical regimes are generally associated with O_3 formation, typically characterized by sensitivity to NO_x or VOCs (Royal Society, 2008; Von Schneidemesser et al., 2015). VOC/NO_x ratios, reactivity of VOCs, biogenic emissions, photochemical reactions and varying meteorological conditions, are considered among the factors influencing these regimes (Von Schneidemesser et al., 2015). Each regime is characterized by different type of sources (O_3 photolysis, formaldehyde HCHO and other intermediate organics) or hydrogen radical sinks as

shown in the reactions 7-11 (Sillman et al., 1999; Royal Society, 2008; Von Schneidemesser et al., 2015).

Sources:

$$O_3 + h\nu \xrightarrow{H_2O} 2OH \quad (7)$$

$$HCHO + h\nu \xrightarrow{O_2} HO_2 + CO \quad (8)$$

Sinks:

$$HO_2 + HO_2 \rightarrow H_2O_2 + O_2 \quad (9)$$

$$RO_2 + HO_2 \rightarrow ROOH + O_2 \quad (10)$$

$$OH + NO_2 + M \rightarrow HNO_3 + M \quad (11)$$

OH radicals play a fundamental role in the chemistry of tropospheric O_3 as they react with CH_4 and CO initiating the chemical reactions which lead to O_3 formation or destruction (Royal Society, 2008). While reaction (11) is one of the most important pathway of O_3 removal via HO_x radicals in polluted urban areas, in regions where NO emissions are high (such as polluted areas or within the forest canopies as a result of microbiological activity) O_3 concentrations can also be reduced due to "NO_x titration" (Von Schneidemesser et al., 2015):

$$NO + O_3 \rightarrow NO_2 + O_2 \quad (12)$$

1.3 Tropospheric O_3 budget

Stevenson et al. (2006) estimated the average lifetime of tropospheric O_3 at 22 (±2) days, showing that it varies with altitude and with time from several weeks in the upper troposphere to 1-2 days within the boundary layer where dry deposition of O_3 occurs. Dry deposition to terrestrial or marine surfaces is the major sink of tropospheric O_3 at the surface (Royal Society, 2008).

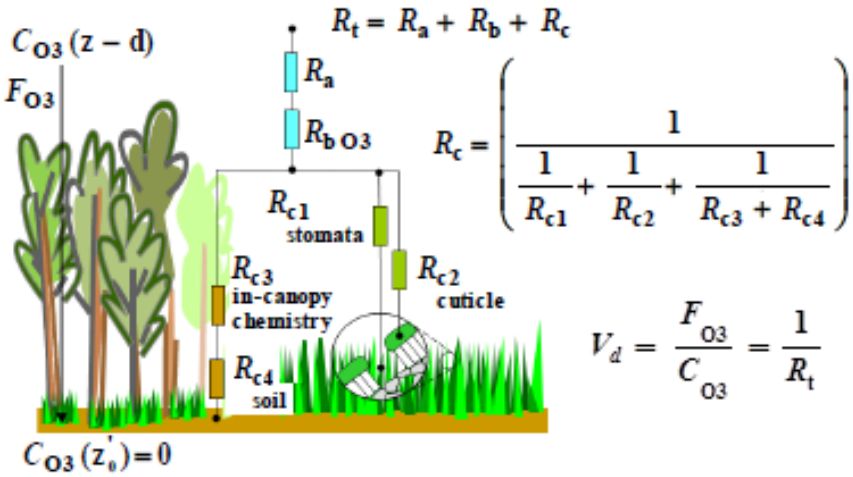

Figure 1.1. Simplified resistance approach representing O_3 dry deposition pathways including the atmospheric resistances (R_a, R_b) and sinks on plant stomata, leaf cuticles, in-canopy chemistry and soil. Figure from Monks et al. (2015).

The atmospheric budget of O_3 at the global scale is defined by the rates of O_3 production and O_3 destruction (Royal Society, 2008). Recent model estimates suggest that the O_3 production in the troposphere accounts for approximately 5110 ± 606 Tg yr^{-1} (Stevenson et al., 2006; Royal Society, 2008) whereas an estimate of the second major source of tropospheric O_3, represented by the stratosphere-troposphere exchange (STE), based on observational constraints is around 550 ± 140 Tg yr^{-1} (Olson et al., 2001; McLinden et al., 2000; Monks et al., 2015). Chemical destruction or chemical loss of 4668 ± 727 Tg yr^{-1} and dry deposition to the surface of 1003 ± 200 Tg yr^{-1} are recent model estimates of the processes closing the O_3 budget (Stevenson et al., 2006; Royal Society, 2008).

The net chemical production, resulting from the balance of the global O_3 tropospheric budget, is about 450 ± 300 Tg yr^{-1} (Stevenson et al., 2006). The large uncertainty of this term is due to the uncertainties in the estimates of gross chemical production and destruction which remain considerable (Wild, 2007; Wu et al., 2007; Monks et al., 2015).

1.4 Modelling global source and sinks of O_3

Dry deposition schemes were developed to quantify the contribution that each deposition pathway provides to the exchange of O_3 (Fowler et al., 2009). The deposition of O_3 from the atmosphere onto surfaces occurs in the absence of precipitation (Seinfeld and Pandis, 2006), and the amount of O_3 depositing to a unit surface area is defined as vertical dry deposition flux (F_{O3}). Dry deposition rates are commonly expressed as a vertical velocity (V_d), with dimensions of ms^{-1}, and are determined by the ratio of the vertical flux (F_{O3}) and the ambient O_3 concentration at a reference height (C_{O3}) (Royal Society, 2008). By making an analogy with electrical circuits, the O_3 dry deposition flux can be represented as an electrical current flowing within a system of resistances, as shown in Figure 1.1 (Fowler et al., 2009).

Each resistance may be in series if just one sink is present at the surface (e.g. sea/fresh water) or in parallel with each term representing a different key process (Fowler et al., 2009).

The O_3 deposition flux (F_{O3}) is commonly measured through micro-meteorological methods (Duyzer et al., 1995; Lamaud et al., 2009; Monteith and Unsworth, 2007; Rummel et al., 2007; Stella et al., 2011b) or enclosure techniques (Altimir et al., 2006; Brueniger et al., 2012). Both methods quantify a combination of source and sinks at the surface (canopy or surface resistance) which is generally calculated as a residual of the total resistance deprived of the turbulent transfer resistance (R_a) and leaf boundary layer resistance (R_b) (Fowler et al. 2009; Ganzeveld et al., 2015).

1.4.1 Atmosphere-biosphere exchange of O_3

Due to its high chemical reactivity, O_3 rapidly deposits to dry surfaces including vegetation, soil and other materials (e.g. buildings) whereas in theory O_3 deposits less quickly onto wet surfaces owing to its low solubility (Royal Society, 2008). As shown in Figure 1.2, dry deposition of O_3 occurs to different pathways such as through the stomata of plant leaves (stomatal deposition), or via non-stomatal pathways (Fowler et al., 2009). Typical non-stomatal deposition pathways are:

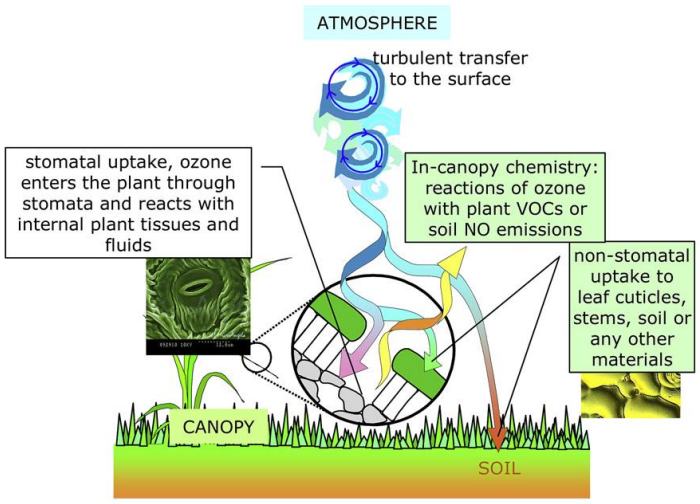

Figure 1.2. Terrestrial O_3 sinks and processes governing the atmosphere-biosphere exchange. Figure from Fowler et al. (2009).

reactions of O_3 with the outer plant surfaces or waxy leaf cuticles and the soils underlying the vegetation canopies (Fowler et al., 2009).

Chemical sinks associated with VOC emissions and other chemical reactions occurring on canopy surfaces, can constitute a significant part of the non-stomatal O_3 deposition (Kurpius and Goldestein, 2003; Gerosa et al., 2005; Cape et al., 2009; Fares et al. 2010a,b).

1.4.2 Plant leaf processes: O_3 stomatal uptake

A review of some of the most common approaches used in Chemistry Transport Models (CTMs) to simulate the stomatal conductance (e.g. the rate of passage of carbon dioxide CO_2 entering, or water vapour exiting, through the leaf stomata), revealed that this parameter is simulated using a multiplicative response function approach first developed by Jarvis (1976) (Flechard et al., 2011). In this approach the maximum expected stomatal conductance for O_3 for the different land cover types

(taken from look-up tables) is multiplied by a number of factors (0 to 1) that describe the impact of non-ideal environmental conditions. According to this approach, specific environmental functions are used to relate some key environmental factors, affecting the stomatal uptake, such as irradiance, temperature, vapour pressure deficit and soil water availability to the stomatal conductance (Emberson et al.,2000a; Büker et al., 2012). Büker et al. (2012) showed that, using this method, properly modelling the characteristics of the environment such as soil texture and soil water holding properties (which usually vary with the surface type) is crucial to simulate the stomatal conductance for O_3 and O_3 stomatal deposition accurately, but also the water vapour loss from the canopies and the plant phenology.

A second method used in GCMs is based on a relationship between the leaf level photosynthesis and the stomatal conductance to water vapour (then corrected by a factor to take into account the different diffusivity of CO_2 and O_3 through air), since CO_2 diffuses before being fixed by photosynthesis (Cox et al., 1999; Fares et al., 2013). Cox et al. (1999) also introduced an additional dependence of the photosynthesis rate on soil moisture availability, as better described in Chapter 2 (Sec. 2.2.4.4). Similarly, in other model approaches the stomata conductance is derived through leaf photosynthesis rate which is calculated inferring the fraction of sunlit and shaded leaves (Val Martin et al., 2014).

1.4.3 Non-stomatal deposition processes

In a recent review of the modelling approaches of O_3 atmosphere-biosphere exchange, Ganzeveld et al. (2015) highlight there is a large body of literature showing that the magnitude of the O_3 non-stomatal deposition can be comparable to the stomatal uptake. Ganzeveld et al. (2015) also point out that quantifying the total O_3 deposition flux is vital for studies of carbon sequestration and the impact of O_3 on plant functioning, as they depend on the accuracy of the partitioning between stomatal and non-stomatal O_3 deposition. According to the most recent experimental evidence, Fowler et al. (2009) point out that ca. 40-60% on average of the total deposition is constituted by the stomatal uptake and the non-stomatal deposition is variable.

In addition, Fowler et al. (2009) state that surface temperature, solar radiation, surface moisture and wind speed play a significant role in affecting non-stomatal deposition. Some key mechanisms leading to an increase in O_3 deposition are identified by Fowler et al. (2009): (i) waxes and other compounds on the plant surface can mediate the decomposition of O_3 which is strongly dependent on surface temperature; (ii) solar radiation controls the photolysis of O_3 which can be affected by the surface properties, and influences the chemical reactions associated with VOC emissions from vegetation canopies; (iii) reactions with compounds in aqueous solutions on plant surfaces can be mediated by surface moisture, in which case the affinity of surfaces for ozone may actually increase with moisture.

1.4.3.1 O_3 interactions with aqueous solutions on leaf surfaces

The external leaf surface is covered with epicuticular waxes and other associated compounds which can be either be deposited onto the foliage such as salts/ions (e.g. $Na^+, K^+, NH_4^+, NO_3^-, SO_4^{2-}$), inorganic gases, and condensable vapours (H_2O, bVOC) or emitted/secreted by the plant (Altimir, 2005; Poitier et al., 2015). Examples of compounds that are emitted or secreted from the interior of the plants and have been found to destroy O_3 at the surface include *cis*-abienol (Jud et al., 2016) and ascorbate (Potier, 2015).

Experimental measurements of O_3 deposition flux over different forests indicate that, despite of its low solubility, the enhancement in the removal of O_3 is mediated by the presence of surface wetness on the foliage surface (Fuentes et al., 1992; Fuentes et al., 1994; Altimir (2005); Altimir et al., 2006). According to Altimir (2005), the reactions in the aqueous solution present at leaf surface, increase the solubility of O_3, with larger pH favouring the dissolution. Experimental evidence showed that the composition of the chemical solution on the foliage is likely to vary with time (Altimir, 2005; Fuentes et al. 1994). The deposition of aerosols on the leaf surfaces, which would bring salts and organic acid, may be responsible for the change of the composition of the potential solution (Altimir, 2005).

Interestingly, Altimir et al. (2006) found that the O_3 non-stomatal contribution to the total O_3 canopy sink over a Pine Forest in Finland become the dominant (larger than

60%) when the canopy conditions are mostly wet.

Coyle et al. (2006) suggested that a combination of ambient sulphur dioxide (SO_2) and ammonia (NH_3) over grassland in Scotland can account for the high level of observed O_3 non-stomatal deposition, which is due to NH_3 increasing the pH of the solution that leads to a considerable sink for O_3. Poitier et al. (2015) indicate that the required chemical reaction rate of O_3 on wheat leaves can be attributed to reactions in mixed water with ascorbate leaking from the leaf apoplasts, with the leakage rate being higher in senescent leaves compared to mature leaves.

1.4.3.2 In-canopy O_3 chemistry sinks

The air composition surrounding the external and inner surfaces of the plant canopies is determined by the gases emitted by the vegetation (bVOC), the viscous boundary layer and the intercellular air space, and is influenced by the micro-climate conditions (Altimir, 2005). According to canopy scale observations, the emitted bVOC and especially the most reactive species can lead to a significant (non-stomatal) sink for O_3 within the vegetation canopy (Kurpius and Goldestein, 2003; Fares et al., 2010a).

Fares et al. (2010a) reported of high levels of O_3 non-stomatal deposition fluxes over a Pinus Ponderosa forest in the USA during spring and summer, attributing this to reactions of bVOC (monoterpenes, sesquiterpenes) with O_3 in the gas-phase occurring within the canopy which are strongly influenced by the temperature.

Kurpuis and Goldestein (2003) partioned the total O_3 flux over a pine ponderosa in Sierra Nevada, reporting that the O_3 in-canopy chemistry sinks was the dominant day time O_3 loss process (45-55%), while the stomata uptake and the non-stomatal deposition accounted for 25-35% and 20% respectively in summer. Fowler et al. (2001) interpreted this O_3 non-stomatal deposition process as temperature dependent thermal decomposition of O_3 on dry surfaces.

Kurpuis and Goldestein (2003) pointed out that the gas-phase reactions of a wider suite of biogenic hydrocarbons (monoterpenes, sesquiterpenes, and related compounds with lifetimes less than 10 mins), whose emissions is exponentially dependent on temperature, could significantly produce O_3 loss within the canopy.

Reaction chamber experiments carried out by Cape et al. (2009) confirmed that the 'steady-state' loss of O_3 (in absence of α-pinene) on 'inert' surfaces is temperature dependent, reporting a common activation energy of 30 kJ mol^{-1}, similar to that associated with O_3 deposition flux to vegetation. In addition, Cape et al. (2009) reported of a dependence of the absolute reaction rate on the effective surface area, with values 14 times greater for aluminium and hydrocarbon wax surfaces than stainless steel.

1.4.3.3 Soil deposition

Massman (2004) provide a first overview of the modelling approaches for O_3 dry deposition to soils, pointing out that wet/dry soil moisture leads to larger/smaller soil resistances with consequences for deposition. Earlier study results (Garland, 1976; Güsten et al., 1996; Massman, 2004) suggest that a relation between soil organic content, soil porosity, soil moisture and soil resistance might exist. Due to lack of knowledge regarding the relations between the above soil resistance and the soil properties, Massman (2004) derived two constant resistance values, respectively a lower value for dry soils and higher one for wet soils. By contrast, as reported by Ganzeveld et al. (2015), more recent experimental measurements indicate that increasing relative humidity at the soil level is a factor controlling O_3 deposition to bare soil. The key mechanism associated with this effect is driven by the changes in soil moisture availability induced by the increase in relative humidity (Stella et al., 2011b; Ganzeveld et al., 2015).

1.4.4 In-canopy turbulent transport and diffusion

Parameterisations of ozone deposition range from big-leaf models, where the canopy exchange is simulated to take place at a single mean height, to multi-layer models, where the canopy is divided into several layers at which exchange takes place. Even the big-leaf models are usually complemented by a further exchange pathway with the soil below, and thus both types of models require a parameterisation of the efficiency of the transport through the canopy. In current modelling approaches the

turbulent transport of O_3 within the canopy is partly captured, and the transport through the quasi-laminar surfaces is by molecular diffusion (Ganzeveld et al., 2015). Ganzeveld et al. (2015) also indicated that two underlying mechanisms associated with canopy turbulence regimes are not yet simulated: (i) the partial or full decoupling of the lower part of canopy which depends on wind speed, density of the vegetation canopy and thermal stratification; (ii) consistent turbulent structures forming above the canopy which can lead to canopy air restoration with consequent transport of heat and mass. Moreover, almost all parameterisations are steady-state models, in which storage of O_3 inside the canopy and its chemical interaction with other compounds such as NO and VOCs cannot be tracked in time, resulting in additional uncertainty. Ganzeveld et al. (2002) showed that a two-layer (crown layer and a canopy-soil layer) representation of the canopy vegetation leads to a better simulation of the main features of the atmosphere-biosphere exchanges of O_3 and NO_x, pointing out that dry deposition and turbulent exchange of O_3 within the canopy are better resolved using this approach.

1.4.5 Simulating O_3 through GCMs and CTMs: overview of existing deposition schemes

In most of GCMs and CTMs, the dry deposition resistance parameterizations first developed by Wesely (1989) are typically used (Fowler et al., 2009; Hardacre et al., 2015), which, for a range of pollutants, includes a Jarvis-type parameterisation for the stomatal pathway (as described in Section 1.4.2), coupled with a simple parameterisation of the cuticular deposition pathway (based on the reactivity and solubility of the pollutant, where the latter assumed to be 0 for O_3) and the deposition through the canopy to the soil. The parameterisation of each pathway uses look-up values that are specific to the surface type and season. Fowler et al. (2009) point out that in these models the effect of soil moisture stress on the stomatal function observed in field measurements (Gerosa et al., 2009) is still poorly simulated. In addition, some processes at the sub-grid level are not well captured due to low model resolution and the aggregation of vegetation and land cover properties (Fowler et al., 2009). Importantly, most models simulate O_3 dry deposition and biogenic emissions of VOC separately not taking into the effects of chemical interactions within the

canopy (Ganzeveld et al., 2015). Due to technical and methodological difficulties, along with a lack of field data, Flechard et al. (2011) highlight that the parameterizations for the O_3 non-stomatal deposition differ between CTMs. The EMEP CTM includes a parameterization for the non-stomatal deposition which considers the effect of increasing surface wetness on the O_3 deposition (Touvinen et al., 2008; Fowler et al., 2009). In the regional model Surfatm-O_3 more developed parameterizations for the non-stomatal deposition were implemented (Stella et al., 2011a). The effect of relative humidity on deposition to leaf cuticles during growing and senescence periods as well as a dependence of soil deposition on the soil surface relative humidity (*RH*) are simulated in the Surfatm-O_3 model (Stella et al., 2011a,b). In MuSICA model a more mechanistic approach for O_3 non-stomatal deposition is applied, modelling O_3 deposition to dry and wet leaves differently during growing and senescence periods (Poitier et al., 2015). Zhang et al. (2003) developed more dynamic non-stomatal parameterizations for O_3 which take into account key environmental factors such as relative humidity (*RH*), leaf area index (*LAI*) and friction velocity (u_*). The Comprehensive Air Quality Model with Extensions (CAMx) photochemical grid model currently implements the Zhang et al. (2003) approach for O_3 modelling studies across Europe (Nopmongcol et al., 2012).

1.5 Impacts of O_3 on the Earth system

1.5.1 Climate

The Earth's radiation budget is strongly affected by the composition of the atmosphere (Isaksen et al., 2009). The role of clouds is also significant as they reflect the incoming component of the solar radiation and absorb the outward thermal radiation component emitted from the surface, then reradiating at the ambient temperature through the effect known as greenhouse effect (Isaksen et al., 2009). In the troposphere compounds like O_3, CH_4 and secondary aerosols (sulphates, nitrates and secondary organic aerosol compounds) can exert a strong influence on the Earth climate due to their radiative properties (Isaksen et al., 2009). In particular, O_3 is

considered the third most significant greenhouse gas contributing to the climate change (Stevenson et al., 2006, 2013). In the Earth system there are several interactions of tropospheric O_3 concentrations and feedbacks between the physical climate and the atmospheric composition (Monks et al., 2015).
Ozone can also affect climate via the interaction with the biosphere: ozone effects on vegetation can reduce photosynthesis and thus the potential of vegetation to sequester CO_2 (Sitch et al., 2007), and ozone stress can affect the biogenic emission of volatile organic compounds that act as aerosol precursors (Monks et al., 2015).

1.5.2 O_3 exposure: health and ecosystems effects

As a secondary air pollutant, O_3 is a powerful oxidant which causes severe issues for human health (Bates, 2005). Short term inhalation of O_3 produces inflammation of the entire respiratory area (Monks et al., 2015). Long term exposure to O_3 can lead to serious chronic health effects and is also considered the cause of 0.47 million premature deaths globally (Von Scheneidemesser et al., 2015). In addition, O_3 is phytotoxic constituent and penetrating the leaf stomata produces reactive oxidants as a consequence of the reactions with the internal tissues of the plant (Monks et al., 2015). The most evident effect of these chemical reactions is represented by a visible injury on the plant leaves (Ashmore et al., 2005). Reduced plants growth and seed production, lower leaf functional area and earlier senescence are some critical effects induced by the exposure of plants to O_3 (Monks et al., 2015). More recent experimental evidence show that the long-term exposure of plants to O_3 also reduces stomatal conductance due to the direct effect of O_3 on photosynthesis (Ainsworth et. al, 2012).

1.6 Influence of climate change on O_3 air quality

Recent reviews highlight there are multiple ways by which climate change influences O_3 air quality (Jacob and Winer, 2009; Fiore et al., 2012; Monks et al., 2015; Von Schneidemesser et al., 2015). The influence of climate change on air quality can

occur through different processes such as: natural emissions, transport and mixing, photolysis rates, chemical reactions and deposition processes (Isaksen et al., 2009). In particular, the hydroxyl radical (OH), due to its central role in the oxidising capacity of the troposphere, represents a key factor in the interaction between the climate and the atmospheric chemistry (Isaksen et al., 2009). Considering that the concentrations of water vapour are predicted to increase in the future, this might lead to a decrease of O_3 concentrations over rural areas (Jacob and Winer, 2009; Monks et al., 2015) and to increases in O_3 production over polluted areas, due to changes in O_3 precursors such as isoprene, PAN and NO_3 induced by climate change (Jacob and Winer, 2009).

In the last years many studies used GCMs incorporating interactive chemistry schemes to investigate the response of O_3 to climate change and examining some chemistry-climate interactions (Fiore et al., 2012). Monks et al. (2015) and Fiore et al. (2012) provide a summary of key climate change-air quality pathways, pointing out that some of these are significant such as increases in temperature over land, changes in atmospheric humidity, and increased occurrence of stagnation episodes associated with changes in the anticyclonic conditions. Overall, climate change is likely to lead to an increase in O_3 in NO_x polluted regions and O_3 loss in remote regions where the concentrations of NO_x are low (Jacob and Winer, 2009; Fiore et al., 2012). Increases in lightning NO_x and in the exchange of stratospheric-tropospheric O_3 are also predicted to occur as a consequence of climate change (Fiore et al., 2012). Although most of the model predictions point toward an increase in O_3 concentrations as a response to climate change (Stevenson et al., 2006), large uncertainties remain on how changes in meteorological factors might lead to changes in biogenic emissions of isoprene and O_3 dry deposition (Monks et al., 2015). Fiore et al. (2012) and Jacob and Winer (2009) point out a low level of confidence for those pathways.

1.7 Global impacts of O_3 on vegetation: present day and future assessments

According to the United Nations Economic Commissions for Europe (UN-ECE), two main approaches are currently used for assessing the regional risk for O_3 damage to vegetation (Simpson et al., 2007). These metrics are based on the AOTX index (Fuhrer et al., 1997) and the method based on the accumulated stomatal flux above a threshold *Y* ($AF_{st}Y$) (Mills, 2004). The AOTX is defined as the integral over time (in ppb hr) of the O_3 concentration above a threshold concentration X, and the integral becomes a proxy for potential damage (Simpson et al., 2007). For crops and forests this concentration threshold is 40 ppb (AOT40). The approach based on the stomatal flux, calculates the integral over time of the stomatal flux above a flux threshold, which varies between 6 nmol m^{-2} s^{-1} (crops) to 1.6 nmol m^{-2} s^{-1} (forests) (Karlsson et al. 2004; Simpson et al., 2007). However, other thresholds are also adopted such as for C3/C4 grass e.g. 5 nmol m^{-2} s^{-1} (Clark et al., 2011). According to Simpson et al. (2007) the AOTX is associated with two practical problems: (i) the height of the measurement height should be at the top of the vegetation canopy whereas the O_3 concentrations used to calculate the AOTX index are usually taken at ~ 3 m; (ii) inconsistency in the accumulation period (growing season) as it can be fixed at May-July or vary from a country to another.

Most recently, it has become increasingly evident that a metric based on a stomatal dose-response relationship is more appropriate for O_3 damage assessments rather than one based on concentrations (Ainsworth et al., 2012). This methodological difference is particularly important under hot/dry meteorological conditions which may strongly influence the O_3 stomatal uptake (Simpson et al., 2007). In addition, climate change is likely to lead to changes in the O_3 exposure to vegetation globally (Ashmore et al., 2005). In order to estimate the O_3 exposure on vegetation globally, more experimental and field data are needed considering that the most of the existing studies are carried out in N. America and Europe (Ashmore et al., 2005). Therefore, considerable uncertainties remain for global O_3 damage assessments both for the present day and in the future. In addition, the non-stomatal deposition sinks are considered fixed in current O_3 damage studies based on accumulated stomatal flux

above a threshold (Touvinen at al., 2009; Emberson et al., 2013). Considering that several studies showed that the non-stomatal deposition is not constant (Fowler et al., 2009) and is sensitive to changes in meteorological factors and to in-canopy chemistry reactions (Fares et al., 2010a,b), this might constitute a further source of uncertainty for assessing present and future O_3 damage.

1.8 Thesis aims

Firstly, this thesis will present the main features of the dry deposition scheme of the global chemistry aerosol model (United Kingdom Chemistry Aerosol model) employed in this study. Some errors were found in the current UKCA dry deposition parameterizations, based on of simplified version of the Wesely (1989) scheme, and the effects of the model corrections of simulated O_3 fields were investigated and quantified. Assessing the impacts of the UKCA dry deposition scheme (here called WES scheme) amendments on modelled O_3 was essential as model outputs are used to support decisions for climate policies and for O_3 damage risk assessment studies.
Large uncertainties in parameterising the non-stomatal ozone deposition term exist in climate chemistry models and model predictions vary greatly (Fowler et al., 2009). The effects of a more mechanistic non-stomatal deposition approach and the blocking of stomata based on Zhang et al. (2003) on the modelled O_3 dry deposition rates and canopy conductance terms (here called ZHG scheme) will be examined in the second part of the thesis.

Secondly, this thesis will compare the performance of both UKCA dry deposition schemes against measurements, with a particular focus on the diurnal and seasonal variations of the dry deposition velocity terms and their partitioning between stomatal and non-stomatal components. The sensitivity of the O_3 non-stomatal deposition to observed environmental factors will also be investigated. A comparison of surface O_3 against observed values in the North Hemisphere and South Hemisphere will be provided, exploring the effect of the change in dry deposition scheme.

Finally, this thesis will provide results from a future climate simulation for the 2090s using RCP 8.5 climate change scenario to study the response of surface O_3 predictions to climate change, and exploring their sensitivities to different dry deposition schemes. The effect of climate change on the dry deposition sink of O_3 was addressed contrasting the two non-stomatal deposition parameterizations (WES vs ZHG). The impact of climate change on the O_3 dry deposition flux partitioning will be also investigated.

The main research questions of this thesis are:

I. Revising ozone dry deposition in the UKCA model and implementing a more mechanistic non-stomatal deposition approach (Chap. 2):

(a) How is O_3 dry deposition represented in UKCA model?

(b) What is the impact of the dry deposition parameterization corrections on surface O_3, O_3 dry deposition and O_3 dry deposition velocity at the global scale?

(c) What are the impacts of a more mechanistic non-stomatal deposition scheme and the blocking of stomata by surface water on O_3 deposition?

(d) What is the impact of the alternative dry deposition scheme on modelled O_3 concentrations?

II. A comparison of dry deposition schemes in the United Kingdom Chemistry Aerosol (UKCA) model with observations (Chap. 3) :

(a) Does UKCA capture the observed diurnal and seasonal variations of O_3 dry deposition velocity?

(b) How do modelled key meteorological factors for dry deposition and specific vegetation parameters compare with observations?

(c) How does the partitioning of the modelled O_3 deposition flux between stomatal and non-stomatal components compare with observations?

(d) What are the key uncertainties related to model structure and model resolution?

(e) Does the use of observed plot-scale environmental factors improve the simulated O_3 non-stomatal deposition compared with modelled large-scale meteorology?

(f) How does modelled surface O_3 compare with observations at the global scale?

(g) To what extent is the simulated surface O_3 sensitive to different dry deposition schemes?

III. The sensitivity of global ozone predictions to dry deposition schemes and their response to climate change (Chap. 4) :

(a) What is the overall impact of climate change induced by the increase in GHGs with RCP 8.5 on modelled O_3 dry deposition and surface O_3 globally?

(b) How do the predicted changes in O_3 dry deposition velocities due to climate change differ between dry deposition schemes?

(c) What drives the changes in O_3 dry deposition rates?

(d) To what extent are the tropospheric O_3 changes induced by climate change sensitive to dry deposition schemes?

(e) What is the impact of climate change on the O_3 dry deposition flux partitioning?

Chapter 2

Revising ozone dry deposition in the UKCA model and implementing an alternative non-stomatal deposition approach

2.1 Introduction

Tropospheric ozone (O_3) is considered a dangerous air pollutant causing damage to ecosystem and human health. Tropospheric O_3 concentration is controlled by the balance among net chemical production, influx from the stratosphere and deposition to the surface (Stevenson et al., 2006; Wu et al., 2007). Dry deposition constitutes the dominant physical loss process accounting for about 25% of the total tropospheric O_3 loss (Lelieveld and Dentener, 2000). Several studies in the literature have shown that different treatments of dry deposition within models lead to a wide range of simulated tropospheric O_3 budgets and contribute to inter-model surface O_3 differences (Stevenson et al. 2006; Wild, 2007; Fiore et al. 2009). Hardacre et al. (2015) presented the first evaluation of global O_3 dry deposition fluxes in global scale chemistry climate models (Fiore et al., 2009; Task Force on Hemispheric Transport of Air Pollution, 2010). It was found that differences between modelled dry deposition fluxes are mainly driven by modelled O_3 dry deposition velocities (V_d) rather than surface O_3. Hardacre et al. (2015) also point out that the discrepancies in modelled V_d over the oceans, grasslands and tropical forests represent the main source of differences between models. As reported in previous evaluation studies for the EMEP (Touvinen et al. 2004, 2009) and AURAMS (Zhang et al. 2002a) models

and in Hardacre et al., (2015), soil moisture deficit and non-stomatal deposition are generally not well represented within models and appear to be an important source of variability between models.

Several studies showed that the ecosystem effects of ozone are more closely linked to the O_3 flux entering the stomata rather than with ambient O_3 concentration (Ashmore et al., 2004; Harmens et al., 2007; Karlsson et al., 2007; Pleijel et al., 2007 Ainsworth et al., 2012). Thus, correctly partitioning the dry deposited O_3 flux between stomatal and non-stomatal sinks at the surface is vital to reduce uncertainties in assessments of O_3 effects (Touvinen et al., 2009; Emberson et al., 2013). In addition, Val Martin et al. (2014) showed that linking dry deposition more closely to vegetation significantly reduced biases in simulated surface O_3.

The United Kingdom Chemistry and Aerosol (UKCA) model (Abraham et al., 2012) simulates the process of dry deposition using a simplified implementation of the resistance analogy scheme of Wesely (1989) (here called WES Orig.), coupled with a prediction of stomatal conductance from the MOSES 2.2 land surface scheme (Essery et al., 2001, 2003). The interactive dry deposition scheme (Sanderson et al., 2006, 2007) consists of three main resistance terms in series (R_a, R_b, R_c). R_a and R_b represent the aerodynamic and quasi-laminar layer processes, respectively, whereas R_c, the canopy resistance, quantifies the affinity of the surface for O_3 uptake, or destruction, and includes the uptake by stomata, leaf surfaces (cuticles), soil, water and other materials present at the Earth's surface.

Thus, R_c takes into account specific chemical and physical properties of the surface, and the structure and physiological properties of the vegetation type itself. The canopy resistance may therefore be split into multiple resistance terms representing the different sinks (stomatal and non-stomatal pathways) at the surface, each operating in parallel. The stomatal uptake is represented by the resistance term R_s whereas R_{cut}, R_{soil} describe the O_3 deposition to leaf cuticles and to soil and whereas R_{ac} defines the in-canopy turbulent exchange of O_3. In the current interactive UKCA dry deposition scheme, the deposition to leaf cuticles is represented by monthly varying values whereas deposition to in-canopy pathways and the soils are simulated through vegetation/surface-specific resistance values. In practice, ozone reaction with leaf cuticle surfaces has been shown to vary with temperature, leaf surface water and

and atmospheric humidity (Coyle et al., 2008; Fowler et al., 2001).

Several atmospheric species are subject to dry deposition in UKCA model; in this study our focus in on O_3. Some errors in the implementation of the UKCA WES Orig. scheme, regarding the stomata resistance R_s and in-canopy aerodynamic resistance R_{ac}, were identified and corrected during this study.

Recent experimental studies have shown that O_3 stomatal uptake by a plant canopy constitutes between 40-60% of the total flux as an annual average and that the non-stomatal deposition varies (Altimir et al., 2006; Gerosa et al., 2003, 2004, 2009; Coyle, 2005; Coyle et al., 2009; Fowler et al., 2009; Fares et al., 2010a; Kurpius and Goldestein, 2003).

In this study, an alternative and simplified version of O_3 non-stomatal deposition approach along with effect of blocking of stomata (Zhang et al., 2003) (here called ZHG scheme) was implemented in UKCA. The ZHG scheme takes into account a dependence of O_3 deposition on some key meteorological factors (such as friction velocity, relative humidity, canopy wetness) and biological parameters such as canopy type and leaf area index. Therefore, among the existing deposition schemes, in this study the ZHG scheme was considered more suited to explore the effect of varying meteorological conditions, and by extension, changing climate on the global O_3 deposition. The ZHG scheme was then used to investigate the sensitivity of simulated surface O_3 to a more dynamic and mechanistic O_3 removal by vegetation and to better understand how the partitioning between stomatal and non-stomatal O_3 flux may vary at both a regional and global scales.

This chapter is organized as follows: Sections 2.2.1-2.2.6 describe the main features of WES Orig. deposition scheme, summarizing the problems found in it and the changes made to correct them. Section 2.2.7 introduces the alternative non-stomatal deposition scheme (ZHG scheme) implemented in UKCA. In Section 2.3.1 the impact of the model corrections on simulated surface concentrations, deposition velocities and fluxes are presented. The effect of the change of the dry deposition scheme on O_3 dry deposition velocities is also presented in Section 2.3.2. Sections 2.4.1-2.4.2 present some discussion of the sources of uncertainty regarding the changes made to the dry deposition scheme and the limitations of the ZHG scheme.

2.2 Methods

2.2.1 UKCA model general description

The coupled climate-chemistry model used for this study was the Hadley Centre Global Environment Model version 3 – Atmosphere only (QESM-A), with the UM (Unified Model) version 7.3 incorporating the UK Chemistry and Aerosol (UKCA) model (O'Connor et al. 2014). The horizontal resolution is 3.75º longitude x 2.5º latitude, with 60 hybrid vertical levels and top height at 84 km. The dynamic time step is 30 min while the UKCA (chemical) time step is 1 hour (O'Connor et al. 2014). Dynamical properties of UM are more fully described in Hewitt et al. (2011). This version of UKCA included a tropospheric chemistry scheme (TropIsop) which incorporates 25 tracers and 41 chemical species (O'Connor et al. 2014). The TropIsop scheme also comprises 25 photolytic reactions, 83 bimolecular reactions and 13 uni- and termolecular reactions (as described in tables (4)-(5)-(6) in O'Connor et al. 2014). The TropIsop scheme also includes the extra Isoprene species and reactions following the Mainz Isoprene Mechanism (MIM) (Pöschl et al. 2000). Emissions are decadal averages centred on the year 2000 based on the gridded dataset of Lamarque et al. (2010). These include surface emissions from nine species (NO, CH_4, CO, HCHO, C_2H_6, C_3H_8, Me_2CO, MeCHO, C_5H_8) and multi-level NO_x emissions from aircrafts.

2.2.2 Surface exchange Scheme: tile approach

UKCA is coupled with the land surface and carbon cycle model MOSES 2.2. In MOSES 2.2, an explicit treatment of the sub-grid land cover heterogeneity was introduced (Essery et al., 2003). Nine surface types were considered in this so-called "tile approach": broadleaf trees (BL), needle leaf trees (NL), C3 (temperate) grass, C4 (tropical) grass, shrubs, urban, water, bare soil and ice (Essery et al., 2001). Apart from those classified as land-ice, each model grid-box can be constituted by a mixture of the eight surface types (Essery et al, 2003). The associated surface type

Table 2.1. Meteorological variables driving MOSES 2.2 (top). Ancillary fields acquired by MOSES 2.2 (bottom).Table contents adapted from Best et al. (2011).

Met. variables	**Units**
↓ comp. of short-wave radiation at the surface	W m^{-2}
↓ comp. of long-wave radiation at the surface	W m^{-2}
Rainfall	kg m^{-2} s^{-1}
Snowfall	kg m^{-2} s^{-1}
u comp. of wind	m s^{-1}
v comp. of wind	m s^{-1}
Atmospheric *T*	K
Atmospheric *q*	kg kg^{-1}
Surface pressure *P*	Pa
Soil/Veg. ancillary fields	**Units**
Grid-box fractions of surface types, Γ_g	
Canopy height for vegetation types, h_c	m
Leaf area index for vegetation types, *LAI*	m^2m^{-2}
Volumetric saturation point for soil θ_s	m^3m^{-3} of soil
Critical volumetric soil moisture content, θ_c	m^3m^{-3} of soil
Volumetric wilting point for soil, θ_w	m^3m^{-3} of soil

fractions are read from ancillary fields. MOSES 2.2 simulates separate surface temperature (T_s), sensible (*H*) and latent heat (*LE*) fluxes, and canopy moisture loads for each tile. Other simulated meteorological parameters such as relative humidity (*RH*), wind speed and its derived variable the friction velocity ($u*$), are modelled as grid-average properties (Essery et al., 2001). As a coupled model, MOSES 2.2 exchanges with the climate model specific meteorological data (Met. Variables,

Table 2.1) and imports ancillary information and specific surface type prescribed values which are required for various soil/vegetation parameters (Soil/Veg. ancillary fields, Table 2.1). Specific vegetation type monthly means leaf area index (*LAI*) values are imported from maps based on the second Simple Biosphere Model outputs (SiB2; Sellers et al., 1996a) derived from NOAA-AVHRR satellite data. The canopy heights (h_c) of each vegetation type within the grid-box are also read from ancillary fields (Essery et al., 2001). The momentum roughness length (z_0) is inferred by setting $h_c/20$ for trees and $h_c/10$ for short vegetation types. An additional modelled vegetation parameter is the capacity of the canopy to hold water (μ_c, in kg m^{-2}) through the interception of rainfall:

$$\mu_c = \rho_m + \alpha_m LAI \qquad \textbf{(2.1)}$$

where ρ_m is the minimum canopy capacity (set to 0.5 kg m^{-2} for all the vegetation types) and α_m is the rate of change of water holding capacity with leaf area index, which is to set 0.05 in the MOSES 2.2 land surface model (Essery et al., 2002; Best et al., 2011). In contrast to the surface exchange, in MOSES 2.2 the sub-grid soil heterogeneity is not represented and the soil temperature and soil moisture content are treated as uniform within each grid-box (Essery et al., 2001; Best et al., 2011). The soil moisture availability of each vegetation type at each soil level is defined by the root density, following an exponential distribution with depth (Essery et al., 2001). Four soil layers of different thickness (0.1, 0.25, 0.65 and 2m) giving a total depth of 3m are currently included in the land surface scheme (Best et al., 2011). The default root depths of the plant types are 3m for BL tree, 1m for NL tree and 0.5m for C3/C4 grass and Shrubs respectively. There are three soil textural classes (fine, medium and coarse) included in MOSES 2.2 and specific properties regarding these land cover classes are based on Wilson and Henderson-Sellers (1985).

2.2.3 Simulation setups

In this study, two different simulation setups were used. A first model simulation (S1) was run to assess the effect of the dry deposition scheme corrections on

modelled O_3 fields with monthly time resolution. A second experiment (S2) was run to estimate the effect of the change (in %) of dry deposition scheme (from the WES scheme, which includes the model corrections, to the ZHG scheme) on annual mean surface O_3 and O_3 V_d and total annual O_3 dry deposition. A third simulation (S3) was performed, with monthly time resolution, to estimate the impact of the alternative dry deposition approach (ZHG scheme) on the annual mean O_3 V_d compared to the WES scheme.

Simulations S1, S2 and S3 were performed for two years and four months, as the first year was discarded to allow model spin-up. For simulations S1 and S2, prescribed monthly mean sea surface temperature and sea ice fields obtained from the observational HadISST data set (Rayner et al., 2003) were used. For simulation S3, physical variables (temperature *T*, zonal wind, *u*, and meridional wind, *v*) were nudged using ECMWF ERA-40 meteorological re-analysis data following the approach described in Telford et al. (2008) to give a more realistic representation of the atmosphere. In all the experimental setups, the same emissions and chemistry scheme were used as described in Sec. 2.2.1.

Some specific diagnostics were created to output the O_3 V_d terms simulated using the different model configurations as described above.

2.2.4 UKCA dry deposition scheme: Wesely-based approach

The dry deposition scheme called *Interactive dry deposition scheme* (hereafter referred to WES Orig.) is used as the default in UKCA to simulate diurnally and seasonally varying dry deposition velocities from the simulated meteorological conditions for the gaseous chemical species: O_3, NO_2, PAN, PPAN, MPAN, HNO_3, H_2O_2, SO_2, CH_4 (Giannakopoulos et al. 1998, Sanderson et al. 2007, O'Connor et al., 2014). The WES Orig. scheme is based on that developed by Wesely (1989) in which the dry deposition flux is treated as an analogue of a current flowing through an electrical circuit (Figure 2.1a) in which the processes controlling deposition consists of three main resistance terms. The aerodynamic resistance R_a represents the resistance to turbulent transport of material through the atmospheric boundary layer to a thin layer of air close to the surface. In this thin surface layer, transport is

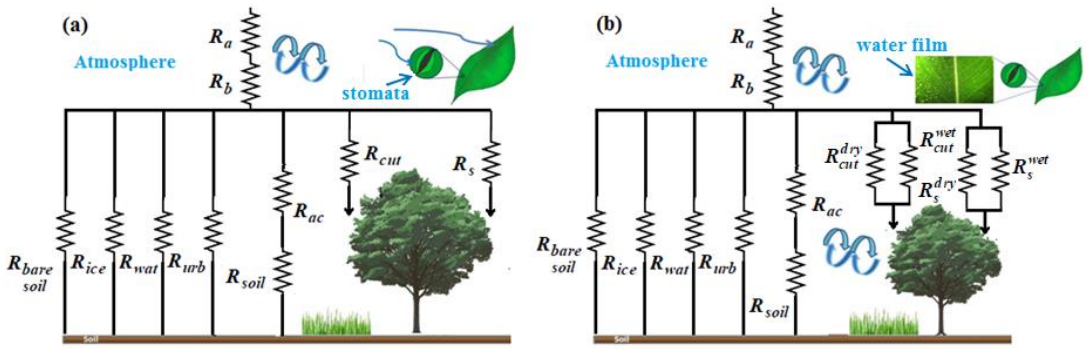

Figure 2.1. Schematic representation of the current UKCA dry deposition based on the Wesely (1989) approach (a). (b) shows the developed UKCA dry deposition scheme based on the Zhang et al., (2003) parameterizations.

characterised by the quasi-laminar resistance R_b which is related to the properties of the dry deposited species as it represents the molecular diffusion of the species through the non-turbulent layer of thin air (thickness of a typically a mm) in contact with the surface (Seinfield and Pandis, 2006). Finally, the canopy resistance R_c, which takes into account the chemical-physical and specific properties of the surface itself, describes the uptake of the species by the vegetated and non-vegetated surfaces.

2.2.4.1 Aerodynamic resistance: R_a

The grid aerodynamic resistance R_a is modelled in UKCA through the following equation for each of the nine surface types:

$$R_a = \frac{\ln(z'/z_0) - \Phi_m}{k\,u_*} \qquad (2.2)$$

where z_0 is the roughness length, Φ_m is the Businger function for momentum, z' is the roughness height for the exchange of the trace gas and sensible heat, u_* is the friction velocity and k is Von Kármán constant (Bentley, 2014;Ganzeveld et al. 1995). Whilst

UKCA takes into account land-cover specific values of h_c (and therefore z_0), it uses grid-average of u_* and heat fluxes to evaluate the functions Φ_m.
For the vegetation surfaces z_0 is calculated by MOSES 2.2 following the relation:

$$z_0 = \omega h_c \tag{2.3}$$

where ω (m m^{-1}) is the rate of change of vegetation roughness with height (e.g. 0.05 for BL and NL trees; 0.1 for C3/C4 grass and shrubs) and h_c (m) is the vegetation canopy height. By contrast, the roughness length over oceans is a function of wind speed and is calculated by the model according to the modified Charnock relationship given by Smith (1988) as follows:

$$z_{0w} = \frac{\nu}{9.1 u_*} + 0.0016 \frac{u_*^2}{g} \tag{2.4}$$

where ν is the kinematic viscosity of air (0.15 m^2 s^{-1}) and g (m s^{-2}) is the gravitational acceleration.

2.2.4.2 Quasi-laminar resistance: R_b

The quasi-laminar resistance R_b, which is gas specific, is computed according to the following relationship:

$$R_b = \ln(z'/z_0) \frac{(Sc/Pr)^{2/3}}{k u_*} \tag{2.5}$$

where Sc is the Schmidt number and Pr is the Prandtl number (Ganzeveld et al., 1995). In UKCA, ln (z'/z_0) is approximated with 2 for vegetated surfaces according to Garratt and Hicks (1973) whereas for non-vegetated surfaces a value of 1 is used according to Brutsaert (1973).

2.2.4.3 Canopy resistance: non-stomatal pathways

The grid surface or canopy resistance R_c is calculated using a so-called “big-leaf” approach, treating the vegetation canopy as though it were a single layer as described

by Monteith (1965). This allows the model to simulate O_3 dry deposition through different pathways: (i) uptake by vegetation canopies through stomata (R_s); (ii) the plant cuticles, a protective film covering the epidermis of leaves constituted by lipid and hydrocarbon polymers impregnated with wax, described by R_{cut}; (iii) the turbulent exchange between the upper canopy and the lower canopy (R_{ac}); (iv) deposition to underlying canopy soil and to the other surface types (R_{soil}) (Smith et al., 2000; Seinfield and Pandis, 2006).

The canopy resistance R_c is then calculated as a combination of stomatal and non-stomatal resistance terms:

$$R_c = \frac{1}{\frac{1}{R_s} + \frac{1}{R_{cut}} + \frac{1}{R_{ac} + R_{soil}}} \quad (2.6)$$

The cuticular resistance for O_3 is modelled for each vegetation type as:

$$R_{cut} = \frac{R_{cut}(O_3)}{LAI} \quad (2.7)$$

where $R_{cut}(O_3)$ is a constant equal to 5000 s m^{-1} independent of vegetation type (Massman et al., 2004).

Deposition to non-stomatal pathways (including external plant surfaces and non-vegetates surfaces), expressed here as a conductance G_{ns} (reciprocal of the non-stomatal resistance), is derived as follows:

$$G_{ns} = \frac{1}{R_{ns}} = \frac{1}{R_{cut}} + \frac{1}{R_{ac} + R_{soil}} \quad (2.8)$$

For the soil underlying the canopies, the resistance changes with surface wetness are taken into account by setting a threshold of soil moisture ratio $\mathcal{E}_{sm}$ (the amount of water per unit volume of soil, divided by the water density). Assuming that a typical soil porosity is ~30-40%, $\mathcal{E}_{sm}$ = 0.3 indicates that the soil is nearly saturated. If $\mathcal{E}_{sm} \leq 0.3$, the soil underlying the vegetation canopies is considered dry and the model assigns specific surface type resistance R_{soil} values taken from Wesely (1989)

as presented in Table 2.2. Otherwise if $\mathcal{E}_{sm} > 0.3$, the soil is considered wet and the model sets R_{soil} to a constant value (500 s m^{-1}) (Massman et al., 2004).

For the non-vegetated surface types, specific land cover type lookup table values are assigned to R_{soil} by the model as shown in Table 2.2.

Table 2.2. Soil resistance R_{soil} and in-canopy aerodynamic resistance R_{ac} lookup table values used in the UKCA dry deposition calculations (WES scheme).

Surface type	R_{soil} (s m^{-1})	R_{ac} (s m^{-1})
Broadleaf tree	200	1425
Needleleaf tree	200	2000
C3 grass	200	95
C4 grass	200	95
Shrub	400	145
Urban	800	0
Water	2200	0
Bare soil	800	0
Ice	2500	na

The in-canopy aerodynamic resistance R_{ac} is surface-type specific and is characterized by seasonal geographical variations as it depends on canopy height and density (Massman et al., 2004). R_{ac} values were not incorporated in the original UKCA dry deposition scheme (WES Orig.). However, appropriate values were implemented in UKCA as described in the following Section 2.2.5.2.

Overall, the non-stomatal deposition approach adopted in WES scheme is a simplification of the scheme suggested by Wesely (1989), who specified 11 vegetation types, because UKCA only uses five. Therefore, the seasonal variations of O_3 non-stomatal deposition are not fully implemented in the WES scheme.

2.2.4.4 Stomatal Resistance for O_3

The bulk stomatal conductance for water vapour is simulated by the land surface model MOSES 2.2. This approach is based on a simple relationship between leaf photosynthesis (A_l) and the stomatal conductance to water vapour, since CO_2 diffuses through stomata before being fixed by photosynthesis (Cox et al., 1999).

The following equation, derived by Cox et al. (1998) and based on the approach developed by Collatz et al. (1991,1992) for C3 and C4 grass respectively, describes the relation between the stomatal conductance to water vapour at the leaf level g_l (m s^{-1}) to the net leaf photosynthesis rate A_l (mol CO_2 m^{-2} s^{-1}) :

$$A_l = \frac{g_l}{1.6\,RT_l}(C_{CO2_l} - C_{CO2\,i}) \quad (2.9)$$

where T_l is the leaf surface temperature (K), R is the universal gas constant (J/mol/K) and C_{CO2_i} and C_{CO2_l} are the internal and leaf surface CO_2 partial pressure (Pa) and 1.6 accounts for the different diffusivity of CO_2 to H_2O. The internal CO_2 pressure calculation is based on the approach developed by Jacob (1994), as follows:

$$C_{CO2\,_i} = F_0\left(1 - \frac{D_l}{D_c}\right)(C_{CO2\,_l} - \gamma_{cp}) + \gamma_{cp} \quad (2.10)$$

where γ_{cp} is photosynthesis compensation point (when CO_2 internal pressure balances phototranspiration), D_l is the leaf surface humidity deficit and F_0/D_c are specific vegetation type calibration parameters (Cox et al., 1999).

Secondly, another key relation is the dependence of leaf photosynthesis on soil moisture which was introduced by Cox et al. (1999) in MOSES 2.2 as follows:

$$A_l = A_p\,\beta \quad (2.11)$$

where A_p is the non-moisture stressed net photosynthesis rate (calculated by subtracting the rate of dark respiration from the gross primary photosynthesis rate), and β is a factor between 0 and 1 that accounts for the moisture availability in the root zone. The empirical factor β is derived as follows (Cox et al., 1999; Best et al., 2011):

$$\beta(\theta) = \begin{cases} 1 & \theta_s > \theta_c \\ \dfrac{\theta_s - \theta_w}{\theta_c - \theta_w} & \theta_w < \theta_s < \theta_c \\ 0 & \theta_s \le \theta_w \end{cases} \quad (2.12)$$

where θ_s is the modelled volumetric soil moisture concentration within the top soil layer whereas θ_c and θ_w are the volumetric soil moisture concentrations at critical and wilting points respectively. θ_c and θ_w vary with the three soil textures (fine, medium, coarse) currently included in MOSES 2.2 (Cox et. al., 1999).

Equations 2.9 and 2.11 are a coupled model of leaf stomatal conductance and net leaf photosynthesis rate, and the leaf stomatal conductance for water vapour (g_l^{wv}) can be derived as follows:

$$g_l^{wv} = 1.6\,RT_l \frac{A_p \beta}{(C_{CO2\,l} - C_{CO2\,i})} \quad \textbf{(2.13)}$$

Assuming that the leaf-level photosynthetic capacity varies proportionally with the vertical distribution of irradiance, the canopy photosynthesis can be calculated integrating the leaf-level photosynthesis up to the canopy level (Cox et al., 1999; Best et al., 2011; Clark et al., 2011). Then, the bulk canopy stomatal conductance for water vapour for each plant type is derived as follows:

$$g_c^{wv} = g_l^{wv} f_{PAR} \quad \textbf{(2.14)}$$

where f_{PAR} is given by:

$$f_{PAR} = \frac{1 - e^{-0.5\,LAI}}{0.5} \quad \textbf{(2.15)}$$

0.5 is the photosynthetic active radiation (*PAR*) coefficient and *LAI* is the leaf area index of the plant type respectively. Finally, the canopy stomatal resistance R_s for O_3, NO_2 and PAN is then calculated:

$$R_s = \frac{\sigma}{g_c^{wv}} \quad \textbf{(2.16)}$$

where σ are diffusion correction factors (square roots of the ratios of the molecular weights of O_3, NO_2 and (PAN, MPAN, PPAN) to water (1.6, 1.6, and 2.6 respectively) accounting for the different diffusivities of these gases to water (Massmann et al., 1998).

2.2.5 O_3 dry deposition loss rate and flux in UKCA

For every chemical time step (1 hour), in each grid box a mean dry deposition velocity is calculated for each dry depositing species as follows:

$$V_d = \frac{1}{R_a (+ R_b + R_c} \quad \textbf{(2.17)}$$

In the real world, deposition occurs only at the surface and turbulence mixes air downwards, constantly replenishing near surface concentrations. However, because turbulent is fast compared with the model (dynamical) time step (30 min), deposition from multiple levels needs to be included to represent this simultaneous mixing and deposition (otherwise the lowest level is likely to become unrealistically depleted). Accordingly, in UKCA dry deposition is not only applied to the bottom level, but also from higher boundary layer levels (Sanderson et al. 2007; O'Connor et al., 2014).

For O_3 as well as the other species, each model layer within the boundary layer contributes to form the total dry deposition flux (F_d) which is calculated as follows:

$$\boldsymbol{F_d = \chi_d \sum_i C_{g_i} \Omega_i} \quad \textbf{(2.18)}$$

where χ_d is the grid dry deposition loss rate (s^{-1}) of the dry deposited gas as output by the model for each grid box, C_g is the gas concentration and Ω is the volume of the grid box, both at each level i respectively. The grid dry deposition loss rate χ_d is:

$$\boldsymbol{\chi_d = -\frac{1}{\tau_m} \log\left[1 - \sum_j \Gamma_{g_j} e^{-\frac{(V_d)_j \tau_m}{h_{BL}}}\right]} \quad \textbf{(2.19)}$$

where Γ_g are the fractions of the 9 surface type j within each grid-box, τ_m the UKCA time step and h_{BL} is the height of the highest model level contained within the boundary layer.

2.2.6 Revising the UKCA dry deposition scheme

2.2.6.1 Changes to stomatal conductance

The current version 7.3 of UKCA (referred to here as WES Orig.) was found to be using incorrect values for stomatal conductance of water vapour (Figure 2.2a). The stomatal conductance for H_2O passed into UKCA from MOSES 2.2 used to calculate the stomatal conductance for O_3 (and oxidised nitrogen compounds or NO_y) included an extra term for evaporation from bare soil, representing a water flux from the surface which does not pass through the stomata.

Figure 2.2a-b show the diurnal variations of modelled canopy stomatal conductance for C3 grass over four seasons for the grid-square over southern Scotland, for the original scheme and the corrected version.

It is clear from Figure 2.2a that in WES Orig. stomatal conductances do not approach zero at night, and reached unrealistically high values especially in winter. The corrected scheme (referred to here as WES), shown in Figure 2.2b, now makes physical sense (Coyle et al. 2009, Fowler et al. 2001).

2.2.6.2 Changes to in-canopy aerodynamic resistance

A second problem identified with WES Orig. was that the in-canopy aerodynamic resistance term R_{ac} was missing for some of the chemical species dry deposited. R_{ac} depends of the specific surface type and is characterized by seasonal geographical variations due to the influence of canopy height and density (Massman et al., 2004). However, WES Orig. scheme represents a simplification of the scheme suggested by Wesely (1989), who specified 11 vegetation types, because UKCA only uses five. Therefore, the seasonal variations of O_3 deposition, associated with geographic changes of the vegetation properties, cannot be considered fully implemented in the UKCA deposition scheme. Consistently with this simplified approach, annual mean R_{ac} values were inferred averaging the seasonal values reported in Wesely (1989). An extra lookup table, containing mean annual R_{ac} values for each of the 5 vegetation types, has been implemented in the model (WES scheme) as presented in Table 2.2.

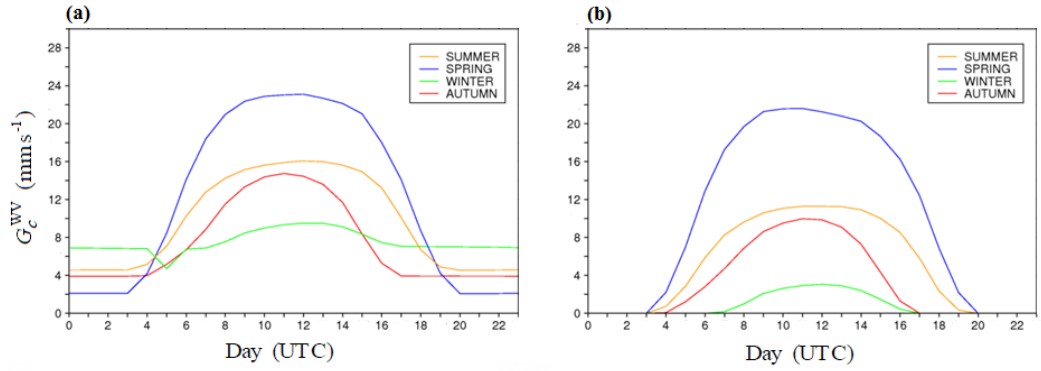

Figure 2.2. (a) shows the seasonal cycle of canopy stomatal conductance for water vapour G_c^{WV} (mm s^{-1}) used in the current UKCA dry deposition scheme (WES Orig.) as output for C3 grass for the model grid centred in the S. Scotland (55N 3.75W). (b) shows the corrected G_c^{WV} used in the revised UKCA dry deposition scheme (WES).

2.2.7 Zhang dry deposition scheme

An alternative dry deposition scheme (hereafter referred as the ZHG scheme), as described in Zhang et al. (2002a, 2002b, 2003), has been incorporated in UKCA with the aim to simulate dry deposition using a similar resistance analogy approach as in the WES scheme, but with a more complex representation of how the non-stomatal resistance terms interact with meteorology. In the WES scheme, non-stomatal O_3 deposition is calculated by assigning constant (annual mean) resistance values only dependent on surface type to R_{ac} and R_{soil} (Table 2.2) and values dependent on monthly mean leaf area indices to the cuticle resistance R_{cut} (equation 2.7). By contrast, in the ZHG scheme which is presented in Figure 2.1b, non-stomatal parameterizations take into account several meteorological factors such as relative humidity, friction velocity, canopy wetness, and biological parameters including canopy type as well as LAI (Zhang et al., 2003). Although the non-stomatal approach adopted with the ZHG scheme is not fully mechanistic (Zhang et al., 2003; Altimir et al., 2006), it is more realistic than the WES scheme (Wen et al., 2014). In the ZHG scheme, deposition rates increase when the canopy surface is wet (Coyle et al. 2009,

Altimir et al. 2006, Zhang et al. 2002b).

The original Zhang et al. (2003) dry deposition scheme was formulated for 26 land-use categories (covering 18 vegetation types). Here, this approach has been simplified, using the five vegetation types available in UKCA (Table 2.3).

Table 2.3. Lookup table values used by UKCA to calculate soil resistance R_{soil}, in-canopy in-canopy aerodynamic (R_{ac0}) and cuticular resistances in dry (C_{d0}) and wet (C_{w0}) conditions in the ZHG dry deposition scheme.

Surface type	R_{soil} (s m^{-1})	R_{ac0}	C_{d0}	C_{w0}
Broadleaf tree	200	250	6000	400
Needleleaf tree	200	100	4000	200
C3 grass	200	20	4000	200
C4 grass	200	25	4000	200
Shrub	400	40	5000	300
Urban	800	0	0	0
Water	2200	0	na	na
Bare soil	800	0	na	na
Ice	2500	0	na	na

As with the implementation of the WES scheme, the ZHG scheme is combined with the canopy stomatal resistance for O_3 (equation 2.16) simulated by MOSES 2.2 land surface model.

Several studies have shown that wetted surfaces inhibit O_3 stomatal uptake, due to presence of a liquid layer on the leaves that blocks stomata, compared to dry surfaces (Erisman et al., 1994; Brook et al., 1999; Zhang et al., 2002b; Altimir et al., 2006; Coyle et al., 2009). In the ZHG scheme, the effect of blocking of the plant stomata is simulated following the empirical approach suggested by Zhang et al. (2003). The stomatal conductance computed by MOSES 2.2 is reduced when the canopy conditions are considered wet, which may occur after rain or dew events as better described in the following section.

2.2.7.1 Implementing the ZHG scheme in UKCA

R_a and R_b are determined by the model as done in the WES scheme (equations 2.2 and 2.5). The canopy resistance R_c is modelled in the ZHG scheme as follows:

$$\frac{1}{R_c} = \frac{1 - W_{bk}}{R_s} + \frac{1}{R_{ns}} \qquad \textbf{(2.20)}$$

where W_{bk} is the fraction of stomata blocked by a thin water film under wet conditions. The fraction of stomatal blocking is simulated by first working out whether the canopy is wet or dry (Brooks et al., 1999). The canopy water content in fraction of area (η_c), between 0 and 1 and is dimensionless, and the grid average relative humidity (*RH)* in % , simulated by the MOSES 2.2, are used by the model to discriminate between wet or dry conditions within the canopy. The former is calculated as follows:

$$\eta_c = \frac{\Psi_w}{\mu_c} \qquad (2.21)$$

where Ψ_w is the average canopy water content (kg m^{-2}) simulated by MOSES 2.2 for each surface type within the model grid and μ_c is capacity of the canopy to hold water (kg m^{-2}) through the interception of rainfall (equation 2.1).

In the model, the canopy is considered dry when $\eta_c \leq 0.1$ and for $RH \leq 80\%$ and R_s remains unchanged. Otherwise, the canopy is considered wet and W_{bk} is estimated as follows (Zhang et al., 2003):

$$W_{bk} = \begin{cases} 0, & I_s \leq 200\ W\,m^{-2} \\ (I_s - 200)/800, & 200 < I_s \leq 600\ W\,m^{-2} \\ 0.5, & I_s > 600\ W\,m^{-2} \end{cases} \qquad (2.22)$$

According to experimental evidence, during most rain conditions the solar radiation is weak ($I_s \leq 200$ W m^{-2}) and W_{bk} is set to 0 because O_3 stomatal uptake is reduced due to closing stomata (Zhang et al., 2002b). However, when clear sky conditions occur immediately after morning dew or rainfall events, a water films can form on the leaves inhibiting O_3 stomatal uptake, when the stomatal resistance is small owing to the solar radiation that becomes sufficiently strong ($I_s > 200$ W m^{-2}) (Zhang et al. 2002b, Brook et al. 1999, Janssen and Romer, 1991). This effect is taken into account by the W_{bk} term with values between 0 and 0.5, effectively enhancing the stomatal and the canopy resistance (eq. 2.20) (Brook et al. 1999; Zhang et al. 2003). The upper limit of W_{bk} was based on experimental evidence (Zhang et al., 2003) indicating that this value was more sensible compared to previous estimations which were too large

(Zhang et al., 2002a).

Secondly, the model determines the cuticular resistance in wet or dry conditions for each vegetation type through the following parameterizations, which were based on empirical fits to the data as reported in Zhang et al. (2002b):

$$R_{cut\_dry} = \frac{C_{do}}{e^{0.03\,RH}\,(LAI)^{1/4}\,u_*}$$
$$R_{cut\_wet} = \frac{C_{wo}}{(LAI)^{1/2}\,u_*} \quad \textbf{(2.22)}$$

where the dimensionless constants C_{d0} and C_{w0} are the result of statistical analysis and are specific values assigned by the model (Zhang et al., 2003) to each vegetation type (as reported in Table 2.3). In particular, the C_{d0} and C_{w0} indicated in Table 2.3 correspond to the lookup table values reported in Zhang et al. (2003) for evergreen broad-leaf tree and need-leaf tree, short crass and forbs, long grass and evergreen broadleaf shrubs.

Finally, the in-canopy aerodynamic resistance R_{ac} is computed as:

$$R_{ac} = \frac{R_{ac0}}{u_*^2}(LAI)^{1/4} \quad \textbf{(2.23)}$$

where R_{ac0} are reference values assigned by the model to each vegetation type according to Zhang et al. (2003) and reported in Table 2.3.

2.3 Results

2.3.1 Combined effects of all model amendments to the WES scheme on O_3 fields

Figures 2.3a, 2.3b and 2.3c show the annual mean global distributions of surface ozone, ozone dry deposition velocity and ozone dry deposition flux as simulated by UKCA using the WES scheme, which includes the revisions of the stomatal conductance (described in Section 2.2.6.1) and the in-canopy aerodynamic resistance

(Sec. 2.2.6.2). Figures 2.4a-2.4b-2.4c present the combined impacts of the model corrections, compared to the original scheme (WES Orig.).

These corrections produced significant changes. Decreased O_3 stomatal uptake and increased non-stomatal resistance reduced O_3 dry deposition velocity over land, particularly over Eurasia, N. America and Central Africa with values reduced by as much as -50% (Figure 2.4b). This is consistent with a decrease of O_3 dry deposition flux over land up to -30%. Reduced O_3 deposition over land led to a greater export of O_3 especially to the Arctic (Figure 2.4a); the increase of surface O_3 over the Arctic led to an increase in O_3 dry deposition over the same area.

As a consequence of all the changes, the model deposits less over land and there is an increase in intercontinental O_3 transport from Asia and N. America to the Arctic.

Moreover, the annual global O_3 dry deposition reduced by -150 $Tg(O_3)$ yr^{-1} (-13%) Due to a reduced surface ozone sink there was a small increase of the O_3 life time (0.7 days; +3.4 %). The model corrections also affected oxidised nitrogen species, with similar percentage reductions in V_d as those found for O_3.

2.3.2 Assessing the impacts of the change of dry deposition scheme on modelled O_3

2.3.2.1 Impact on global O_3

As presented in Figures 2.5a-b-c, the change from the WES to the ZHG scheme produced significant effects on the annual mean global distributions of surface O_3, O_3 V_d and O_3 dry deposition flux. Figure 2.5b shows that the ZHG scheme led to a considerable increase of O_3 V_d in the NH across Eurasia and N. America of as much as +40%. This is reflected in a decrease of O_3 flux of up to -20% over the same areas and to an increase of as much as +20% over tropical regions and E. Asia (Figure 2.5c). The change of dry deposition scheme produced important changes to surface O_3 concentrations, with a decrease of up to -20% over most land surfaces in the NH and an increase of up +20% over tropical areas and E. Asia (Figure 2.5a).

In addition, the ZHG scheme led to an increase of O_3 deposition over the oceans in the SH and a decrease in the NH which reflected changes of O_3 concentrations. However, as shown in Figure 2.5b, O_3 V_d over water surfaces did not exhibit any

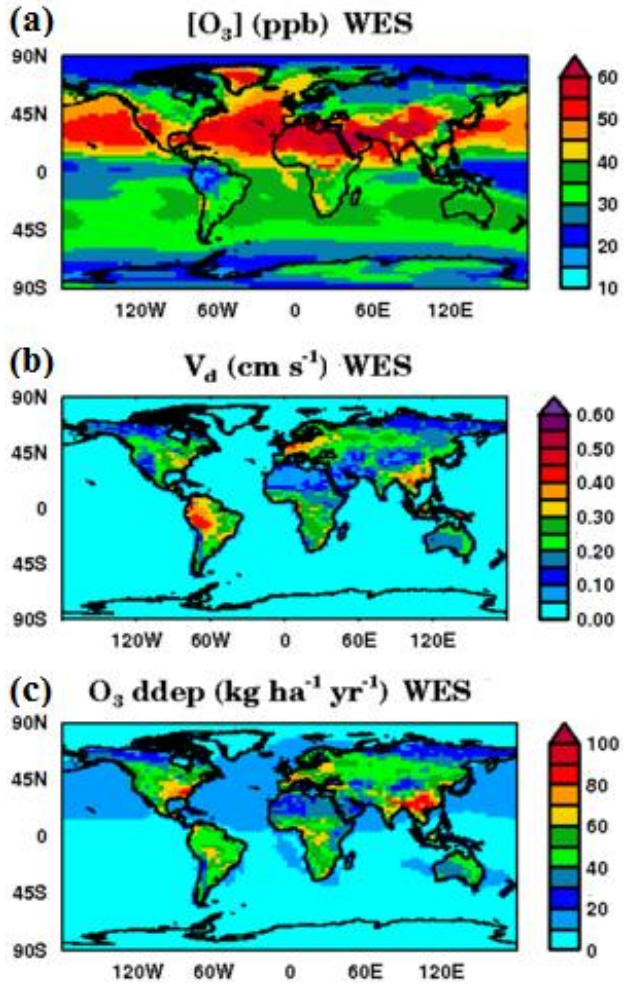

Figure 2.3. Annual average of surface O_3 concentration (ppb) (**a)**, annual average of grid O_3 dry deposition velocity V_d (cm s-1) (**b**), total annual O_3 dry deposition (kg ha^{-1} yr^{-1}) (**c)** as simulted by the UKCA for a non-nudged simulation for 2000 using the dry deposition scheme which include all the model corrections (WES scheme).

significant change as the ZHG parameterizations were only applied to the vegetation surfaces. Figure 2.6 also shows that the change of scheme leads to a hemispheric difference of O_3 concentration throughout the troposphere. In particular, ZHG exhibits larger surface O_3 (up to 16%) than WES over the lower tropical troposphere whereas more uniform and smaller changes (up to -4%) are simulated throughout the mid-latitude NH compared to WES. By contrast, ZHG leads to an increase in O_3 (up to 10%) in the Arctic lower troposphere.

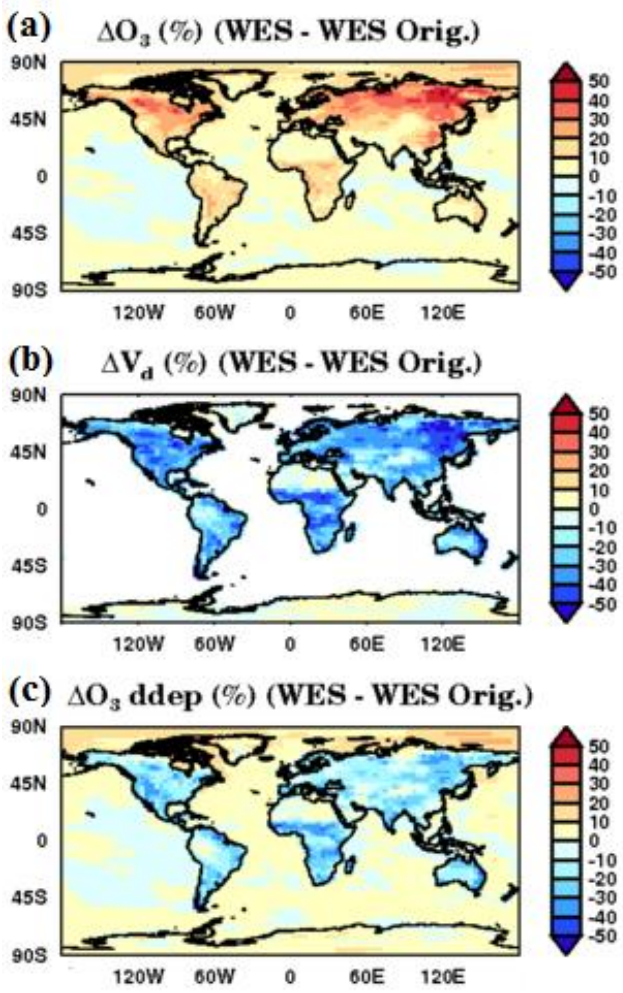

Figure 2.4. (**a)-(b)-(c)** show the differences in (%) between modelled surface O_3, grid O_3 V_d and O_3 dry deposition using the revised scheme (WES scheme) and the existing one (WES Orig.) respectively.

2.3.2.2 Effects on O_3 dry deposition velocity

The effect of the change from WES to ZHG dry deposition scheme on modelled O_3 was further assessed. This was done by investigating how regional differences in simulated V_d for broadleaf and needle-leaf trees as well as C3 grass (Figure 2.7) contribute to variations of the annual average grid V_d at the global scale (Figure 2.8). In Figure 2.7 only the V_d simulated for grid-squares containing more than 5% of

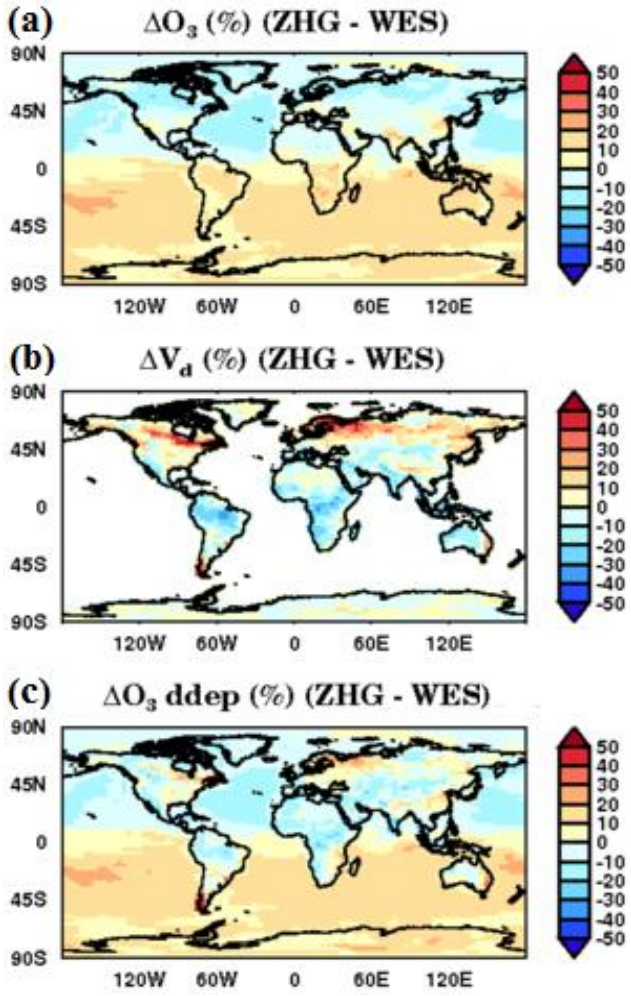

Figure 2.5. Differences (in %) between modelled annual mean surface O_3 (**a**), grid O_3 V_d (**b**) and total annual O_3 dry deposition (**c**) simulated using the ZHG scheme and WES scheme respectively.

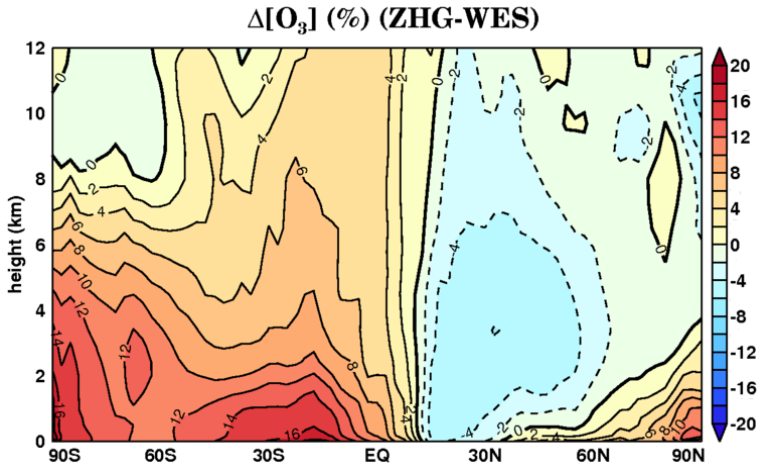

Figure 2.6. Zonal annual mean difference (%) between tropospheric O_3 rations simulated with ZHG and WES schemes.

broadleaf (a-b) and needle-leaf trees (d-e) as well as grids with more the 20% of C3 grass (g-h) were presented. By contrast, the grid V_d simulated with both the schemes, which are made of weighted fractions of V_d for each vegetation type in the grid square (as explained of Section 2.2.4), were introduced in Figures 2.8a-b.

Simulated grid V_d values over the oceans were masked as they were very small with WES and ZHG. In addition, ZHG did not lead to any significant change of V_d over the oceans compared to WES, so the differences between the two schemes were not shown. Figure 2.7c-f-i show that the ZHG scheme leads to considerable differences in simulated O_3 V_d for each vegetation type compared to WES. Deposition velocities for O_3 simulated using the ZHG scheme show a larger variability across North America, Europe and Eurasia than WES.

The most significant differences of V_d are simulated for needle leaf trees over the northern hemisphere (NH) boreal forests (up to +60%) (Figure 2.7f) and over C3 grass across the NH with differences as much as +40% (Figure 2.7i).

By contrast, ZHG led to more regionally varying changes in V_d for broad-leaf forests (BL) than WES (Figure 2.7c). In particular, V_d increases over BL (up to +30%) in the NH at mid-high latitudes whereas decreases of up to -25% over tropical forested regions were simulated. Overall, Figure 2.8c shows that as a result of the change from WES to ZHG, O_3 V_d increases as much as +30% over vegetated areas in the NH whereas a considerable reduction is found over tropical forested regions (by up to -30%).

2.3.2.3 Changes in stomatal and non-stomatal deposition

The differences in V_d simulated by using the ZHG and the WES schemes in UKCA can be explained taking into account the changes in the O_3 stomatal (G_s) and non-stomatal (G_{ns}) conductance terms predicted by the model as a result of change of dry deposition scheme. Figures 2.9c-f-i reveals that the ZHG scheme, as a response to occurrence of wet canopy conditions, leads to a decrease of the O_3 stomatal conductance by up to -15% over areas in Europe and N. America mainly covered by C3 grass (Figure 2.9i) and more significantly over tropical forests as much as of -30% (Figure 2.9c).

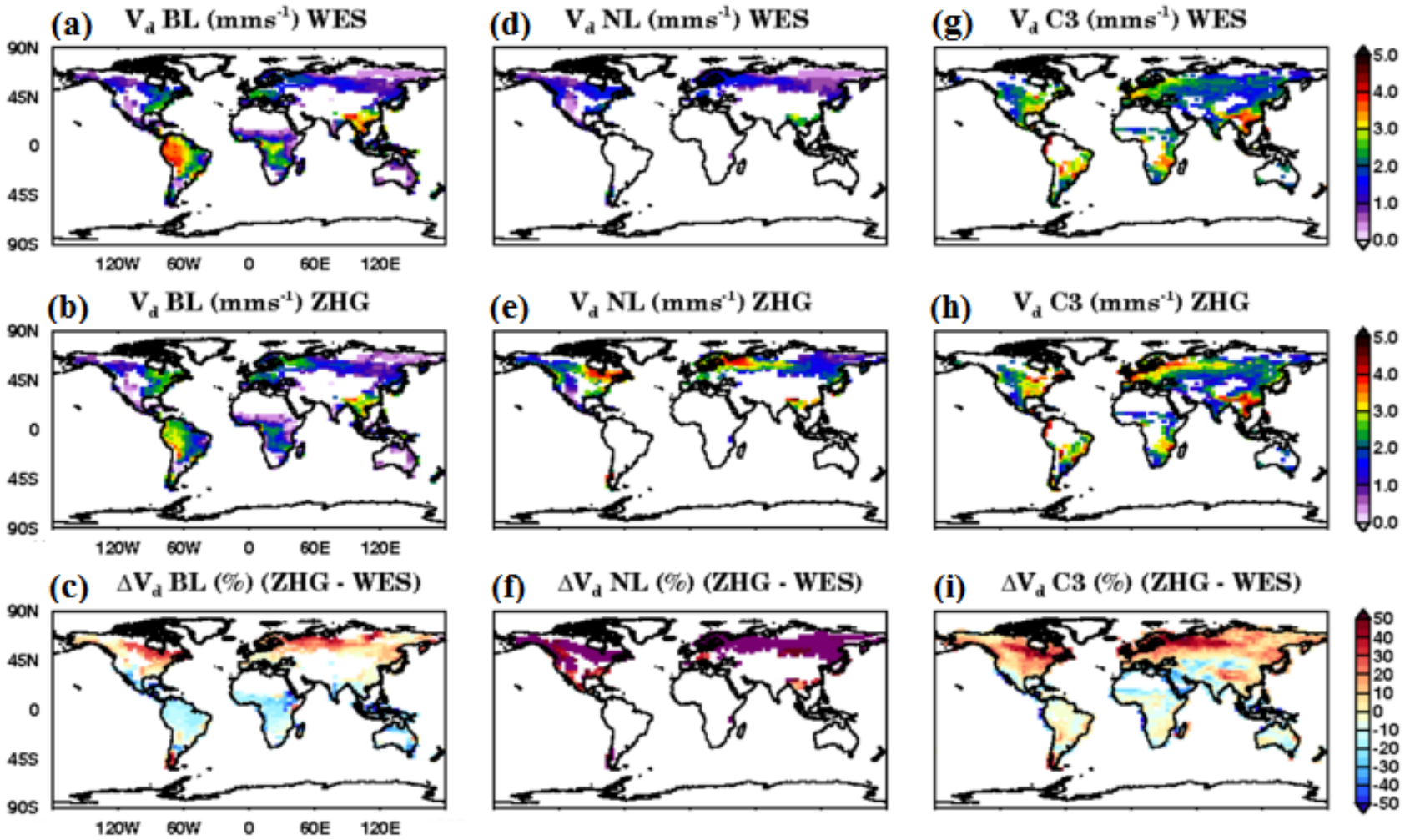

Figure 2.7. (**a)-(d)-(g)** show the global annual mean of V_d for broad-leaf (BL) and needle-leaf (NL) trees and C3 grass respectively as simulated in a nudged configuration with the WES scheme. Figures **(b)-(e)-(h)** show the modelled V_d for the same vegetation types using the ZHG scheme **(c)-(f)-(i)** present the relative differences (in %) in V_d as a result of the change from WES to ZHG scheme. Only V_d values for grids with fractions of BL-NL ≥ 5 % and C3 ≥ 20% are shown. Grid V_d values over the oceans were masked.

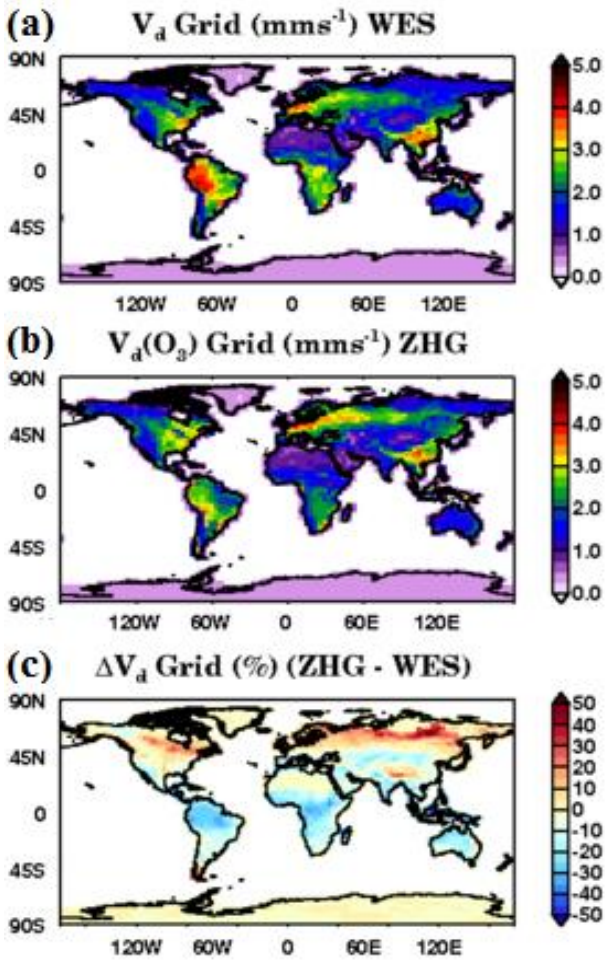

Figure 2.8. (a)-(**b**) show the annual mean grid O_3 V_d (mms^{-1}) simulated using WES and ZHG schemes respectively. (**c**) presents the difference (in %) in O_3 V_d as a result of the change of scheme from WES to ZHG scheme,

The ZHG scheme led to considerable increases of G_{ns} (by up to -70%) over the NH coniferous forests compared to WES (Figure 2.10f). By contrast, G_{ns} simulated with ZHG for BL forest and C3 grass appear more regionally varying than WES. Increases in G_{ns} as much as of + 40% for BL trees are simulated with ZHG in the NH at mid-high latitudes whereas decreases (up to -40%) were found over tropical regions (Figure 2.10c). Interestingly, ZHG led to larger G_{ns} over regions covered by C3 grass across the NH, with increases by up to +50% over Eurasia and E. Asia.

2.3.2.4 Impact on the O_3 dry deposition flux partitioning

Figure 2.11 presents how the fraction of the O_3 non-stomatal deposition to the total O_3 flux over vegetated surfaces varied as a result of the change of dry deposition scheme. Overall, the ratio G_{ns}/G_c increased with ZHG especially over boreal coniferous forests and for C3 grass across the NH, with latitudinal gradients (Figure 2.11f-i). The model shows less uniform changes of G_{ns}/G_c for BL trees with regional differences in the NH (Figure 2.11c). This means that the ZHG scheme led to an increase of the non-stomatal deposition for high latitude regions in the NH and to a more uniform reduction of G_{ns}/G_c indicating an increase in the stomatal deposition.

2.4 Discussion

2.4.1 Interpreting the effects of the deposition corrections on model outputs

The current UKCA dry deposition scheme has been revised correcting errors in earlier versions and to update the partitioning of surface O_3 flux according to the current understanding of the processes (Fowler et al., 2001; Zhang et al., 2002b, 2003; Coyle et al., 2009). A model analysis was designed to assess the impact of the model amendments on O_3, allowing exploration of the sensitivity of surface O_3 to changes in canopy uptake. With the corrected dry deposition scheme (WES), the model shows larger surface O_3 concentrations in the NH than in SH (Figure 2.4a). Although other factors contribute to high O_3 concentrations in the NH such as the enhanced industrial O_3 precursor emissions (Cooper et al., 2014; Monks et al., 2015), this is consistent with less O_3 dry deposited especially over those areas in the NH and in the Tropics covered by vegetation (Figure 2.4c).

Both the model corrections led to a significant decrease of O_3 V_d globally and in particular in the NH (Figure 2.4b). Of the two scheme amendments, the addition of the in-canopy aerodynamic resistance R_{ac} is the dominant one and leads to a considerable decrease of V_d (up to -0.20 cm s^{-1}) especially over boreal and tropical regions. In contrast, the effect of the correction to the canopy stomatal conductance (G_s) on surface

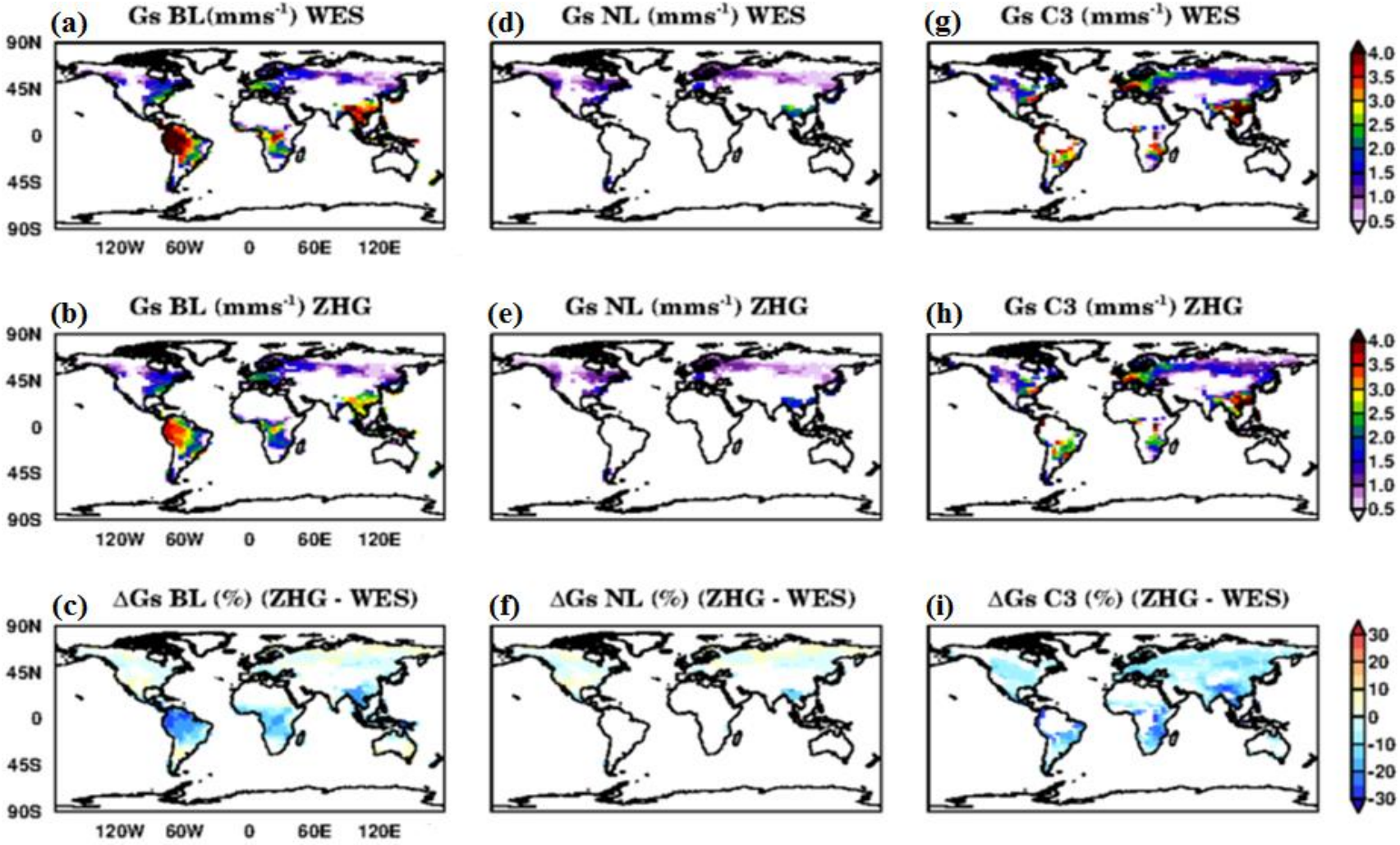

Figure 2.9. (a)-(d)-(g) show the annual mean stomatal conductance for O_3 (G_S) as simulated with WES scheme for BL-NL trees and C3 grass. **(b)-(e)-(h)** show G_S simulated with ZHG scheme for the same vegetation type. **(c)-(f)-(i)** present the annual mean relative difference (in %) between G_S simulated with ZHG compared to WES. Only G_S values for grids with fractions of BL-NL ≥ 5 % and C3 ≥ 20% are shown.

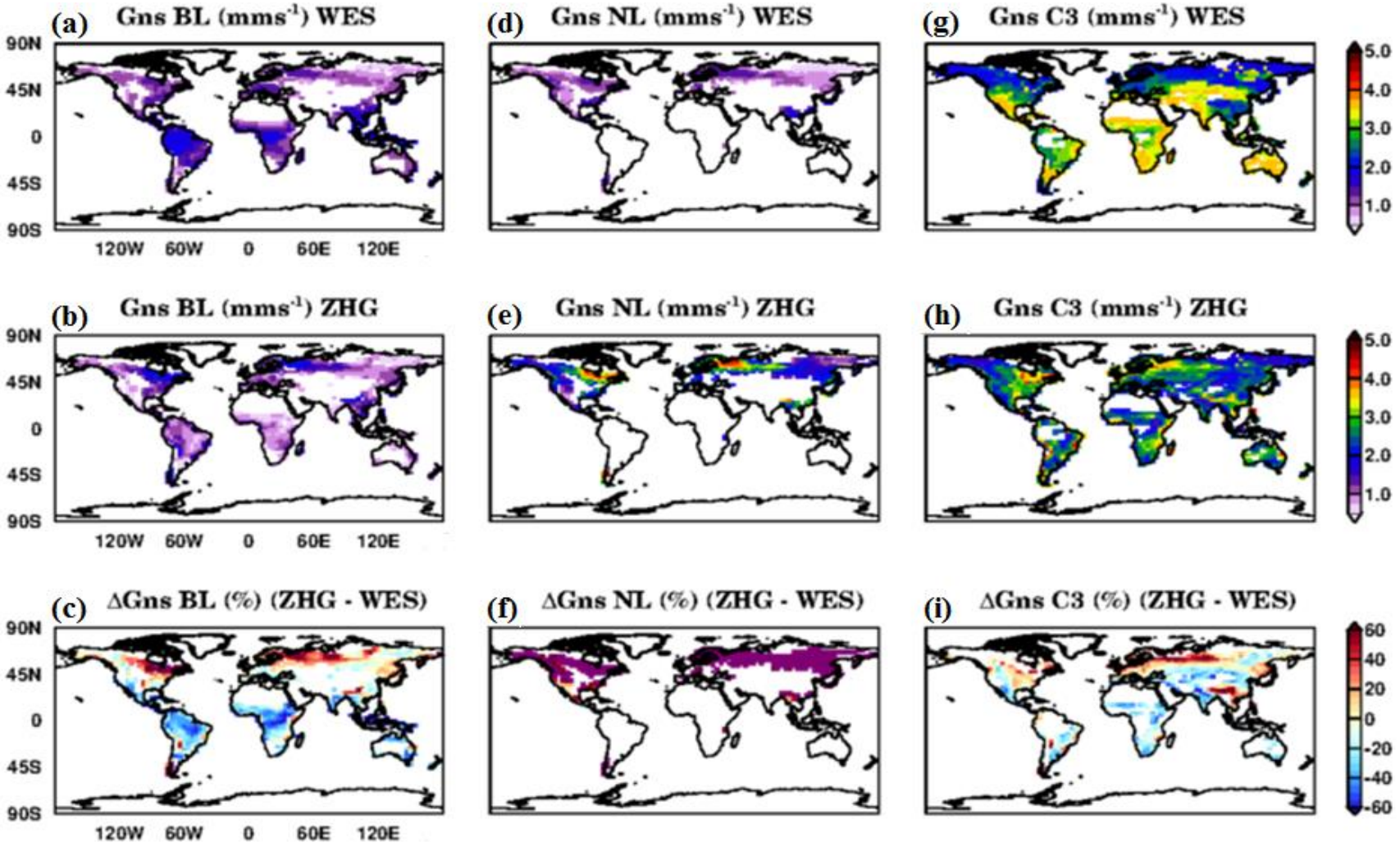

Figure 2.10. (a)-(d)-(g) show the annual mean non-stomatal conductance for O_3 (G_{ns}) as simulated with WES scheme for BL-NL trees and C3 grass. **(b)-(e)-(h)** show G_{ns} simulated with ZHG scheme for the same vegetation types. **(d)-(f)-(i)** present the annual mean relative difference (in %) between G_{ns} simulated with ZHG compared to WES. Only G_{ns} values for grids with fractions of BL-NL ≥ 5 % and C3 ≥ 20% are shown.

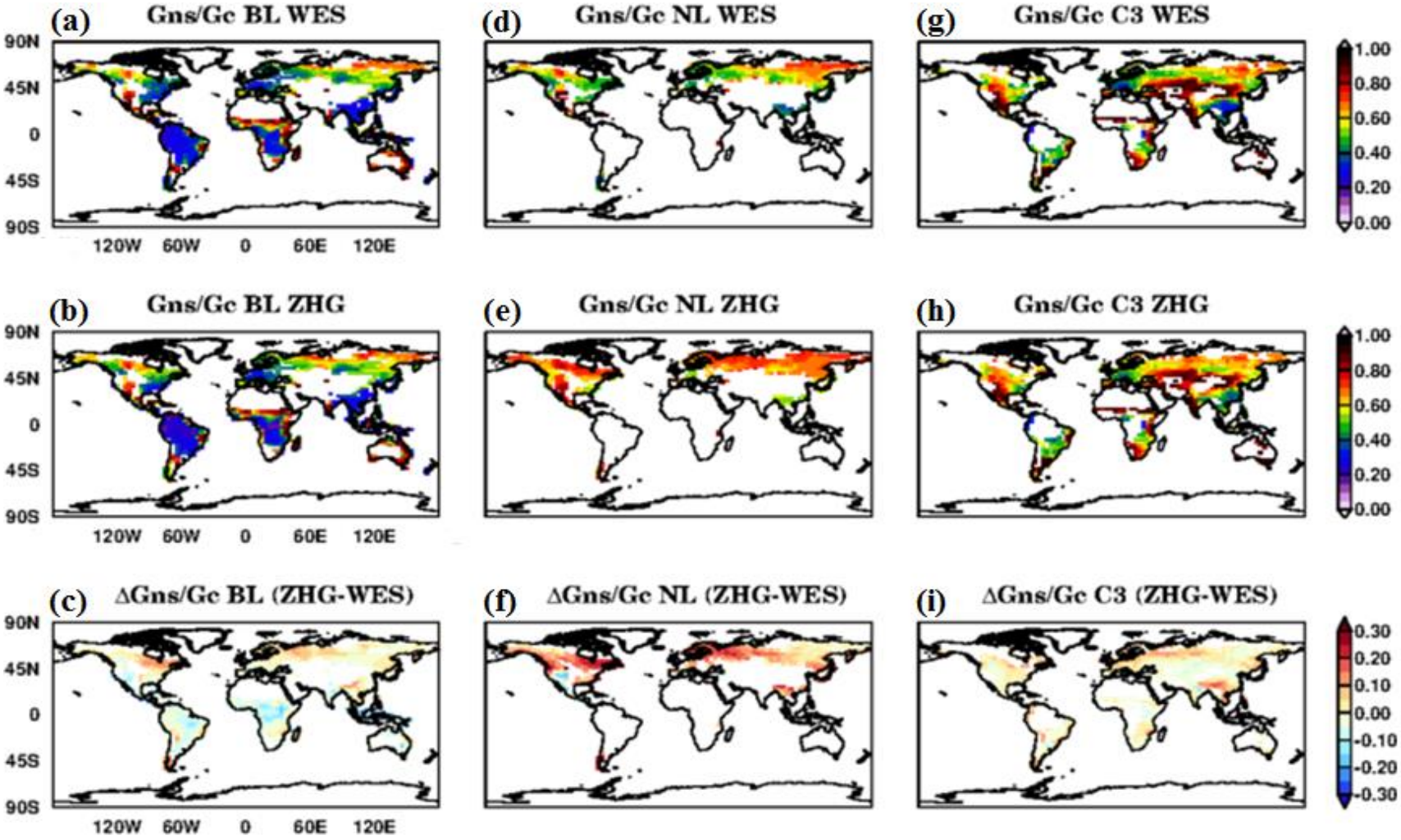

Figure 2.11. (a)-(d)-(g) show the annual mean ratio (G_{ns}/G_c) between non-stomatal conductance G_{ns} and the total canopy conductance G_c (= G_s+G_{ns}) simulated by UKCA using WES for BL-NL trees and C3 grass. **(b)-(e)-(h)** show the ratio G_{ns}/G_c modelled with ZHG for the same vegetation types. **(c)-(f)-(i)** present the absolute differences between G_{ns}/G_c simulated with ZHG and WES. Only G_{ns}/G_c values for grids with fractions of BL-NL ≥ 5 % and C3 ≥ 20% are presented.

O_3 was generally smaller but was significant over those areas dominated by C3 grass (up to +4 ppb across parts of Eurasia and N. America) as a consequence of a decreased V_d and a smaller O_3 deposition flux. This is due to the removal of the soil evaporation contribution from the bulk canopy stomatal conductance for water vapour, which was proportionally larger for short canopies compared to forests as the fraction of bare soil contributing to the evaporation term is scaled by the density of leaves (Best et al., 2011). In addition, the relative change of G_s was largest during night time and in winter when surface O_3 concentrations are relatively small, whilst the addition of R_{ac} decreased the deposition at all the times.

As a result of all the model amendments, a smaller total annual O_3 deposition (996 Tg yr^{-1}) was found. This corresponds to -13% reduction of the total annual O_3 deposition compared to the original UKCA dry deposition scheme (1146 Tg yr^{-1}). The revised value brings UKCA more in line with ACCENT (Atmospheric Composition Change: the European Network of excellence; Stevenson et al., 2006) estimate (all models mean ± standard deviation, 1003 ± 200 Tg yr^{-1}) and ACCMIP (Atmospheric Chemistry and Climate Model Inter-comparison Project; Young et al., 2013) estimate (all models mean, 937 Tg yr^{-1}).

Annual mean surface O_3 and its spatial distribution simulated using the corrected model version (WES scheme) showed similar values to O'Connor et al. (2014). This study reported that HadGEM2-UKCA compares well with both the ACCENT ensemble mean (sits within ± standard deviation) in most altitudes and regions and performs well in simulating the amplitude of the seasonal cycle and the absolute concentrations. O'Connor et al. (2014) noted a low bias in surface O_3 in the NH at mid-latitude regions. In particular, at Northern high latitudes (Barrow 71°N 157°W) although UKCA reproduces the summertime concentrations well, it fails to capture the autumn-winter maximum which is underestimated by 50% (O'Connor et al., 2014). Some potential causes of these discrepancies are discussed in that study. However, among these causes, potential shortcomings in the dry deposition approach within the model are not considered.

This study showed that using WES scheme, surface O_3 mixing ratios increased considerably (by up to 10 ppb; +50%) over lands in the NH due to a drastic change of the O_3 deposition removal rate (up to -0.3 cms^{-1}; -40%) which led to a relevant

reduction of the total annual O_3 deposited over vegetated surfaces (up to -30%). Thus, these changes may have potential implications for O_3 modelling studies and should be considered in the future UKCA model versions.

The model corrections did not cause any significant change of V_d over the Arctic. However, UKCA exhibits an increase of surface O_3 (up to +6/7 ppb) over the Arctic suggesting that this change is mainly driven by more O_3 being transported from land, as a consequence of a reduced O_3 deposition (Figure 2.4c).

Finally, although we partitioned the impact of both the model amendments on surface O_3, NO_2 and PANs, the stomatal conductance and R_{ac} corrections were simultaneously applied to all these species. As a result of these changes, higher surface NO_x and PANs concentrations may promote O_3 production over the Arctic (Hirdman et al., 2010; Monks et al., 2015) and less NO_2-PAN dry deposited especially over rural areas in the NH may lead to further O_3 chemical loss (Wild, 2007; Royal Society, 2008). However, these effects were not isolated in this study. Further investigations of the impact of changes in NO_y deposition on O_3 are a priority in the future studies.

2.4.2 Impact of the ZHG scheme relative to the WES scheme on global O_3

Figure 2.5b shows that the ZHG scheme causes V_d increases over much of the high-latitude NH land, but V_d decreases in the tropics, and over most land in the SH. This leads to a hemispheric divergence in effects on O_3 concentrations, with decreases of ~10% across much of the NH, and similar magnitude increases across much of the SH. Figure 2.6 also reveals that this hemispheric difference in O_3 concentration exists throughout the troposphere, with the larger values simulated with ZHG over the lower tropical troposphere (up to +16%) compared to WES.

It is interesting to note that in an evaluation of 15 state-of-the-art global models within the ACCMIP project, Young et al. (2013) found that models have a systematic high bias of ~10/20% in the NH and a similar low bias in the SH for tropospheric column O_3.

This study represented the first attempt to explore the sensitivity of modelled global surface O_3 to an alternative non-stomatal deposition approach and to the effect of

blocking of stomata. Although the total annual O_3 dry deposited did not change considerably from WES scheme to ZHG (994 Tg yr^{-1}), the latter did lead to significant changes of the O_3 V_d over land.

The results of this study highlight that tropospheric and surface O_3 concentrations are sensitive to a more dynamic representation of non-stomatal O_3 deposition and to the effect of blocking of stomata.

2.4.3 Discussing non-stomatal O_3 deposition approaches

Analysis of measured ozone fluxes has shown that the fraction of O_3 deposition to vegetative surfaces occurring through stomatal pathways constitutes the predominant part of the total O_3 flux during the day and in the growing season (Cieslik, 2004; Altimir et al., 2006; Gerosa et al. 2003, 2004; Coyle et al., 2009), whilst the non-stomatal O_3 flux to leaf and other surfaces was the dominant term annually (Fowler et al. 2001; Mikkelsen et al., 2004; Coyle et al., 2006). Both surface sinks (stomatal and non-stomatal) are highly variable with time, depending on multiple biological and meteorological factors as well as chemical-physical processes taking place on the leaves both during dry and wet conditions (Fuentes et al., 1992; Fowler et al., 2001; Coyle et al., 2009; Fowler et al., 2009; Fares et al., 2010a). Surface temperature, surface wetness, solar radiation and wind all influence O_3 non-stomatal deposition (Coyle et al., 2009; Fowler et al., 2009). It is therefore unreasonable to assume a simplified non-stomatal deposition approach, as earlier models imply (Wesely, 1989). In the current UKCA model (with the WES scheme), the non-stomatal deposition component is represented only through deposition to leaf cuticles R_{cut} (taking into account a dependence on specific seasonal vegetation type LAI; Massman et al., 2004) and towards the surfaces underlying the vegetation canopies (explicitly assigning annual surface type dependent values to the in-canopy aerodynamic resistance R_{ac} then summed in series to specific surface type resistances R_{soil} (Wesely, 1989). Surface wetness leads to an increase of the soil resistance underlying the vegetation canopies (Massman et al., 2004) and this effect is taken into account in the UKCA model by simply assigning a constant value (500 s m^{-1}) to R_{soil} based on a discrimination between wet or dry surfaces that is worked out by the

model through a soil moisture content ratio threshold $\mathcal{E}_{sm}$ as described in Section 2.2.4.3.

In this study, Zhang et al. (2003) parameterizations were included in UKCA to provide a representation of the non-stomatal flux that is closer to the current understanding of the process and to explore the sensitivity of O_3 V_d and surface O_3 to a more climate sensitive O_3 non-stomatal deposition component. Zhang et al. (2003) cannot be considered a fully mechanistic approach (Altimir et al., 2006; Massman et al., 2004) as processes such as aqueous-phase chemistry and chemical-physical mechanisms occurring on the leaves are not included (Fuentes et al., 1992; Zhang et al., 2003; Fowler et. al., 2001; Coyle et al., 2009). A better understanding of how the partitioning between stomatal and non-stomatal fluxes may vary is also a fundamental requirement for O_3 risk assessment studies (Gerosa et al., 2003, 2004; Touvinen et al., 2009; Fares et al., 2010b; Emberson et al., 2013).

2.4.4 The effect of blocking of stomata

In this study, a simplified approach of the effect of blocking of leaf stomata has been implemented in UKCA model. This effect occurs owing to a thin film of water which may form on the leaves after rain or dew events and the canopy conditions become wet along with a strong solar irradiation (Zhang et al. 2002b, 2003). The model uses the canopy wetness (η_c,, eq. 2.21) simulated for each vegetation type and an average grid relative humidity as a proxy to work out the wetness conditions within the canopy.

In UKCA, this effect led to a decrease of the annual mean $G_s(O_3)$ by up to -15% over those areas in Europe and N. America mainly covered by C3 grass (Figure 2.9i) and more significantly over tropical (broadleaf) forests as much as of -30% (Figure 2.9c). The larger decrease of G_s over the Amazon forest and Central Africa as much as -25%, indicates a larger sensitivity of $R_s(O_3)$ to the more frequent wet canopy conditions simulated over tropical regions.

In summary, this analysis revealed that simulating stomatal blocking effect using the Zhang et al. (2003) approach can lead to an increase of the O_3 stomatal resistance especially over tropical areas. This is consistent with experimental studies indicating

that changing canopy wetness regimes can influence O_3 uptake by vegetation (Fuentes et al., 1994; Grantz et al., 1997; Altimir et al, 2006).

However, the stomatal blocking effect taken into account in this study cannot be considered fully represented in UKCA owing to: (i) the fraction of the canopy effectively covered by water is not resolved as this method only empirically assumes that the canopy is not usually completely covered by water (Brooks et al. 1999; Zhang et al. 2002b); (ii) the model does not take into account the variability in the stomatal distribution between the abaxial (upper) leaf surfaces and adaxial (lower) leaf surfaces, which is a specific property of the vegetation type (James et al. 1999). Therefore, more work is needed to improve the representation of the stomatal blocking effect in UKCA model.

2.4.5 Changes of the O_3 deposition flux partitioning

The results presented in this study have shown that the ZHG scheme leads to significant changes of the partitioning between modelled stomatal and non-stomatal O_3 flux. One of the most important features emerging from this study is that using the ZHG scheme the model shows that the ratio between stomatal and non-stomatal O_3 deposition varies with different environmental conditions (Fowler et al, 2009), especially over those areas covered by coniferous forests in the NH and over tropical broadleaf forests.

In particular, as shown in Figure 2.11, the ratio G_{ns}/G_c between non-stomatal conductance and the total canopy conductance increased considerably especially for needle leaf forests and C3 grass in the NH indicating that most of the O_3 flux simulated by UKCA using ZHG scheme now occurs via non-stomatal pathways (maxima values up 70% for NL tree and up to 60% for C3 grass) which is more in line with field measurements (Fowler et al., 2001; Gerosa et al., 2003, 2004; Mikkelsen et al., 2004; Altimir et al., 2006; Coyle et al., 2009; Fares et al., 2010a; Stella et al., 2011a). The model shows that G_{ns}/G_c for broad leaf forest varies more regionally, with increases simulated in the NH and decreases over tropical areas.

2.5 Conclusions

The main conclusions taken into consideration in this study can be summarized as follows:

- The assessment of the impact of the stomatal conductance G_s and the in-canopy aerodynamic resistance R_{ac} corrections applied to O_3 in the current UKCA dry deposition scheme revealed that as a result of both the changes the model shows a large increase of surface O_3 over land in the NH with values as much as 12 ppb (+50%) higher on annual average.
- Both the model amendments increased the canopy resistance globally leading to a substantial reduction in dry deposition rates for O_3. The R_{ac} amendment (seasonal annual mean values) led to a decrease of O_3 dry deposition velocity. The stomatal conductance change led to a smaller increase of O_3 dry deposition which turned out to be more evident over those areas mainly covered by grass where the stomatal uptake was more significant. As the model corrections were simultaneously applied to NO_2 and PANs, more work is needed to isolate the effect that changes of surface NO_x and PANs might have on O_3 production over Arctic regions and O_3 chemical loss over rural areas.
- The model corrections led to a reduction of the total annual dry deposition (-150 Tg(O_3) yr^{-1}; -13%) which brings UKCA more in line with ACCENT and ACCMIP estimates (Stevenson et al., 2006; Young et al., 2013).
- An alternative non-stomatal deposition scheme based on Zhang et al. (2003) along with effect of surface water on foliage blocking of leaf stomata, was implemented in UKCA. The implementation of the ZHG scheme in UKCA led to a significant impact on surface O_3 globally, with a decrease of as much as -20% over land at high-mid latitude continental regions and in increase by up to +20% over tropical regions and East-Asia on annual average. ZHG also leads to changes in O_3 concentrations throughout the troposphere compared to WES, with increases up to +16% over the tropics and to decreases (up to -4%) over mid-latitudes in the NH. This might represent a potential improvement of the hemispheric bias in modelled

O_3 compared to satellite observations (Young et al., 2013).

- The ZHG scheme did lead to significant changes of the O_3 V_d over lands, with an increase of as much as +40% and a decrease of up to -30% over tropical regions. The total annual O_3 dry deposited did not change from ZHG to WES scheme.
- In UKCA the stomatal blocking effect led to an increase of the O_3 stomatal resistance (by up to +30%) over tropical regions and to a moderate and spatially uniform increase in in the NH (up to +10%). This result is consistent with studies which have shown that changing canopy wetness regimes can influence O_3 uptake by vegetation (Fuentes et al., 1994; Grantz et al., 1997; Altimir et al., 2006). However, more work is needed to fully represent this effect in UKCA. Two factors were considered significant: (i) an effective simulation of the fraction of the vegetation canopies covered by water film. (ii) the calculation of the stomatal distribution between abaxial and adaxial leaf surfaces.
- This study also revealed that as a result of the implementation of the ZHG scheme, modelled O_3 V_d exhibits significant regional variations and latitudinal gradients especially in the NH, indicating a larger sensitivity of V_d to different local climate conditions. Large V_d differences were mainly driven by changes of the non-stomatal conductance terms both in space and in time.
- The results presented in this study showed that the ratio between stomatal and non-stomatal O_3 deposition fluxes varies with different environmental conditions and it is not constant (Fowler et al., 2009).

Chapter 3

A comparison of dry deposition schemes in the UKCA model with observations

3.1 Introduction

Ozone (O_3) is found in the troposphere as a consequence of the transport from the stratosphere and is produced through chemical reactions represented by the oxidation of hydrocarbons and carbon monoxide (CO) in the presence of nitrogen oxides (NO_x) (Royal Society, 2008). In the troposphere, the role of O_3 is central as it drives the chemical oxidation through the subsequent production of OH radicals (Monks et al., 2015). Tropospheric O_3 is considered a dangerous and reactive air pollutant causing damage to vegetation (Fowler et al., 2009) and human health (Monks et al., 2015; Von Schneidemesser et al., 2015) and is also the third most significant greenhouse gas (IPCC, 2013; Stevenson et al., 2013).

Chemical destruction and dry deposition to the Earth surfaces are the main processes which lead to the removal of O_3 from the troposphere (Stevenson et al., 2006), with the latter estimated to contributing for about 25% of the total atmospheric O_3 loss (Lelieveld and Dentener, 2000).

Global O_3 processes are usually studied with chemistry transport models (CTMs) and climate-chemistry models (GCMs). Discrepancies in the dry deposition approaches within models contribute to differences in inter-model O_3 concentration and simulated tropospheric O_3 budgets (Stevenson et al., 2006; Wild, 2007; Fiore et al., 2009; Hardacre et al., 2015). In models, O_3 dry deposition is highly parameterized

(Fowler et al., 2009; Hardacre et al., 2015) and the O_3 deposition flux (F_{O3}) is usually calculated by multiplying the O_3 with a deposition velocity (V_d), which is commonly estimated by applying a resistance analogy approach proposed by Wesely (1989). Large uncertainties therefore remain in modelling O_3 deposition and a mechanistic representation of this process in global models has not been included yet (Fowler et al., 2009; Wu et al., 2011). This is associated with difficulties in simulating the large spatial and temporal variability and complexity of O_3 dry deposition processes which depend on the meteorological conditions, the properties of the vegetation types and specific characteristics of the surfaces as well as the rapid in-canopy O_3 chemistry reactions (Wu et al., 2011; Hardacre et, 2015).

Hardacre et al. (2015) presented the first evaluation study of global O_3 dry deposition fluxes in the TF HTAP global scale chemistry climate models (Task Force on Hemispheric Transport of Air Pollution). It was found that differences between modelled and observed O_3 dry deposition fluxes are mainly driven by the modelled deposition velocity (V_d) rather than by surface O_3, the discrepancies in modelled V_d over the oceans, grasslands and tropical forests representing the main source of differences between models and observations.

Soil moisture deficit (affecting the stomatal conductance) and the O_3 non-stomatal deposition are generally not well simulated within models and were identified as key sources of variability between models (Zhang et al., 2002a; Touvinen et al. 2004, 2009; Hardacre et al., 2015).

Recent studies have shown that O_3 stomatal and non-stomatal uptake by vegetation each constitute 40-60% of the total flux as an annual average (Gerosa et al., 2003, 2004, 2009; Altimir et al., 2006; Coyle et al., 2009; Fowler et al., 2009; Stella et al., 2009; Fares et al., 2010a). In CTMs and GCMs the O_3 non-stomatal deposition is commonly represented in a very simplified way (Fowler et al., 2009). Properly simulating the ratio between O_3 stomatal and non-stomatal deposition within models is important (Fowler et al., 2009; Hardacre et al., 2015), as the O_3 stomatal uptake causes damage to the plants.

There is an increasing recognition that ecosystem effects of O_3 are more closely linked to the O_3 flux entering the stomata rather than O_3 concentrations (Ainsworth et al, 2012; Ashmore et al., 2004; Harmens et al., 2007; Karlsson et al., 2007; Pleijel et

al., 2007). Thus correctly partitioning the dry deposited O_3 flux between stomatal and non-stomatal sinks at the surface is vital to improve the quality of O_3 effects assessment (Touvinen et al., 2009; Emberson et al., 2013). Val Martin et al. (2014) showed that coupling dry deposition processes to vegetation phenology can significantly reduce biases in simulated surface O_3.

In this study, the United Kingdom Chemistry and Aerosol (UKCA) model (Abraham et al., 2012) is used to simulate the process of dry deposition using a revised version of a simplified implementation of the resistance analogy scheme of Wesely (1989) (and better described in Chap. 2, Sec. 2.2.4), coupled with a prediction of stomatal conductance from the MOSES 2.2 land surface scheme (Essery et al., 2001, 2003).

An alternative non-stomatal deposition approach (Zhang et al., 2003) was implemented in UKCA in order to investigate the sensitivity of surface O_3 to a different dry deposition scheme to explore the effect of changing the partitioning between stomatal and non-stomatal O_3 flux at both regional and global scales (Chap. 2, Sections 2.2.7-2.3.2). In principle the Zhang scheme introduces some additional dynamic responses to meteorological drivers (friction velocity, u_*; relative humidity, *RH*; leaf area index, *LAI*; in-canopy moisture) which are desirable for chemistry and climate models as they open up possibility for capturing responses of V_d to global climate change. By contrast the Wesely-type schemes deploy fixed look-up tables of resistances that represent the (near present-day) conditions at which the underlying measurements were made.

In this study, the performance of both UKCA dry deposition schemes is compared against measurements, with a particular focus on the diurnal and seasonal variations of the dry deposition velocity terms and their partitioning between stomatal and non-stomatal components.

An analysis is presented of the extent to which the differences observed reflect e.g. (a) inconsistencies in site meteorology caused by the low spatial model resolution, (b) limitations due to the use of generic vegetation type properties, (c) problems with the parameterizations of the dry deposition schemes.

This chapter is organized as follows: Section 3.3 describes the long and short-term O_3 flux data sets and the measurements techniques used to collect them along with the method applied to compare model outputs with observations. Section 3.4.1

presents the results of the comparison of modelled O_3 dry deposition velocity and canopy conductance terms against observed flux measurements for forest and grass/crop sites as well as an evaluation of some key environmental factors. A comparison of surface O_3 against observed values in the North Hemisphere and South Hemisphere is also provided in Section 3.4.2. Section 3.4.3 presents an analysis of the O_3 deposition flux partitioning, contrasting two different dry deposition schemes (WES scheme as described in Sec. 2.2.4-2.2.6 and ZHG scheme as described in Sec. 2.2.7). Section 3.4.4 presents some discussion about the source of discrepancies between simulated and observed dry deposition velocity terms interpreting the role of some environmental conditions. In Section 3.4.5, an analysis of the O_3 parameterizations is also provided discussing positive and negative aspects of the dry deposition schemes considered in this study. Finally, recommendations for further improvements of O_3 dry deposition in UKCA are provided in Section 3.4.6.

3.2 Simulation setup

In this study the simulations were conducted using UKCA model as described in Chap. 2 (Sections 2.2.1-2.2.2). The chemistry scheme adopted in the version of UKCA used in this study (called TropIsop) includes a tropospheric chemistry scheme and the extra Isoprene related species and reactions following the Mainz Isoprene Mechanism as already outlined in Sec. 2.2.1 (Pöschl et al., 2000; O'Connor et al., 2014). Emissions used for this study were decadal averages centred on the year 2000 and are based on the gridded dataset of Lamarque et al. (2010). These include surface emissions from nine species (NO, CH_4, CO, HCHO, C_2H_6, C_3H_8, Me_2CO, MeCHO, C_5H_8) and multi-level NO_x emissions from aircrafts.

Several simulations were performed to evaluate UKCA model outputs using the two different dry deposition schemes against O_3 data for different years. All model simulations were run for two years and 4 months to allow model spin up. For these simulations, the model dynamical variables (temperature *T*, zonal wind *u* and meridional wind *v*) were constrained with ECMWF ERA-40 meteorological re-

analysis data to give a more realistic representation of the atmosphere (better described in Telford et al., 2008).

For the simulation regarding the assessment of modelled surface O_3 with observations, prescribed monthly mean sea surface temperature and sea ice fields obtained from the observational HadISST data set (Rayner et al., 2003) were used.

3.3 Data and Methods

3.3.1 Description of O_3 data and measurement techniques

In this study five long term and three short term data sets were used for evaluating O_3 dry deposition velocity terms and to assess micrometeorological data and environmental conditions within some reference model grids (Table 3.1). In all data sets (apart from Harvard Forest for which only V_d is provided), the observed canopy conductance G_c (=1/R_c) was derived from the measurements as residual from Eq. (2.17).

Measured stomatal conductance data for O_3 were available for most of the sites and it was estimated applying energy balance principles using measured water vapour fluxes during dry conditions (when transpiration dominates the latent heat flux), which was then extrapolated to all conditions (Gerosa et al., 2003; Altimir et al., 2006; Coyle, 2005); Rannik et al., 2012; Fares et al., 2014). Here, the exact approach differed between authors of the various studies. It needs to be emphasised that the directly measured-derived entity is the total resistance ($R_t = R_a + R_b + R_c$) and that a comparison of canopy resistances relies on R_a and R_b being parameterised and modelled correctly. An additional modelling step is introduced when dividing R_c into the stomatal and non-stomatal components.

Micrometeorological flux measurement techniques break down under highly stable stratification when vertical transport is no longer driven by friction processes. Under these conditions the sum of R_a and R_b becomes very large and R_c is derived as a small difference between two large terms, with much increased uncertainty. Consequently, measurement data were filtered during analysis to remove highly

stable, calm night-time conditions. This is taken into account by re-sampling the modelled time-series to match the coverage of the available filtered dataset. However, as a result the night-time values of the average diurnal cycles presented here are likely to be biased towards larger values both in the measurements and modelled values.

To summarize, R_c values derived with $u_* < 0.2$ m s^{-1} and $u_* > 2.0$ m s^{-1}, $(R_a + R_b) > 500$ s m^{-1} and $(0 < L < 5)$ m were rejected (Nemitz et al., 2009). In addition, values of R_c inferred with sensible heat flux $H > 600$ W m^{-2} were also discarded as they were considered physically unreasonable (Nemitz et al., 2009).

Monthly mean surface O_3 data from the World Data centre for Greenhouse Gases archive (http:// ds.data.jma.go.jp/gmd/wdcgg/) were used to assess modelled surface O_3 using both WES and ZHG schemes. The surface O_3 data were collected (through air sampling techniques) at monitoring sites located both in the North and South Hemisphere for different periods (Table 3.2).

3.3.2 Comparing model outputs with observations

In both WES and ZHG schemes, surface atmosphere exchange processes at the grid and sub-grid scales are taken into account for modelling O_3 V_d terms using the same tile approach as described in Chap. 2 (Sec. 2.2.2). UKCA is coupled with MOSES 2.2 and therefore some key meteorological and vegetation parameters are acquired from it whereas some others are provided by the climate model. MOSES 2.2 simulates specific surface type temperature (T_s), sensible (H) and latent heat (LE) fluxes whereas friction velocity (u_*), relative humidity (RH) and net global solar radiation (I_s) are modelled as grid-average properties. Some diagnostics such as vapour pressure deficit (VPD), the Bowen ratio (ratio between sensible heat flux and latent heat flux) (ψ_B) were not available. VPD for each the vegetation type was inferred applying the method described in Monteith and Unsworth (1990). To do this, the grid average relative humidity and the specific surface type temperatures were used respectively. The ψ_B were calculated simply dividing the surface type H by the LE for each vegetation type. Some specific diagnostics (not available in the original model configuration) were created in order to output some model variables.

Table 3.1. Summary of data sets used to assess UKCA O_3 deposition velocity and canopy conductance terms and to evaluate modelled environmental conditions. ECM stands for eddy covariance method and GM for gradient method.

Vegetation type	Location	Period	Method	Variables	Reference
		Long term			
Scots pine forest (*Pinus sylvestris)*	Hyytiala, Finland (61°51′ N, 24°17′ E)	1 Jan. 2002 - 31 Dec. 2002	ECM	V_d (22m), G_c, G_s	Rannik et al. (2012)
Norway spruce forest *Picea abies)*	Ulborg, Denmark (56°17′ N, 8°25′ E)	1 Jan. 1999 - 31 Dec. 1999	GM	V_d (18/36m), G_c	Mikkelsen et al. (2004)
Pine plantation (*P. Ponderosa L.*)	Blodgett Forest, USA (38°53′ N, 120°37′W)	1 Jan. 2002 - 31 Dec. 2002	ECM	V_d(35m), G_c, G_s	Fares et al. (2010a)
Holm Oak Forest (*Quercus ilex L.*)	Castelporziano, Italy (41°42′ N, 12°21′ E)	1 Jan.2013 - 31 Dec. 2013	ECM	V_d (12m), G_c, G_s	Fares et al. (2014)
Red Oak (*Quercus rubra*), Red maple (*Acer rubrum*)	Harvard Forest, USA (42°32′ N, 72°11′ E)	Jan. 1992 - Dec. 2001	ECM	V_d(30m)	Munger et al. (1996)
Grassland (Lolium perenne)	Easter Bush, S. Scotland, UK (55°52′ N, 3°12′W)	1 Jan. - 31 Dec. 2002	ECM	V_d(13m), G_c , G_s	Coyle et al. (2006)
Grassland (*Festuca arundinaceae*, *Trifoulium repens*, *Plantago lanceolata*)	Sarrazola, Portugal (40°42′ N, 8°37′)	1 Feb. - 30 Sep. 1995	ECM	V_d , G_c	Pio et al. (2000)
		Short term			
Oak Forest (Quercus robur)	Alice Holt, UK (51°7′ N, 0° 51′ W)	July - 18 Aug. 2005	ECM	V_d, G_c , G_s	Coyle et al. (2006)
Barley Field	Comun Nuovo, Italy (45°42′ N, 9°30′ E)	April - May 2002	ECM	V_d, G_c , G_s	Gerosa et al. (2004)

Table 3.2. Summary of surface O_3 monitoring sites and dataset periods (World Data centre for Greenhouse Gases) used to assess UKCA model surface O_3 concentrations at the global scale.

location and altitude (m a.s.l)	Period
Barrow (71.32ºN, 156.60ºW), 11m	1974-01-01 - 2014-12-31
Mace Head (53.33ºN, 9.90ºW), 8m	1997-01-01 - 2014-12-31
Trenidad Head (41.05ºN, 124.15ºW), 120m	2003-01-01 - 2014-12-31
Niwot Ridge (40.0°N, 105.59°W), 3528m	2004-01-01 - 2010-12-31
Mauna Loa (19.54°N, 155.58°W) 3397m	1973-09-01 - 2014-12-31
Barbados (13.17°N, 59.43°W), 45m	1989-04-01 - 2014-12-31
Capo Verde (16.85°N, 24.87°W), 10m	2007-01-01 - 2014-12-31
Mt. Waliguan (36.28°N, 100.90°E), 3810m	1995-01-01 - 2013-12-31
Ryori (39.03°N, 141.82°E), 260m	1990-01-01 - 2014-12-31
Tsukuba (36.05°N, 140.13°E), 25m	1988-08-01 - 2015-11-30
Bukit Koto Tabang (0.20°S, 100.32°E), 864m	1997-09-01 - 2014-12-31
Mt. Kenya (0.06°S, 37.30°E), 3678m	2003-01-01 - 2008-11-30
San Lorenzo (25.37°S, 57.55°W), 133m	1997-01-01 - 2007-12-31
El Tololo (30.17°S, 70.80°W), 2220m	1995-11-01 - 2014-11-30
Cape Point (34.35°S, 18.48°E), 230m	1983-01-01 - 2014-12-31
Cape Grim (40.68°S, 144.68°E), 94m	1982-01-01 - 2014-12-31
Lauder (45.03°S, 169.67°E), 370m	2003-11-01 - 2014-12-31
Ushuaia (54.85°S, 68.31°W), 18m	1994-11-25 - 2008-12-31
Syowa (69.00°S, 39.58°E), 16m	1997-01-01 - 2014-12-31
South Pole(89.98°S, 24.80°W), 2810m	1975-01-01 - 2014-12-31

These model diagnostics are: O_3 V_d, stomatal conductance for O_3 ($G_s = 1/R_s$), O_3 non-stomatal conductance ($G_{ns} = 1/R_{ns}$), cuticular conductance ($G_{cut} = 1/R_{cut}$), in-canopy aerodynamic+soil conductance $G_{inc.+s.} = 1/(R_{ac}+R_{soil})$. All the resistance terms simulated using the WES scheme and the ZHG scheme (for each surface type) are described in Sec. 2.2.4 and 2.2.6 respectively. O_3 V_d is calculated for both the WES and ZHG scheme (for each surface type) using eq. 2.17.

For this study, a model diagnostic to output the volumetric soil moisture as fraction of saturation (θ_s) at the root zone was not available. Thus, θ_s was inferred using the

eq. 2.12, which defines the surface type specific soil moisture stress factor $\beta(\theta)$ as a function of θ_s, θ_w and θ_c (as described in Sec. 2.2.4.4). θ_s was inferred by inverting $\beta(\theta)$ (eq. 2.12) that is available in UKCA as a diagnostics and using the θ_w/θ_c values which are imported from an ancillary file for the model grids considered for the comparison with observations.

Finally, in order to compare the modelled surface O_3 with observations, the whole time series was used for each monitoring site to infer climatological monthly mean surface O_3 concentrations and the standard deviations respectively. Due to the different monitoring site elevations, the model was sampled at the corresponding heights.

3.3.3 Model performance analysis

UKCA model performance was assessed applying descriptive statistics such as Mean Absolute Error (MAE) in s m^{-1} and Mean Relative Bias (MRB) in % to the modelled R_a, R_b and R_c resistance terms and O_3 dry deposition velocity using WES and ZHG dry deposition schemes as shown in Touvinen et al. (2004). MAE and MRB statistical metrics are calculated as follows:

$$\mathrm{MAE} = \frac{1}{N}\sum_{i=1}^{N}\left| x_{\mathrm{mod}_i} - x_{\mathrm{obs}_i} \right|$$
$$\mathrm{MRB} = \frac{1}{N}\sum_{i=1}^{N}\frac{2(x_{\mathrm{mod}_i} - x_{\mathrm{obs}_i})}{(x_{\mathrm{mod}_i} + x_{\mathrm{obs}_i})} \qquad \textbf{(3.1)}$$

where x_{mod} and x_{obs} are the modelled and the observed parameters expressed as hourly values respectively. The Ulborg data set was particularly scattered so the use of the median of the observed and modelled resistance terms and O_3 V_d was preferred to assess the statistical model performance for that monitoring site.

3.3.4 Sensitivity analysis of the ZHG non-stomatal deposition to observed environmental factors

As described in section 2.2.7, ZHG scheme introduced in UKCA an explicit dependence of the O_3 non-stomatal deposition on: (a) key meteorological factors (u_* and *RH*); (b) specific vegetation type parameter such as the area of the surface taking part in the process per unit ground area (e.g. the leaf are index *LAI*): (c) the surface (grid average) canopy wetness conditions.

Off-line sensitivity tests on the total O_3 non-stomatal conductance (G_{ns}) and its components were conducted: the cuticular (G_{cut}) conductance and the in-canopy aerodynamic+soil (G_{inc+s}) conductance. This was done by simultaneously replacing the above modelled environmental factors with those derived from observations carried out over three vegetation types in Europe: Holm Oak (*Quercus ilex*) at Castelporziano, IT, (41°41′ N, 12°21′ E); Scots Pine (*Pinus sylvestris*) at Hyytiälä, FIN (61°51′ N, 24°17′ E); grassland dominated by Ryegrass (*Lolium perenne*) at Easter Bush, UK, (55°52′ N, 3°12′ W). One year off-line simulations were performed with hourly time resolution to partition the response of the modelled G_{ns} to each environmental factor change (u_*, *RH*, *LAI*) respectively (as described in Sec. 2.2.7.1) and to test their combined effect. This allowed to exploring the sensitivity of G_{ns}, G_{cut} and G_{inc+s} using ZHG parameterizations on a diurnal and seasonal base to each measured environmental factor and to investigate the source of uncertainties between modelled and inferred O_3 non-stomatal deposition.

3.4 Results and discussion

3.4.1 Evaluating ozone dry deposition velocity against observations using WES and ZHG schemes

Dry deposition velocity (V_d), canopy conductance (G_c) and canopy stomatal conductance for O_3 (G_s) terms were simulated using the WES and ZHG deposition schemes and compared against observations primarily focusing on their diurnal variability. A total of nine long term datasets were used to compare the two UKCA

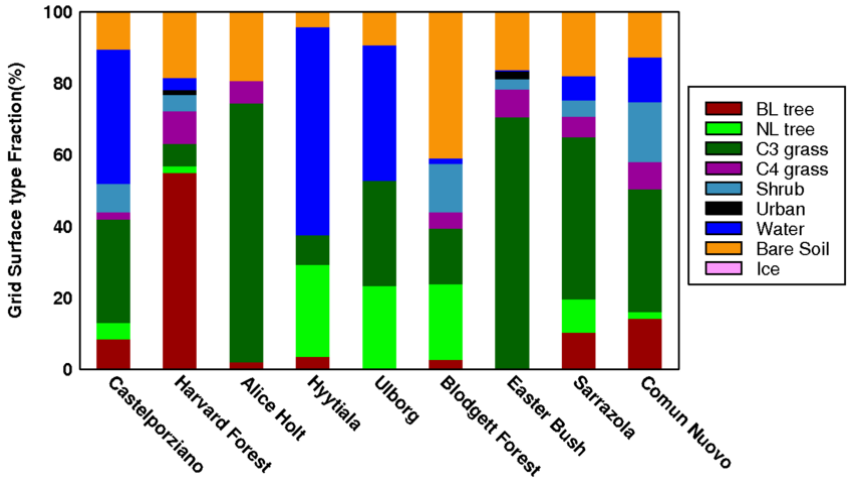

Figure 3.1. Surface type fractions (in %) of model grids used to compare the WES and ZHG dry deposition schemes with observations.

dry deposition schemes with observations, and the performance was investigated in more detailed against three datasets collected over a broadleaf forest (Castelporziano, IT) dominated Holm Oak (*Quercus ilex*), coniferous forest (Hyytiälä, FIN) dominated by Scots Pine (*Pinus sylvestris*) and grassland (Easter Bush, SCO) dominated by Ryegrass (*Lolium perenne*). Table 3.3 presents a summary of the model performance statistics for R_a, R_b, R_c and V_d compared with all the long-term and short-term datasets used in this study. The contribution of the nine different surface types to the model grids containing the different measurement sites is shown in Figure 3.1, to aid the interpretation of the comparison results. For the model-measurement comparison, the modelled fluxes were re-sampled to match the periods that have passed the measurement data filter criteria and account for instrument downtime (Sec. 3.3.2). As a result of this, the presented diurnal cycles are biased towards higher turbulence conditions and may not reflect the true diurnal cycle of the exchange, but modelled and measured values should be comparable. For the non-stomatal conductances, the WES and ZHG routines implemented in UKCA were also

Table 3.3. Model performance statistics for the hourly mean of the resistances R_a, R_b, R_c and O_3 V_d for the long term data sets and short-term data sets used to assess WES and ZHG schemes. (*) refers to the model performance statistics for the hourly median of R_a, R_b , R_c and O_3 V_d . R_a and R_b are modelled using the same algorithm in both WES and ZHG scheme.

Monitoring sites	R_a		R_b		Model version	R_c		V_d	
	MAE (s m^{-1})	MRB (%)	MAE (s m^{-1})	MRB (%)		MAE (s m^{-1})	MRB (%)	MAE (mm s^{-1})	MRB (%)
Hyytiälä	106	57	12	25	WES	157	10	1.0	8
					ZHG	153	23	1.8	40
Ulborg	202	107	48	-99	WES	173*	120*	10.0*	-142*
					ZHG	200*	69*	9.0*	-120*
Blodgett Forest	160	87	22	34	WES	298	34	2.1	-45
					ZHG	247	50	2.7	-53
Castelporziano	91	97	34	2	WES	455	24	1.5	12
					ZHG	490	-4	1.4	-8
Harvard Forest	na	na	na	na	WES	na	na	7.4	-82
					ZHG	na	na	7.1	-67
Alice Holt	458	43	60	33	WES	36	66	4.7	1
					ZHG	35	81	4.5	-14
Easter Bush	28	-29	34	-33	WES	142	42	3.0	-27
					ZHG	158	8	2.8	-0.1
Sarrazola	62	-28	40	-15	WES	411	16	1.6	15
					ZHG	428	8	2.2	10
Comun Nuovo	na	na	na	na	WES	160	4	1.6	-4
					ZHG	162	2	1.7	0.2

used off-line with the actual data recorded at the various field sites (in terms of meteorology and canopy characteristics) to isolate the impacts of model structure and input parameters on the agreement of the modelled results with measurements (Sec. 3.3.4). For each measurement site, a comparison of modelled and measured meteorological parameters is also provided as presented in the following sections.

3.4.1.1 Broadleaf tree

Figure 3.2 compares the average diurnal cycle of simulated G_c-G_s-G_{ns} and V_d for broadleaf tree against measurements collected in summer (JJA) at the Castelporziano estate (41°41′ N, 12°21′ E), Italy, within a typical coastal Mediterranean forest dominated by Holm Oak trees. To aid the investigation of the reasons for discrepancies, the comparison of modelled and measured meteorological and environmental factors at the site is shown in Figure 3.3.

Overall Figure 3.2 demonstrates that, although the agreement between measured and modelled total canopy conductance is reasonable, the partitioning into stomatal and non-stomatal component differs greatly between the modelled and measurement-derived estimates. In particular, Figure 3.2a shows that the observed G_c values at the Castelporziano site are large especially in the morning, with significant day-to-day variability as indicated by the vertical bars. Modelled and observed values of G_c exhibit a peak in the middle of the morning followed by a decrease afterward towards the evening, although the WES scheme shows a moderate rise again in the afternoon. The WES scheme predicts larger G_c values compared with the ZHG scheme throughout the day. Although night time G_c seem better calculated by the WES scheme, modelled day time G_c using ZHG appears to be better correlated with observations. Bearing in mind that the measurement derived split of G_c into G_s and G_{ns} is not without uncertainty (see Section. 3.3.1), the comparison of these conductances can provide additional information on the reasons behind the model/measurements discrepancies of G_c.

As shown in Figure 3.2b modelled G_s present bimodal diurnal patterns with a first maximum predicted in the morning and a second one in the afternoon. In the WES and ZHG schemes, in which G_s is predicted by MOSES 2.2 (with moisture modification in the ZHG scheme), G_s shows a large diurnal variability, with the latter

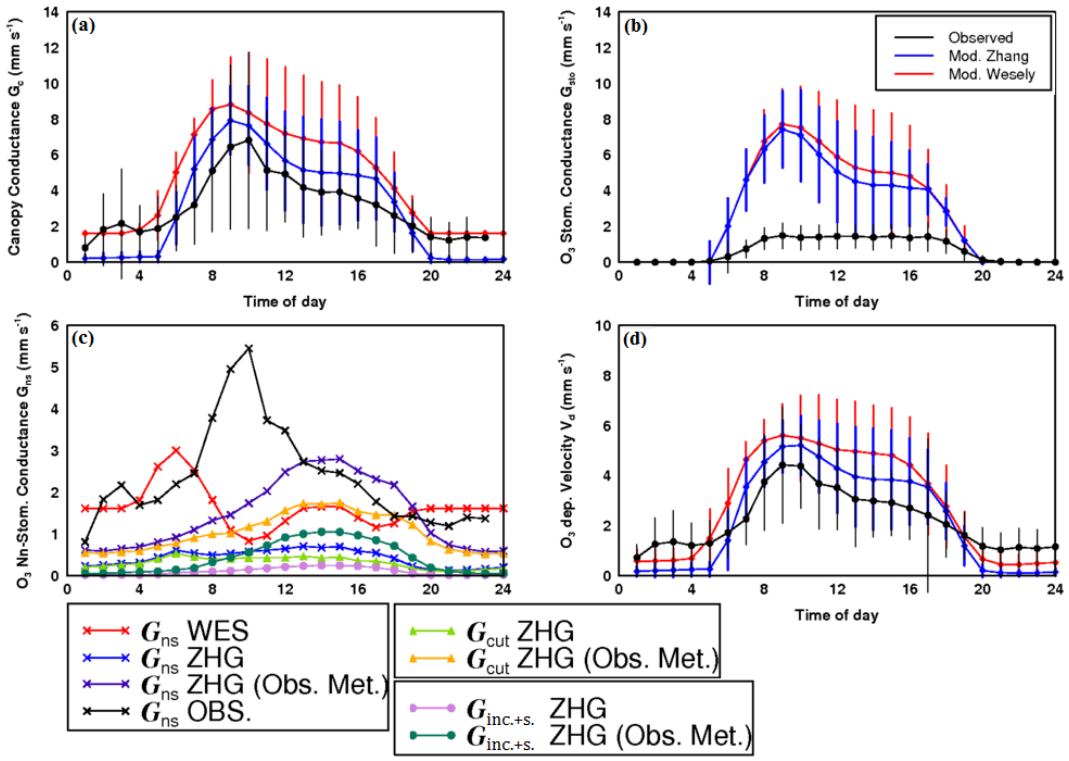

Figure 3.2. Diurnal cycles of modelled canopy conductance G_c (mm s^{-1}) (**a**), canopy stomatal conductance for O_3 G_s (mm s^{-1}) (**b**) and O_3 dry deposition velocity V_d (mm s^{-1}) (**d**) for BL tree against observed values in summer 2013 at the monitoring site of Castelporziano, IT, (41°41' N, 12°21' E). Total observed and modelled non-stomatal conductance G_{ns} (mm s^{-1}) and non-stomatal conductance terms (G_{cut} and $G_{inc.+s.}$) modelled by UKCA in a nudged configuration and off-line using u_*, *RH* and *LAI* measured at Castelporziano in 2013 (**d**). Coloured bars indicate the range of variability of modelled variables using WES and ZHG schemes whereas black vertical bar shows the standard deviation of the observed values.

scheme leading to smaller values until the morning peak is reached and around the second maximum in the afternoon. By contrast, observed G_s at Castelporziano showed more uniform diurnal variations with values a factor of four smaller than the model predictions. As shown in Figure 3.2b, the larger differences between simulated and observed G_s were detected in the morning.

The measurements-derived values of G_s at this site are small, probably due to severe water stress (Gerosa et al., 2005; Gerosa et al., 2009; Fares et al., 2014), which seems not properly represented in the model as shown in Figure 3.4.

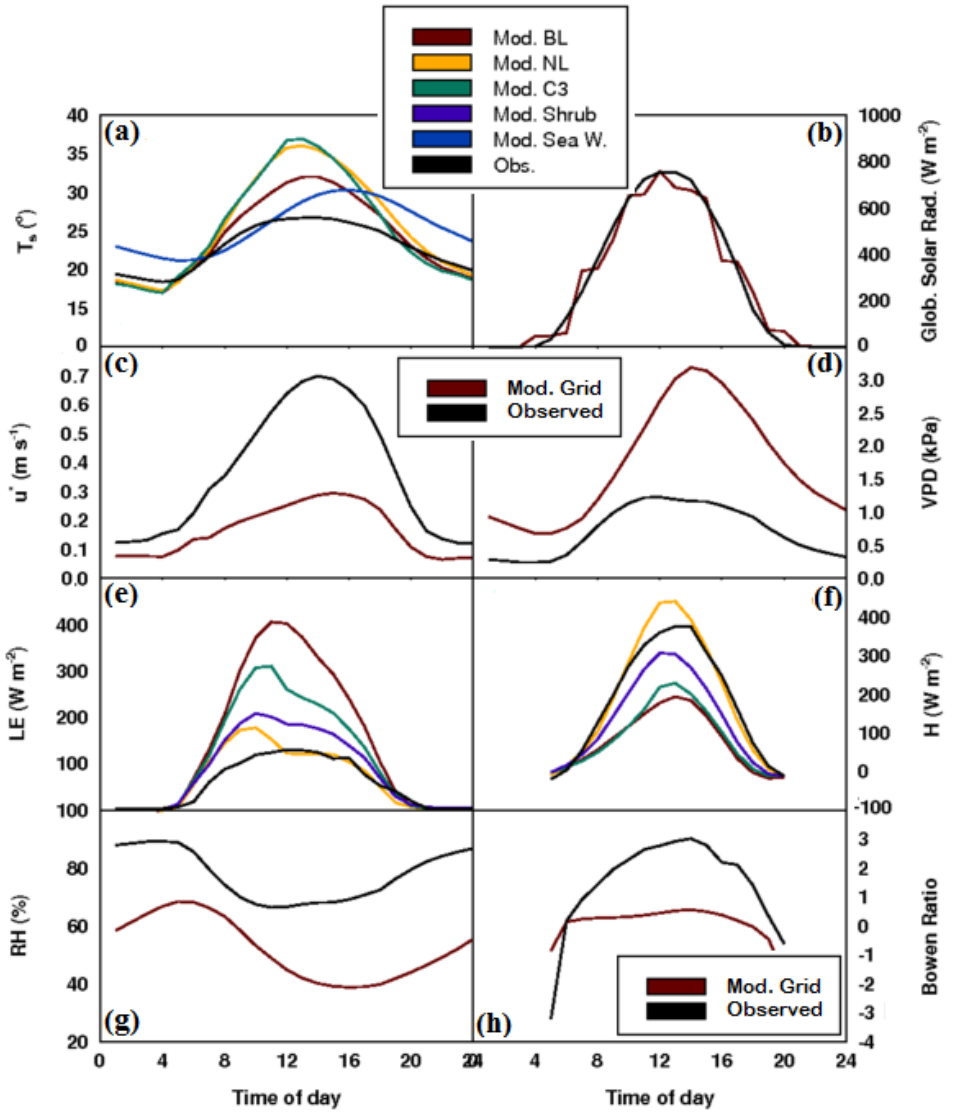

Figure 3.3 Comparison of the seasonal (summer-JJA) diurnal cycle of modelled meteorological and environmental factors with observations collected at the monitoring site of Castelporziano (42º41' N,12º 21' E) in 2013. '(**b)-(c)-(d)-(g)-(h)**' show modelled grid-average variables whereas (**a)-(e)-(f)** present environmental factors simulated for each surface type within the model grid. The modelled vapour pressure deficit *VPD* (**d)** was inferred using a tile surface temperature and a grid average relative humidity.

It appears that the average modelled soil moisture content (SMC_{mod}) at the root zone (the root depth for BL tree is 3 m) shows considerably larger values than observed

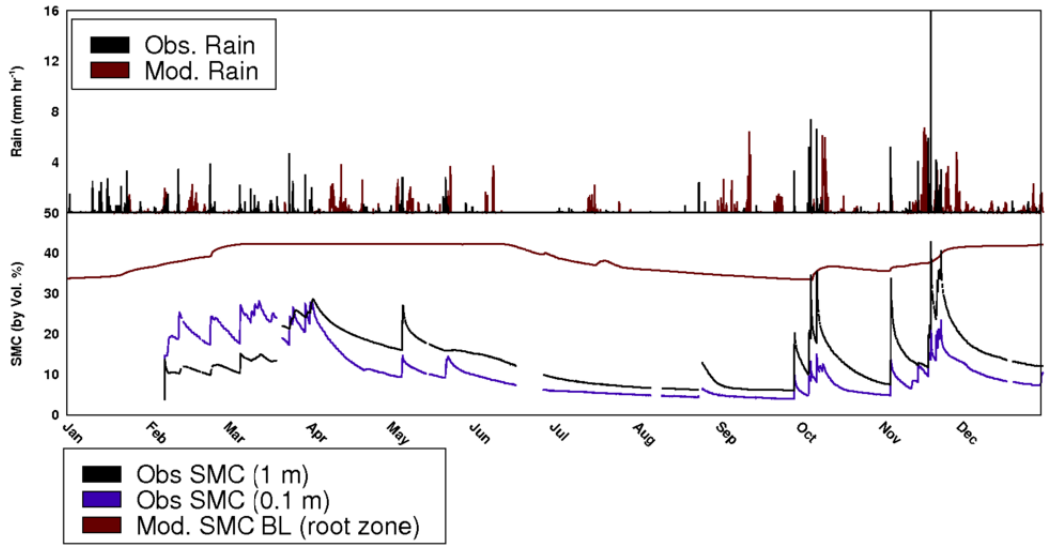

Figure 3.4. Comparison of the modelled grid hourly time series of rain precipitation rate (mm hr^{-1}) and the average modelled volumetric soil moisture content (*SMC*) as a fraction of saturation (%) at the roots level (within 3m) against observed hourly values at 0.1 m and 1 m soil depths measured at the Castelporziano site in 2013.

values (SMC_{obs}) at 1 m throughout the year especially in summer, suggesting slightly different water availability down the root zone compared to the model. As shown in Figure 3.3e, modelled latent heat fluxes (*LE*) over the Castelporziano grid exceed 400 W m^{-2} on average. Such latent heat flux were reported over a mixed coniferous/deciduous forest in N.E America by Finkelstein et al. (2000) and Pleim et al. (2001) who pointed out that their respective forests were unstressed by soil moisture, but the heat fluxes observed at Castelporziano were much smaller (~100 W m^{-2}). Moreover, the model predicts a very different Bowen ratio (ψ_B = ratio of sensible to latent heat flux) during summer (ψ_B ~ 0.5) than implied by the measurements (ψ_B ~ 3), which appears to be related to the much higher vapour pressure deficit (*VPD*) (Figure 3.3d) calculated using the surface temperature simulated by the model for BL tree and the average ambient grid relative humidity used to drive the latent heat fluxes.

The grid cell containing Castelporziano (Figure 3.1) is dominated by C3 grass and

sea water and covers such a disparate variety of Mediterranean broadleaf evergreen forests which can be quite vulnerable to drought such as *Quercus ilex* (Gerosa et al., 2009; Vargas et al., 2013). Thus, in addition to underestimating soil moisture stress, the model also overestimates the latent heat flux (and thus stomatal conductance) by not being able to reproduce the negative feedback of increased *RH* in a forest situated in a tile dominated by other land cover types.

Stomatal conductance measurements in a much more temperate beech (*Fagus sylvatica L.*) of the Abetone forest (44º07′N, 10º40′) in the Northern Apennines, Italy (1230 m), only 290 km from Castelporziano, were more akin to those predicted by the model throughout the day, with larger values up to 10 mm s^{-1} in the morning, followed by a decrease towards the evening (Magnani et el., 1998).

Figure 3.2c reveals that in summer, significant differences exist between observed and modelled G_{ns} using the WES and the ZHG scheme. Modelled G_{ns} using both WES and ZHG scheme show slightly different diurnal variations compared to observed values at Castelporziano. G_{ns} simulated with the WES scheme appears to peak earlier in the morning whereas ZHG predicts smaller values throughout the day. When the ZHG scheme is driven with measured u_*, *RH* and *LAI* at Castelporziano, a much larger total O_3 non-stomatal conductance is simulated, with an average value closer to that derived from the measurements, but a markedly different diurnal pattern. A sensitivity analysis revealed that moving from modelled to measured input parameters increased both individual pathways contributing to G_{ns} (i.e. cuticular and soil deposition), with u_* having the largest effect (not shown). The difference in the diurnal cycle may, at least in part, be due to the fact that the flux measurements were not corrected for storage effects. NO_x emitted by microbial soil activity during night then stored in the canopy as well as moisture accumulating on the leaves in the early morning, represent a chemical sink for O_3 within the Castelporziano forest (Gerosa et al. 2005, 2009) and might account for the discrepancy between observed and modelled G_{ns} using ZHG scheme.

As presented in Figure 3.2d, observed values of O_3 V_d show a large variability during the day and, with a broad maximum occurring in the morning around 10 am, in agreement with previous studies carried out over deciduous and mixed forests (Finkelstein et al., 2000; Pleim et al., 2001; Wu et al, 2011). The rapid increase of O_3

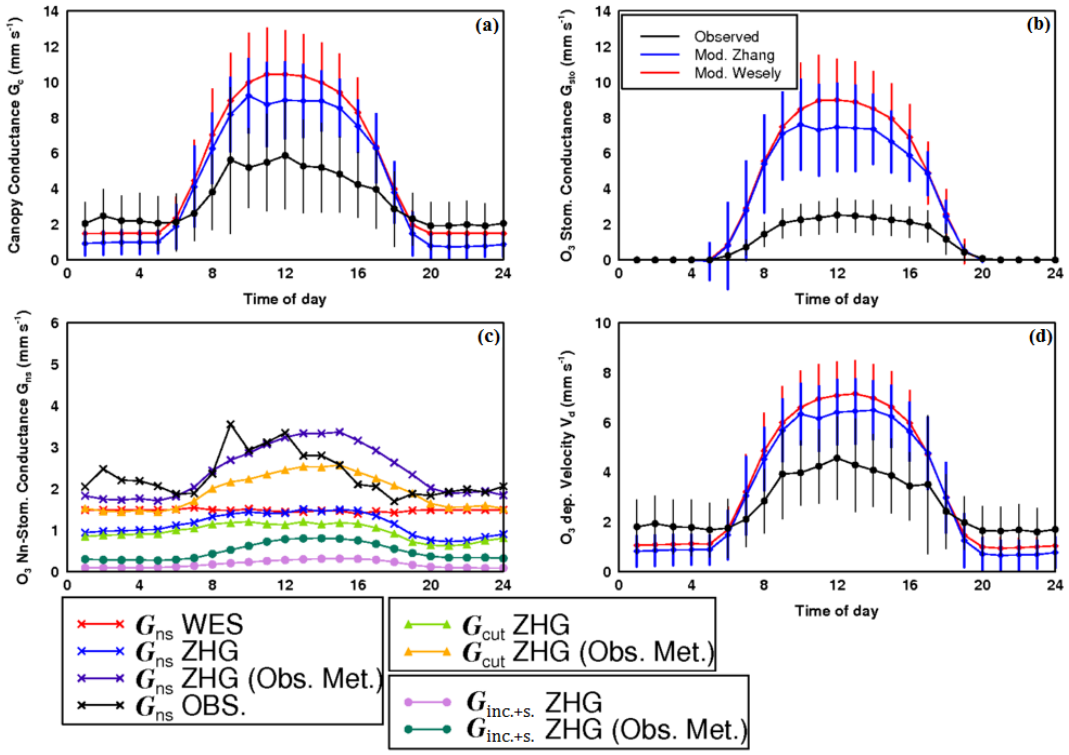

Figure 3.5. Diurnal cycles of modelled canopy conductance G_c (mm s^{-1}) (**a**), canopy stomatal conductance for O_3 G_s (mm s^{-1}) (**b**) and O_3 dry deposition velocity V_d (mm s^{-1}) (**d**) for BL tree against observed values in spring 2013 at the monitoring site of Castelporziano, IT, (41°41' N, 12°21' E). Total observed and modelled non-stomatal conductance G_{ns} (mm s^{-1}) and non-stomatal conductance terms (G_{cut} and $G_{inc.+s.}$) modelled by UKCA in a nudged configuration and off-line using u_*, *RH* and *LAI* measured at the site of Castelporziano in 2013 (**d**). Coloured bars indicate the range of variability of modelled variables using WES and ZHG schemes whereas black vertical bar shows the standard deviation of the observed values.

V_d in the morning corresponds to the time when the stomata are fully open (Gerosa et al., 2005; Magnani et al., 1998), and this pattern seems better captured by ZHG scheme. However, the observed peak in V_d seems to be more associated with the maximum in O_3 non-stomatal deposition observed in the morning (Figure 3.2c), bearing in mind though that the observed fluxes were not corrected for storage effects. During night time the model underestimates V_d whilst G_c was very similar between the measurements and the model using WES scheme.

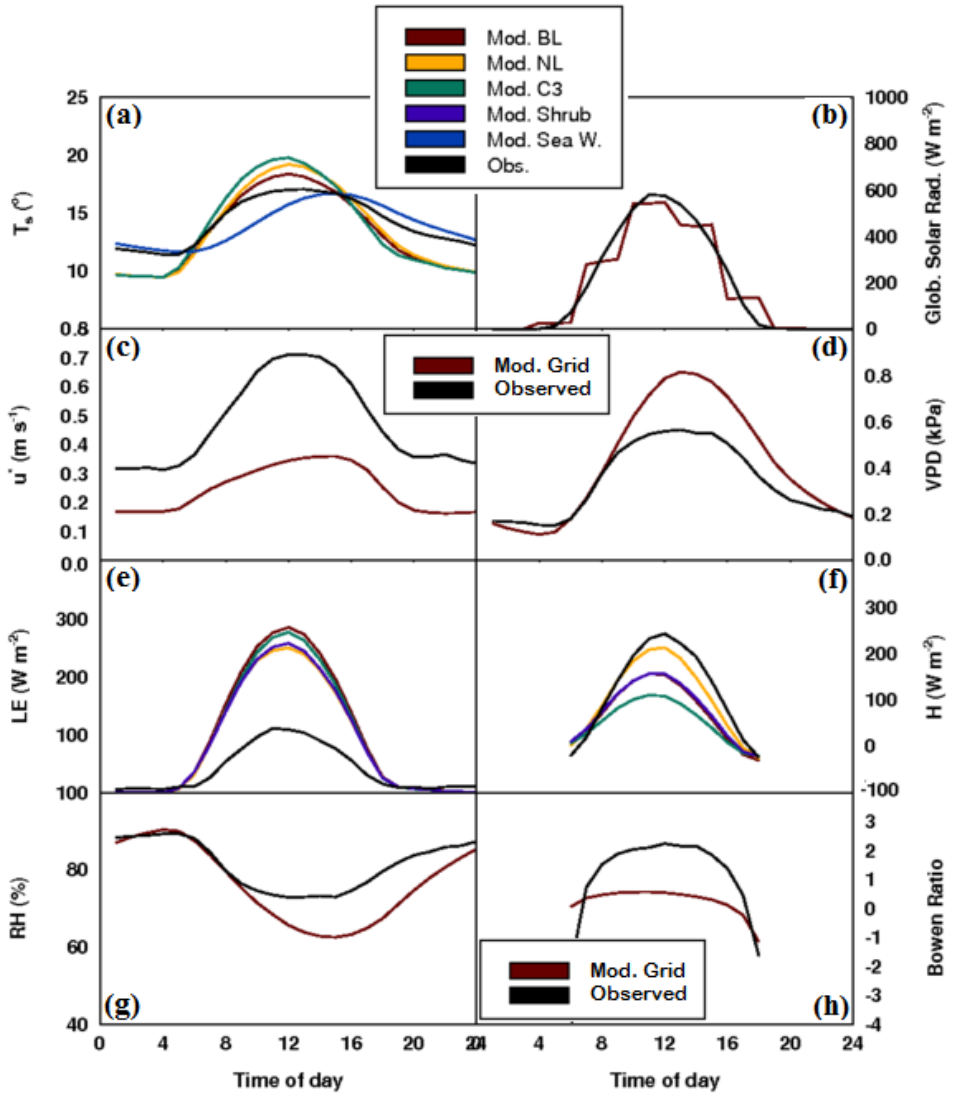

Figure 3.6. Comparison of the seasonal (spring-MAM) diurnal cycle of modelled meteorological and environmental factors with observations collected at the monitoring site of Castelporziano (42º41' N,12º 21' E) in 2013.

This is due to the additional influence of u_*, and being underestimated by the model (Figures 3.3c) resulting in a systematic over prediction of R_a and R_b (Table 3.3). Figure 3.5a revealed that in spring, ZHG scheme led to lower G_c values throughout the day compared to WES. Observed G_s showed values a factor of three lower than

modelled values. However, simulated G_s using the ZHG scheme was closer to observations. Interestingly, Figure 3.6e shows that latent heat fluxes simulated in spring over each of the vegetation types (within the model grid containing Castelporziano) exhibit similar values as well as VPD_{mod} which is closer to the observed VPD_{obs} compared to summer (Figure 3.6d), although the model still greatly overestimates G_s compared with the measurements (Figure 3.5b). Hence, this might confirm that differences between simulated and observed G_s are more due to some environmental conditions not properly represented in the model which reflected in larger calculated LE fluxes for BL trees, rather than differences in *VPD*.

As shown in Figure 3.5c, the ZHG scheme driven with measured meteorology provides an encouragingly good fit of modelled G_{ns} to the measured values. Again, most of the gain in model performance is caused by switching from modelled to measured u_*. In addition, this might suggest that especially in summer the O_3 non-stomatal deposition (Figure 3.2c) is more driven by underlying photochemical or photolytic processes (Fowler et al., 2001; Coyle et al., 2006) whereas in spring the influence of atmospheric turbulence may be more important and better resolved by the ZHG scheme using observed environmental factors (Figure 3.5c).

Finally, Figure 3.5d revealed that both the WES and the ZHG schemes capture the observed V_d diurnal variations in spring. Both the WES and the ZHG scheme appear to calculate lower V_d values during night time and higher values during the day. However, the ZHG scheme V_d estimates seem better correlated with observations.

3.4.1.2 Needleleaf tree

Figure 3.7 show a comparison of modelled G_c-G_{ns}-G_s and V_d for needle leaf tree against observations collected over a Scot pine forest in Hyytiälä, Southern Finland (61°51′N, 24ºN17′E) during the growing season (from March until the end of August). In spring, observed G_c exhibits a large variability and the maximum values are found during daytime (Figure 3.7a). In spring, observed G_c exhibits a large variability and the maximum values are found during daytime (Figure 3.7a). Compared with measurements, the WES scheme appears to calculate G_c values smaller than those predicted by the ZHG scheme, and captures well the diurnal variations.

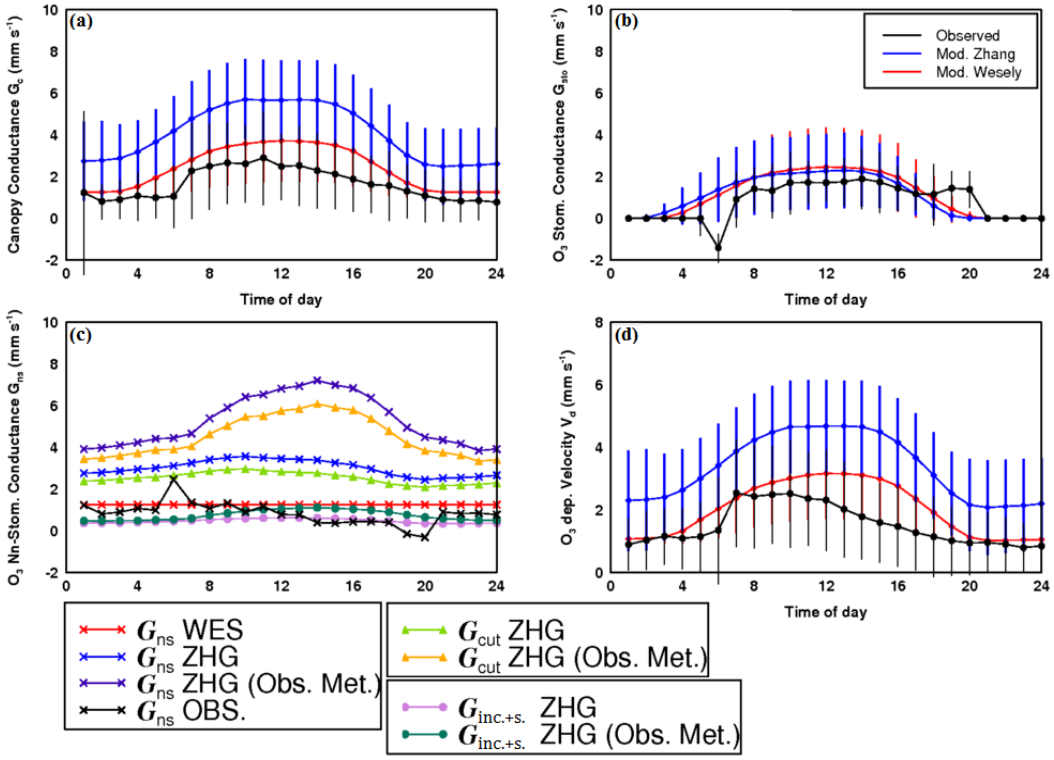

Figure 3.7. Diurnal cycles of modelled canopy conductance G_c (mm s^{-1}) (**a**), canopy stomatal conductance for O_3 G_s (mm s^{-1}) (**b**) and O_3 dry deposition velocity V_d (mm s^{-1}) (**d**) for NL tree against observed values in spring 2002 at the monitoring site of Hyytiälä, FIN, (61°51'N, 24°N17'E). Total observed and modelled non-stomatal conductance G_{ns} (mm s^{-1}) and non-stomatal conductance terms (G_{cut} and $G_{inc.+s.}$) using modelled and observed meteorological conditions (u_*, *RH* and *LAI*) are shown in (**d**).

The ZHG scheme systematically led to higher G_c values than observations by a factor of two (~2 mm s^{-1}).

Figure 3.7b reveals that in spring the large diurnal cycle of G_s is well simulated by the model using both the WES and the ZHG scheme. Both ZHG and WES appear to calculate similar G_s values. Observations derived G_{ns} do not show a clear diurnal cycle whereas ZHG scheme leads to larger values during daytime (Figure 3.7c).

As shown in Figure 3.8g, the model predicts the occurrence of more frequent wet conditions (high *RH*) than is reflected in the observations throughout the day. The model grid containing Hyytiälä (Figure 3.1) is dominated by sea/fresh water (~60%)

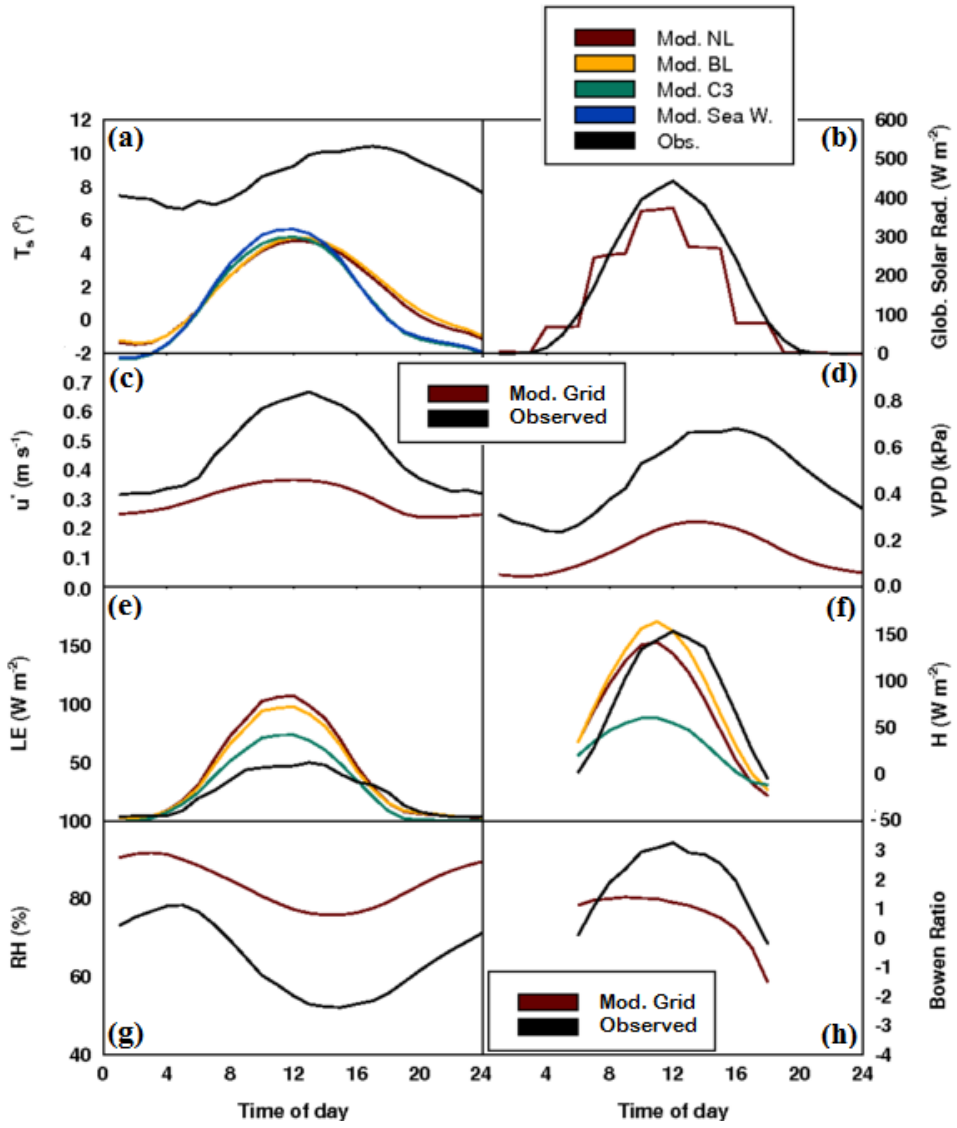

Figure 3.8. Comparison of the seasonal (spring-MAM) diurnal cycle of modelled meteorological and environmental factors with observations collected at the monitoring site of Hyytiälä, FIN, (61ºN51'N, 24ºN17'E) in 2002. '(**b)-(c)-(d)-(g)**' show modelled grid-average variables whereas (**a)-(e)-(f)** present environmental factors simulated for each surface type within the model grid. The modelled vapour pressure deficit *VPD* (**d)** was inferred using a tile surface temperature and a grid average relative humidity.

and this could potentially account for that discrepancy. According to the ZHG parameterizations implemented in UKCA (described in Sec. 2.2.7.1), in spring the

model appears to deposit more onto leaf cuticles in wet canopy conditions, leading to G_{ns} being a factor of three larger than observations.

Thus, larger *RH* and lower u_* values simulated by the model (Figures 3.8c-g), numerically explains why the model led to that difference. By contrast, simulating offline G_{cut} and $G_{inc.+s.}$ using observed u_*, *RH*, *LAI* showed that including a more realistic representation of these environmental factors led to a larger disagreement, revealing that the non-stomatal deposition onto leaf cuticles in the ZHG scheme is very sensitive to atmospheric turbulence (Figure 3.7c). This analysis might suggest that in spring in Hyytiälä the non-stomatal deposition is not driven by u_* and canopy moisture as assumed in the model (Figure 3.7c).

As with G_c, V_d diurnal variations are better captured by the WES scheme whereas the ZHG scheme led to considerable larger V_d values throughout the day, with the most significant differences calculated during daytime (Figure 3.7d). Figure 3.7d also reveals that the difference between modelled and observed V_d can be also attributed to a disagreement between modelled and observed (inferred using measured micro-meteorological variables) aerodynamic and quasi-laminar resistances R_a and R_b and may represent a further source of discrepancy. Therefore, differences in u_* and atmospheric stability factors such as (z_0/L) can lead to over prediction of R_a, R_b values (Table 3.3) contributing to the discrepancy between modelled and observed V_d.

Figure 3.9a shows that in summer, measured G_c values are high during the day with an extended maximum occurring around 10 am. Both WES and ZHG schemes successfully reproduce the observed G_c variations and daytime values with the maximum of the modelled V_d occurring later (around midday), with ZHG leading to slightly larger values during the morning and night time. Figure 3.9b reveals that modelled G_s values were higher than observations, even with the reductions imposed by the stomatal blocking implemented in the ZHG scheme.

Both modelled *LE* and *H* fluxes agreed well with observed values in summer (Figures 3.10e-f). However, observed day time *VPD* values were a factor of five higher than modelled values (Figure 3.10d) suggesting that high *VPD* could account for lower stomatal conductance values observed in Hyytiälä. This is consistent with Sturm et al. (1998) who showed that over a Scot pine forest in Germany during summer, when plants were not water stressed, the canopy conductance decreased

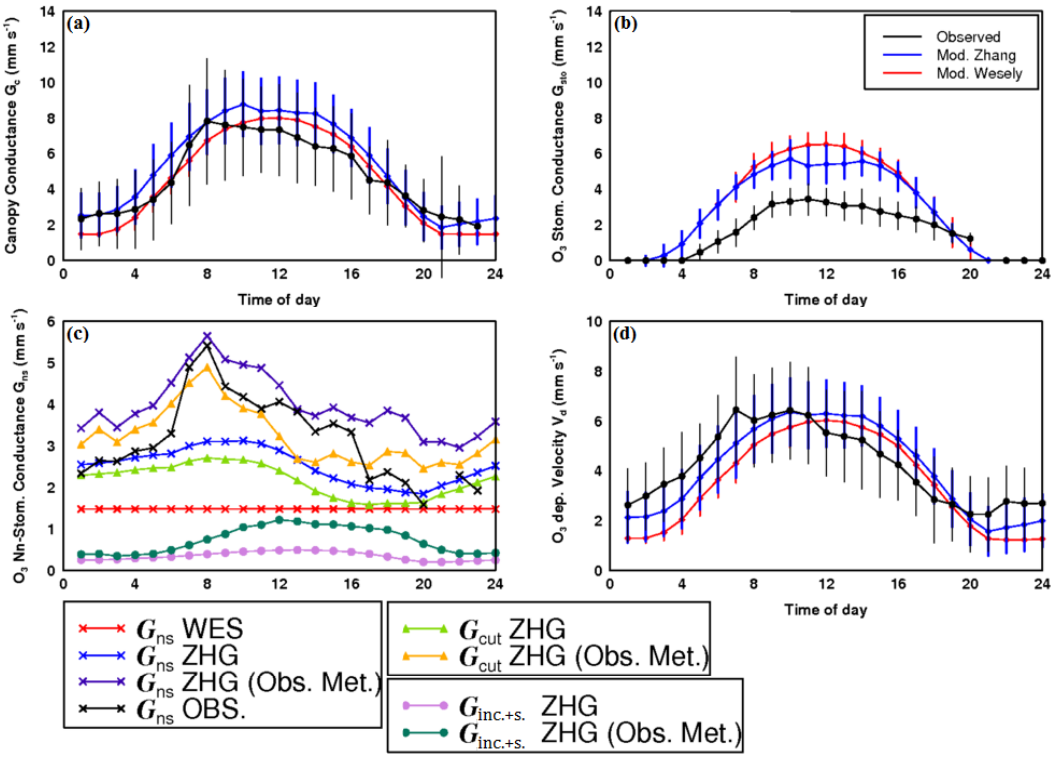

Figure 3.9. Diurnal cycles of modelled canopy conductance G_c (mm s^{-1}) (**a**), canopy stomatal conductance for O_3 G_s (mm s^{-1}) (**b**) and O_3 dry deposition velocity V_d (mm s^{-1}) (**d**) for NL tree against observed values in summer 2002 at the monitoring site of Hyytiälä, FIN, (61°51'N, 24°N17'E). Total observed and modelled non-stomatal conductance G_{ns} (mm s^{-1}) and non-stomatal conductance terms (G_{cut} and $G_{inc.+s.}$) using modelled and observed meteorological conditions (u_*, *RH* and *LAI*) are shown in (**d**).

once *VPD* reaches values around 1.1kPa, leading to stomatal closure.

Figure 3.9c reveals that the observed non-stomatal conductance rises quickly in the morning reaching the maxima value around 8 am then followed by a decrease towards evening. ZHG scheme led to larger G_{ns} values compared to WES, with the former showing an extended maxima occurring throughout the day. By contrast, once modelled offline using measured u_*, *RH* and *LAI*, G_{ns} agreed encouragingly well with measurements showing that the morning G_{ns} peak as well as its diurnal variations are better captured using the ZHG parameterizations (Figure 3.9c).

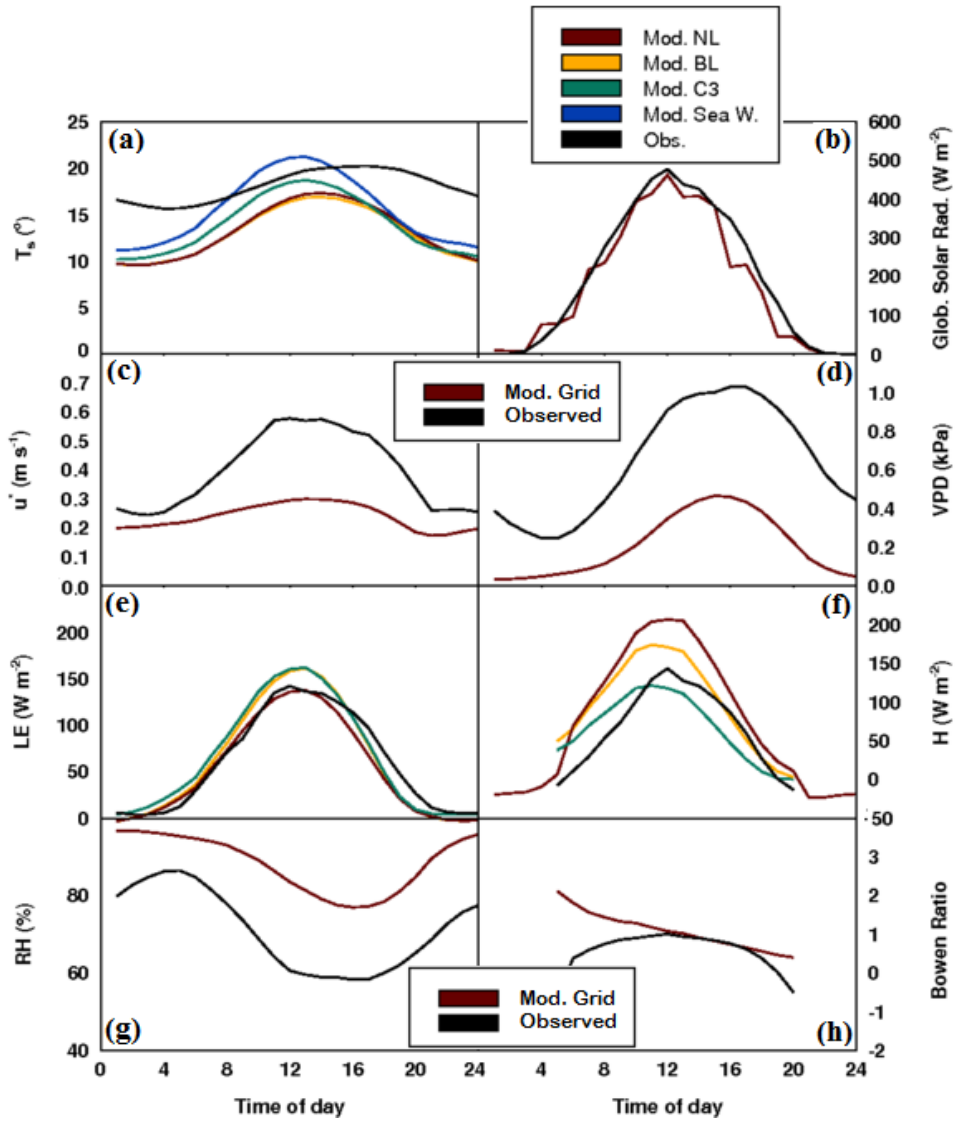

Figure 3.10. Comparison of the seasonal (summer-JJA) diurnal cycle of modelled meteorological and environmental factors against observations collected at the monitoring site of Hyytiälä, FIN, (61°51'N, 24°N17'E) in 2002.

A more realistic representation of turbulent and moisture regimes within the canopy through measured u_* and *RH*, led to an increase of O_3 deposition onto leaf cuticles in particular during the morning and towards in-canopy pathways throughout the day (Figure 3.9c). This is consistent with Altimir et al. (2006) who found that the non-stomatal O_3 deposition maxima coincided with surface wetness peaks occurring

in the morning and particularly in dry canopy conditions.

Finally, as shown in Figure 3.9d, in summer the large diurnal cycle of V_d and daytime values were well reproduced using both the WES and the ZHG schemes whereas night time values appear to be better reproduced by ZHG scheme. However, both schemes did not quite capture the midmorning V_d maximum as reported in other field studies over European coniferous forests (Pileegard et al., 1995; Touvinen et al., 2001; Keronen et al., 2003) and in N. America (Finkelstein et al., 2000). This skewness, however, could be an artefact in the measurements due to storage fluxes not being accounted for in the flux analysis.

3.4.1.3 C3 grass

Figure 3.11 compare the hourly modelled and measured G_c, G_s, G_{ns} and O_3 V_d averaged in summer (JJA) in 2002 at the grassland site of Easter Bush in the South-East of Scotland (55º52′N, 3º12′W). In summer, the observed G_c shows high values and an extended maximum occurring during the day (Figure 3.11a). Figure 3.11a also shows that measured G_c is highly variable during day time compared to night time. At this site, modelled G_c calculated using both WES and ZHG schemes exhibit a similar diurnal pattern, with the latter leading to slightly larger values except for the middle of the day. However, although UKCA captures quite well the large diurnal G_c variability, modelled G_c using both WES and ZHG scheme is underestimated in the early morning and more systematically during night time.

The G_s diurnal cycle is well captured by both WES and ZHG schemes (Figure 3.11b). However, modelled G_s values using both schemes were larger than the observed values, with the latter leading to smaller values during the day. This seems to be related to a larger surface temperature (Figure 3.12a) and a larger *VPD* (Figure 3.12d) calculated for the Easter Bush grid rather than the effect of soil moisture stress (data not available for this site), as indicated by the magnitude of the values of both observed and simulated *VPD*. In addition, modelled *LE* (Figure 3.12e) and *H* fluxes (Figure 3.12f) agree well with the observed values collected in Easter Bush (Coyle, 2005). As a result of the stomatal blocking effect implemented in the model better described in Sec. 2.2.6.1), ZHG scheme leads to a significant decrease of G_s at this site (up to -3 mm s-1) (Figure 3.11b).

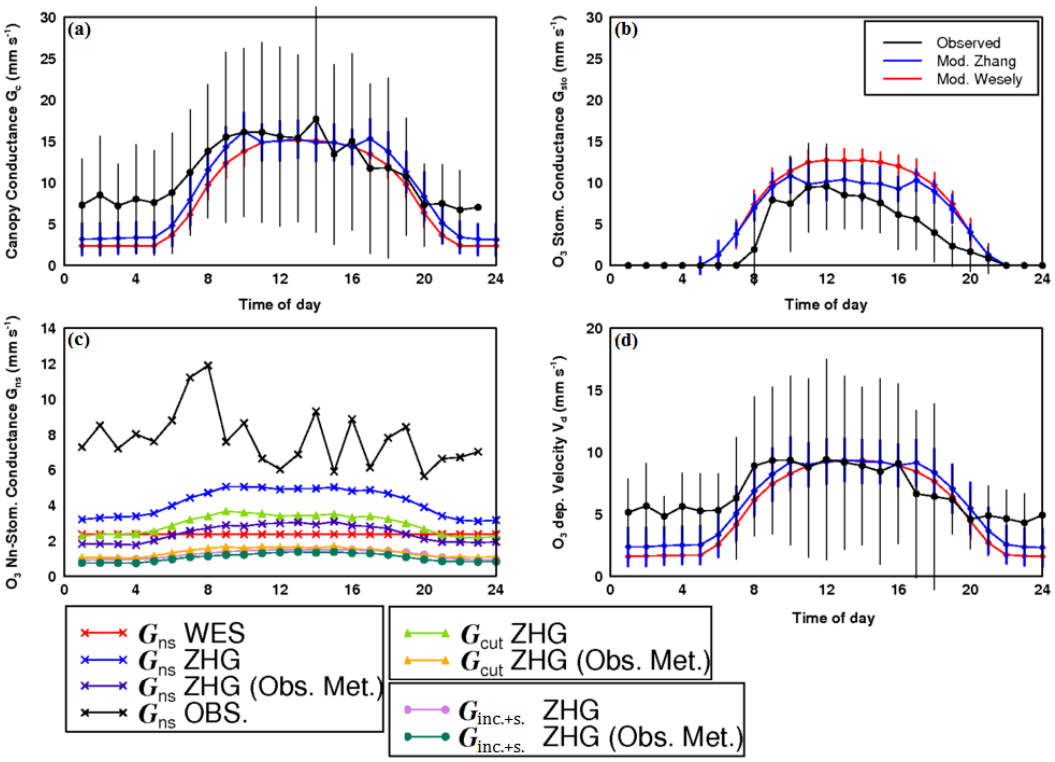

Figure 3.11. Diurnal cycles of modelled canopy conductance G_c (mm s^{-1}) (**a**), canopy stomatal conductance for O_3 G_s (mm s^{-1}) (**b**) and O_3 dry deposition velocity V_d (mm s^{-1}) (**d**) for C3 grass against observed values in summer 2002 at the monitoring site of Easter Bush, SCO, (55°52′N, 3°12′W). Total observed and modelled non-stomatal conductance G_{ns} (mm s^{-1}) and non-stomatal conductance terms (G_{cut} and $G_{inc.+s.}$) using modelled and observed meteorological conditions (u_*, *RH* and *LAI*) are shown in (**d**).

Figure 3.11c reveals that the modelled non-stomatal G_{ns} component is significantly under-predicted by the model using both the schemes, with the ZHG scheme leading to slightly larger values during the day. Figure 3.11c also shows that the observed non-stomatal conductance is fairly constant over the day, with some scatter, and an indication of a possible morning peak. This is in agreement with field studies which showed that during the growing season the stomatal term represents the dominant part of the total O_3 deposition flux over a grassland (Coyle et al., 2006; Meszaros et al., 2009) or a considerable part (47%) in summer (Plake et al, 2015).

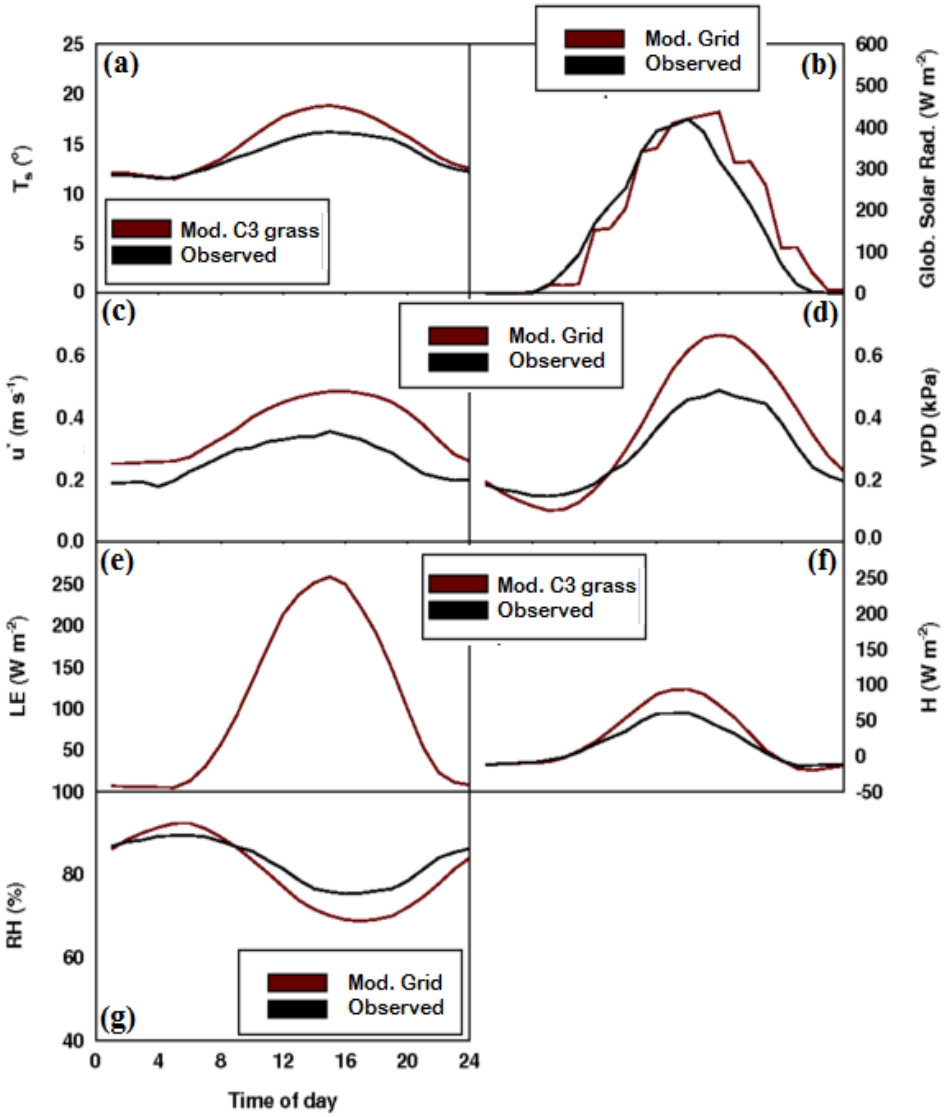

Figure 3.12. Comparison of the seasonal (summer-JJA) diurnal cycle of modelled meteorological and environmental factors with observations collected at the monitoring site of Easter Bush, SCO, (55º52'N, 3º12'W) in 2002. '(**b)-(c)-(d)-(g)**' show modelled grid-average variables whereas (**a)-(e)-(f)** present environmental factors simulated for C3 grass within the model grid. The modelled vapour pressure deficit *VPD* was inferred using the surface temperature simulated for C3 grass and the grid average relative humidity.

Other studies reported a dependence of O_3 non-stomatal deposition on *RH* with values above 60-70% leading to a larger O_3 non-stomatal component whereas values below that threshold led to more O_3 deposited towards stomata (Coyle et al., 2009;

Lamaud et al., 2009). At Easter Bush, Coyle et al. (2006) did not observe any dependence of G_{ns} on u_* over dry grass surfaces. However, that study did report a dependence of the total G_{ns} on u_* in wet canopy conditions (RH > 70%) with increasing u_* leading to an increase of the O_3 non-stomatal deposition. As shown in Figure 3.11c, this study revealed that even simulating G_{ns} off-line using measured u_*, RH, LAI led a further considerable decrease of non-stomatal deposition throughout the day, primarily due to the effect that the measured u_* was smaller than the modelled values. This indicates that the ZHG scheme did not capture some underlying processes occurring at Easter Bush. Thermal decomposition of O_3 on dry canopy surfaces which increases as the temperature increases (Fowler et al, 2001, 2009; Coyle et al., 2009) as well as O_3 aqueous chemistry occurring on the leaves due to dissolved SO_2 and NH_3 (Fuentes et al, 1992; Coyle et al., 2009), might represent O_3 sinks not resolved by the ZHG non-stomatal parameterizations.

Figure 3.11d shows that in summer observed O_3 V_d exhibits a large diurnal variability which is well reproduced by UKCA using both WES and ZHG. However, modelled night time V_d appear to be underestimated with both the schemes. As described in section 3.3.1, the uncertainties of the measured G_c ($1/R_c$) is associated with the errors on R_a and R_b which depends on u_*. As shown in Figure 3.12c, the model tends to over predict u_* leading to underestimate both R_a and R_b (Table 3.3). A different R_b parameterization used by Colye (2005) (developed for a more rough and rigid vegetation such as moorland or needle leaf trees (Garland, 1977) might also contribute to the systematic bias in R_b. This partly accounts for the large differences between modelled and observed G_c during night time and also for daytime V_d values. This is more evident in spring as the difference between modelled and observed u_* turns out to be larger (here not shown).

3.4.2 Surface O_3 evaluation

3.4.2.1 Northern Hemisphere

Figure 3.13 shows a comparison of UKCA modelled surface O_3 using the WES and the ZHG scheme against observations in the Northern Hemisphere. The seasonal cycle and absolute values of surface O_3 are simulated well by UKCA at the northern mid-latitudes with both WES and ZHG schemes, with the latter leading to a lower relative annual bias (4%) for the remote site of Mace Head (Table 3.4).

Although UKCA captures the spring maximum in surface O_3, it appears that modelled and observed surface O_3 at Mace Head are not well correlated with observations independent of the scheme, especially during summer and autumn. By contrast, O'Connor et al (2014) reported a better correlation and lower bias for that site, where the previous non-revised UKCA dry deposition scheme was used for that study.

For the polluted site of Niwot Ridge, the model appears to over predict the summer maximum by up to 27 ppb using WES and by up to 21 ppb using ZHG. A better correlation with observed surface O_3 is calculated with ZHG for Trinidad Head as well as a reduction in the annual bias compared to WES. At the northern high latitude site of Barrow, modelled surface O_3 does not agree very well with observations using both WES and ZHG.

However, the latter seems to reduce the surface O_3 bias during summer. For the background sites in the tropical regions, the seasonal cycle of the surface O_3 observations is simulated well using both WES and ZHG as shown for the sites of Mauna Loa and Barbados. However, modelled surface O_3 at the Barbados is systematically overestimated by as much as of 30 ppb with WES and by up to 22 ppb with ZHG, the latter led to a smaller annual bias and a slightly better correlation for this site.

By contrast, the model performs better at Mauna Loa using WES, apart from the first two months of the year. For the Capo Verde grid, the model shows large surface O_3 during the summer. This may be related to O_3 transported from the African continent as a result of emission from biomass burning and industrial activities, which appear

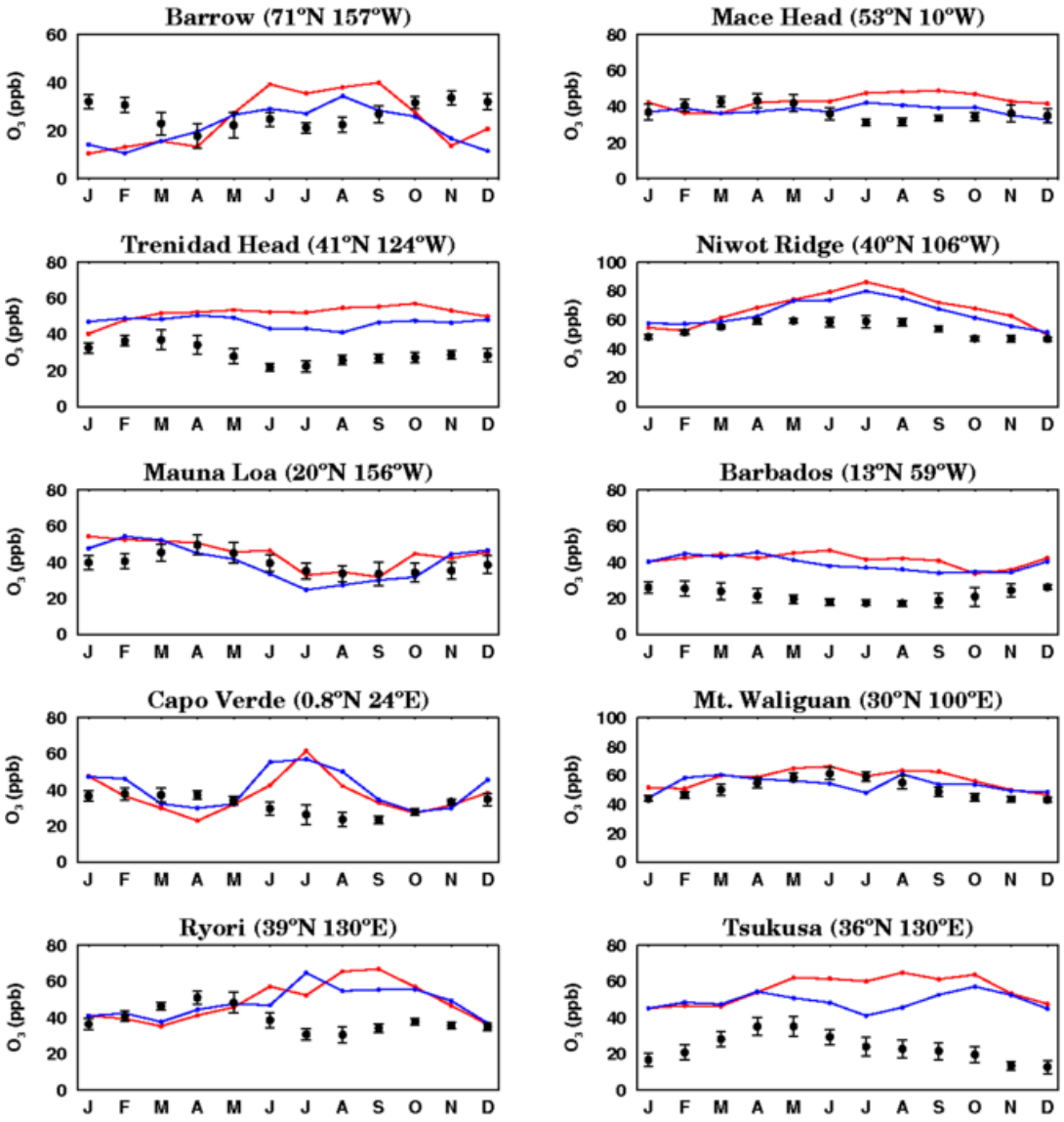

Figure 3.13. Comparison of annual monthly mean surface O_3 concentrations (ppb) simulated using WES (in red) and ZHG (in blue) schemes against observations measured at North Hemisphere monitoring sites. Black dots indicate observed monthly mean O_3 concentrations. Black vertical bars show the standard deviation of the observed values within the period of measurement (Table 3.2). The annual mean bias (%) and the correlation coefficients are summarized in Table 3.4.

Table 3.4. Relative annual mean bias between modelled surface O_3 using WES and ZHG schemes and observations (in %); correlation coefficients *r* between modelled monthly mean surface O_3 concentrations simulated using WES and ZHG schemes and observed values measured at NH monitoring sites.

NH sites	Bias WES (%)	Bias ZHG (%)	*r* WES	*r* ZHG
Barrow	-2	-13	-0.33	-0.50
Mace Head	19	4	-0.77	-0.34
Trinidad Head	84	64	-0.43	0.72
Niwot Ridge	25	20	0.73	0.75
Mauna Loa	13	-37	0.70	0.63
Barbados	97	84	-0.20	0.44
Capo Verde	22	33	-0.31	-0.24
Mt. Waliguan	14	7	0.84	0.34
Ryori	31	29	-0.53	-0.51
Tsukusa	160	133	0.33	0.18

to affect the overall grid cell but not the actual Capo Verde monitoring site.

In East Asia, modelled surface O_3 agrees very well with observations over Mt. Waliguan, with both the seasonal cycle and absolute values well reproduced by the model using both the schemes. However, the ZHG results in a lower correlation with observations (Table 3.4). Over Japan (Ryori, Tsukusa), the model shows a poor capability to simulate surface O_3 observations although ZHG seems to reduce the bias during summer and to slightly improve the correlation of modelled surface O_3 against observations at the site of Tsukusa (Table 3.4).

3.4.2.2 Southern Hemisphere

Figure 3.14 presents a similar comparison of modelled surface O_3 with observations collected in the Southern Hemisphere. The model simulates well the seasonal variations surface O_3 at the Indonesian site of Bukit Koto Tapang, with WES scheme

Table 3.5. Relative annual mean bias between modelled surface O_3 using WES and ZHG schemes and observations (in %); correlation coefficients *r* between modelled monthly mean surface O_3 concentrations simulated using WES and ZHG schemes and observed values in the SH sites.

SH sites	Bias WES (%)	Bias ZHG (%)	*r* WES	*r* ZHG
Bukit Koto T.	44	56	0.81	0.69
Mt. Kenya	-	-	-	-
St. Lorenzo	103	114	0.36	0.58
El Tololo	42	48	0.2	0.57
Cape Point	64	82	0.19	0.48
Cape Grim	47	64	0.33	0.78
Lauder	59	70	-0.37	-0.44
Ushuaia	49	66	0.65	0.84
Syowa	18	29	-0.18	0.53
South Pole	-1	9	-0.43	-0.15

leading to a lower annual bias (44%) and better correlation with observed values compared to ZHG (Table 3.5). In S. America (St. Lorenzo, El Tololo, Ushuaia), the model performance is not very good. The model fails to capture the observed surfaceO_3 seasonal cycle with both the schemes. Modelled surface O_3 bias using both WES and ZHG scheme is larger during the southern hemisphere summer compared to the winter (by up to 20 ppb). A similar positive surface O_3 bias with observations was reported by Pacifico et al. (2015) over the Amazon forest, although a different UKCA model configuration, chemistry scheme and emissions were used for that modelling study. The ZHG scheme slightly improved the correlation between modelled and observed surface O_3 for the S. America sites, but it led a large positive bias. For the African sites of Cape Point and Mt. Kenya the model largely overestimates the absolute surface O_3 values, failing to capture the observed seasonal variations. The model performs similarly over Lauder, although the discrepancy between modelled and observed surface O_3 especially in the SH winter.

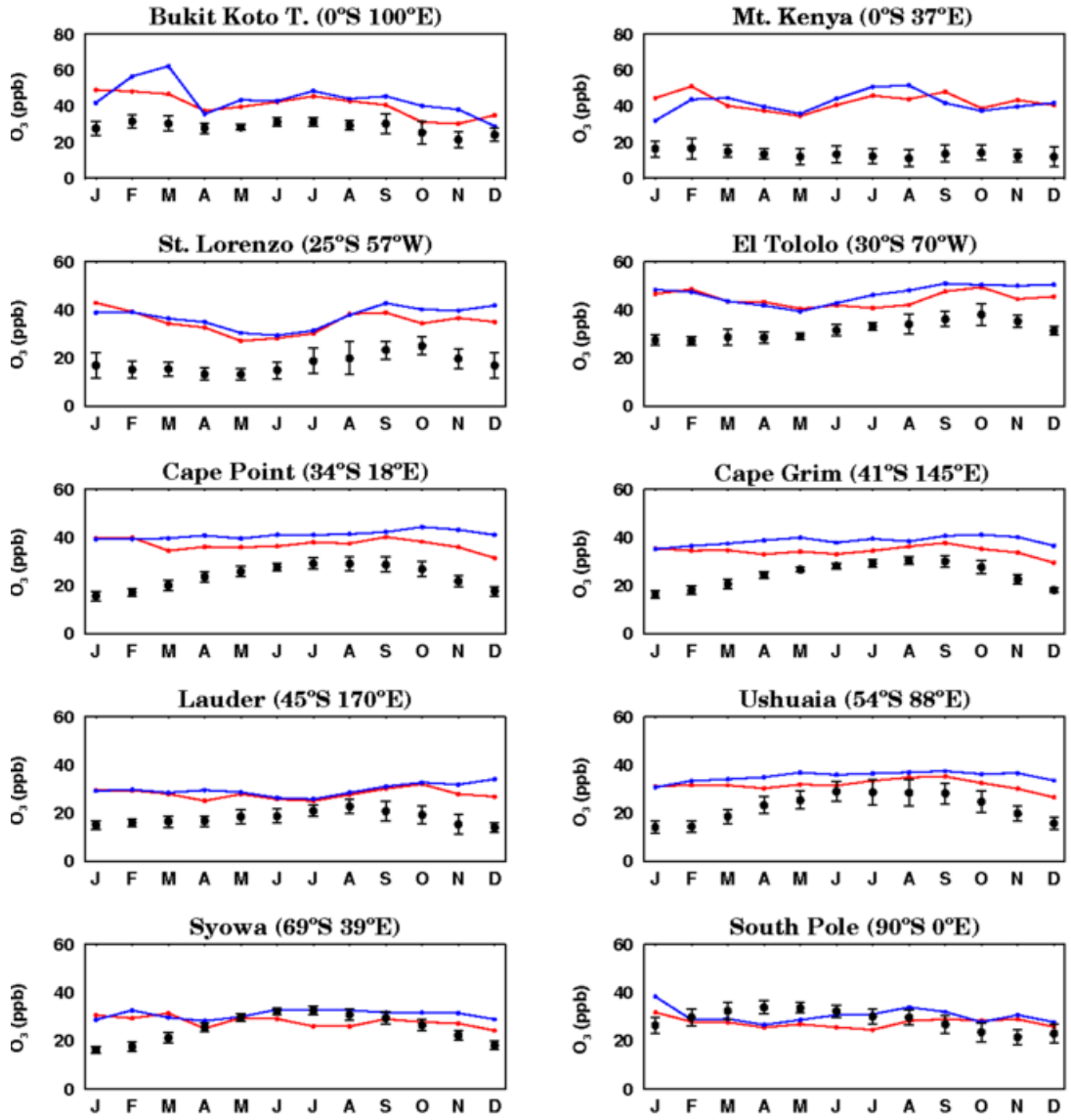

Figure 3.14. Comparison of annual monthly mean surface O_3 concentrations (ppb) simulated using WES (in red) and ZHG (in blue) schemes against observations measured at North Hemisphere monitoring sites. Black dots indicate observed monthly mean O_3 concentrations. Black vertical bars show the standard deviation of the observed values within the period of measurement (Table 3.2). The annual mean bias (%) and the correlation coefficients are summarized in Table 3.5.

3.4.3 Partitioning of the O_3 deposition flux: WES vs ZHG

Figure 3.15 presents a comparison of the seasonal variations of the fraction of O_3 deposition occurring via stomatal and non-stomatal pathways as simulated using the WES and ZHG schemes for three model grids including monitoring sites mainly covered by C3 grass (Easter Bush), coniferous forest (Hyytiälä) and a broadleaf forest (Castelporziano), together with the estimate derived from the observations.

As with the previous comparisons, measured and modelled data have both been filtered for periods during which the measurements are invalid and all monthly averages may be biased towards more turbulent conditions, in particular during night.

At Easter Bush, the modelled stomatal term using the WES scheme shows a larger relative contribution than predicted by the ZHG scheme during summer with the latter leading to stomatal fractions which are closer to observations (Coyle et al., 2006). At Easter Bush, the overall non-stomatal component of the total O_3 flux increased considerably using the ZHG (+80% on annual average) compared to the WES scheme, with the larger differences calculated by the model in summer and in autumn. As shown in Figure 3.15b, the modelled O_3 non-stomatal deposition over C3 grass calculated with the ZHG scheme (62%) was closer to the observed value (59%) on annual average (Coyle, 2005) and is consistent with Fowler at al. (2001) who reported that 60-79% of the total O_3 flux over a nearby moorland in the SE of Scotland (Auchencorth Moss) was constituted by the non-stomatal component. Both sites fall into the same model grid cell and would be considered as C3 grasslands by the model.

Figure 3.15d shows that at Hyytiälä, during the growing season the modelled stomatal component of the total O_3 flux to needle leaf forest using the WES scheme represents around 60% of the total O_3 flux on average. By contrast, the ZHG scheme led to an increase of the non-stomatal fraction (up to 60%) on average compared to WES throughout the growing season (Figure 3.15e).

However, substantial differences in the partitioning of the simulated stomatal and non-stomatal O_3 deposition between the schemes were found during spring and summer. Because the stomatal exchange is modelled similarly within both schemes

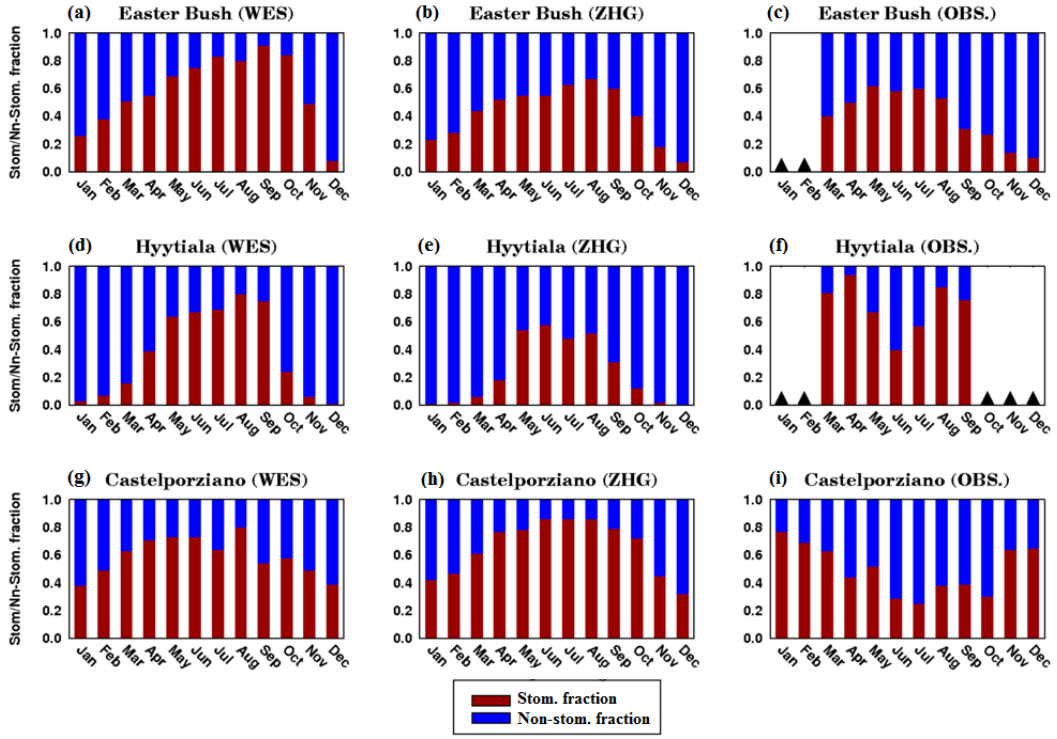

Figure 3.15. Partitioning of monthly mean deposition occurring towards stomatal (shown in red) and non-stomatal (shown in blue) pathways as simulated by UKCA using WES and ZHG schemes compared to observations for three model grids including the following vegetation types: C3 grass (top (**a-b-c**) at Easter Bush, (55N 3.75E), needle leaf forest at Hyytiälä,(62.5N 22.5E) (middle (**d-e-f**) and broadleaf forest at the monitoring site of Castelporziano (42.5N 11.25E) (bottom (**g-h-i**).'▲' indicates that the O_3 flux partitioning was not possible due to missing observed data.

(except for the additional blocking by water layers added in the ZHG predicting larger non-stomatal deposition). As shown in Figures 3.15d-e, the WES scheme showed a larger stomatal seasonal cycle with a maximum of the stomatal uptake predicted in summer whereas ZHG scheme led to lower stomatal fraction in spring (Mar-Apr.-May) than in summer.

At Hyytiälä, the O_3 non-stomatal component calculated using the ZHG scheme considerably increased in summer compared to WES scheme which was closer to observations (Rannik et al., 2012) but it appears to overestimate the non-stomatal fractions compared to observations in spring and in the early autumn. By contrast, in

the same periods both stomatal and non-stomatal fractions modelled with WES scheme seem in better agreement with the observed values (Altimir et al., 2006; Rannik et al., 2012). According to Rannik et al. (2012), the average (from 2001 to 2010) non-stomatal component contribution to the total O_3 canopy conductance during the growing season comprised from 25% to 45%.

Altimir et al. (2006), who made eddy-covariance measurements at the site from 2002 to 2003, reported similar O_3 non-stomatal conductance values throughout the growing season. Taking into account the night-time O_3 non-stomatal deposition values, Altimir et al. (2006) calculated that the O_3 non-stomatal component contribution varied from 25% to 42% in dry conditions (RH < 70%) to 59-65% under wet conditions. Figures 3.8g and 3.10g showed that the model tends to predict more frequent wet conditions and this might partly explain why the ZHG scheme leads to larger O_3 non-stomatal deposition estimates than WES in these periods.

As shown in Figures 3.15g-h, at the Mediterranean forested site of Castelporziano, the modelled stomatal term using both the WES and the ZHG scheme was always larger than the non-stomatal component in spring and in summer. The ZHG scheme led to a decrease of the non-stomatal component in summer compared with the WES scheme. In summer, both schemes predicted small contributions of the non-stomatal deposition (28% WES scheme; 14% ZHG scheme) on average whereas the observations made at Castelporziano suggest that non-stomatal O_3 deposition represents the dominant part of the total O_3 flux (up to 70%) (Gerosa et al., 2005, 2009; Fares et al., 2014). By contrast, in the cooler season the discrepancy between modelled and observed stomatal and non-stomatal components appear less evident (not-shown).

The observation-derived O_3 non-stomatal deposition component is calculated as the residual of the canopy conductance deprived of its estimated stomatal component (Fowler et al., 2001; Gerosa et al., 2005, 2008; Fares et al., 2014). As discussed in more detail above, the Mediterranean evergreen Holm Oak forest experiences severe water stress which results in reduced stomatal opening, limiting evapotranspiration and the stomatal ozone flux and this is not reflected in the modelled soil moisture. Magnani et al. (1998) showed that in summer the canopy stomatal conductance over the aforementioned mature beech forest in the centre of Italy reached values up to

10 mm s^{-1} in the morning, which is more in line to that simulated by the model for BL tree (Sec. 3.4.1.1). Similarly, Coyle et al. (2006) reported that at Alice Holt, an Oak forest in the SE of England, in summer the O_3 stomatal component was frequently larger than the non-stomatal term (median 40-50% of the total flux). Therefore, not properly representing the environmental conditions along with an improper representation of the vegetation types within the model, might account for such a large difference between partitioning of the modelled and observed O_3 flux over BL forests.

3.4.4 Effect of the grid resolution, generic land characteristics and model nudging

This study attempts to isolate the relative uncertainties associated with model inputs and model structure on the performance of the O_3 non-stomatal dry deposition parameterisation against measurements. It is obvious that a global model will never be able to reproduce the conditions at a particular measurement site completely. One uncertainty relates to the very limited number of land cover types (LCs), an aspect where the UKCA implementation adds further uncertainty to the original models of Wesely (1989) and Zhang et al. (2003), both of which were formulated for a more detailed classification. Table 3.6 compares the *LAI* assigned by the MOSES2.2 land surface module in comparison with measurements, revealing considerable differences for individual sites. Similarly, semi-natural moorland, agricultural grassland and C3 crops would all be described by a single land cover class (C3) irrespective of plant species, management or nitrogen input. Further uncertainty is introduced by the limited spatial resolution and the fact that certain parameters are only predicted at the grid cell level, which are very large (~280 x 390 km at mid-latitudes) and not for each LC type individually. Crucially, the deposition schemes as implemented in UKCA use a single value of u_* and surface *RH* for all LC types within a grid cell. For all the measurement sites considered in this work, the average modelled grid value of u_* tends to represent an overestimate for short vegetation types and an underestimate for forest sites, and switching to a measured value of u_* greatly improved the performance of the non-stomatal conductance parameterization of the ZHG scheme (G_{ns} of the WES scheme is insensitive to u*) (Figures 3.2, 3.5

Table 3.6. Comparison of model prescribed (**M**) and observed (**O**) single-sided Leaf Area Index (*LAI*) (m^2 m^{-2}) values. (*****) represent *LAI* values modelled using observed canopy heights measured at Easter Bush (Coyle, 2005).

	BL tree						**NL tree**						**C3 grass/ crop**					
	Castelporziano		**Harvard F.**		**Alice Holt**		**Hyytiälä**		**Ulborg**		**Blodgett F.**		**Easter Bush***		**Sarrazola**		**Comun Nuovo**	
	M	**O**	**M**	**O**	**M**	**O**	**M**	**O**	**M**	**O**	**M**	**O**	**M**	**O**	**M**	**O**	**M**	**O**
Jan.	3.8	3.7	0.9	na	2.2	na	3.8	6.0	3.7	na	3.9	na	1.8	0.6	2.5	na	1.3	na
Feb.	3.8	3.7	1.3	na	2.2	na	3.8	6.0	3.8	na	3.8	na	1.8	0.6	2.4		1.2	na
Mar.	3.9	3.7	1.6	na	2.3	na	3.9	6.0	3.9	na	3.9	na	1.7	0.6	2.5		1.3	na
Apr.	4.1	3.7	2.6	na	3.4	na	4.1	6.0	4.0	na	4.2	na	2.4	1.0	2.6		2.1	
May	4.3	3.7	5.0	na	4.8	na	4.3	7.0	4.2	na	4.8	na	2.9	2.3	2.5		3.1	2.0-5.5
June	5.1	3.7	7.3	3.4	5.1	5.0	5.1	8.0	5.3	8.0	5.2	na	3.8	1.3	1.9	2.5-4.5	3.6	
July	6.0	3.7	7.2	3.4	4.5	5.0	6.0	8.0	5.8	8.0	5.2	na	3.8	1.8	1.6		3.7	
Aug.	5.3	3.7	7.2	3.4	4.0	5.0	5.3	8.0	5.3	8.0	5.1	na	3.4	1.2	1.4		3.4	na
Sep.	4.6	3.7	6.9	na	3.7	na	4.6	7.0	4.8	na	5.0	na	2.9	1.1	1.3		3.0	na
Oct.	5.0	3.7	4.4	na	3.2	na	5.0	6.0	4.5	na	4.6	na	2.3	0.7	1.6		2.3	na
Nov.	3.9	3.7	2.6	na	2.8	na	3.9	6.0	4.4	na	4.3	na	2.9	0.6	2.0	na	1.8	na
Dec.	3.8	3.7	1.9	na	2.9	na	3.8	6.0	3.8	na	4.0	na	1.8	0.4	2.2	na	1.4	na

Table 3.7. Modelled prescribed (**M)** and observed (**O**) canopy heights (m) for the model grids and monitoring sites considered for this study.

	Canopy height, h_c (m)	
BL tree	**M**	**O**
Castelporziano	11.4	14.9
Harvard F.	19	20.0
Alice Holt	13.2	18
NL tree		
Hyytiälä	17.4	14-18
Ulborg	8.9	na
Blodgett F,	20.9	4-7
C3/Crop		
Easter Bush	1.0	0.05-0.4
Sarrazola	1.2	0.1-0.8
Comun Nuovo	1.3	0.2-1.0

Table 3.8. Modelled prescribed (**M)** surface type and observed (**O**) roughness properties for the model grid and monitoring sites considered for this study.

	Roughness length z_0 (m)	
BL tree	**M**	**O**
Castelporziano	0.57	1.49
Harvard F.	0.95	1
Alice Holt	0.66	na
NL Tree		
Hyytiala	0.85	0.93
Ulborg	0.45	na
Blodgett F.	1.05	(0.2-0.35)
C3/Crop		
Easter Bush	0.1	0.005-0.04
Sarrazola	0.12	0.01-0.08
Comun Nuovo	0.13	0.02-0.1

and 3.9). The degree to which u* is incorrectly estimated for a given site depends on the LC mix in the particular grid cell.

Miao et al., (2006) clearly showed that modelled O_3 V_d is influenced by the land cover and synoptic weather conditions, revealing that the model resolution accounts for systematic differences in diurnal variations of modelled O_3 V_d using ZHG scheme. In addition, the different representation of u_* along with canopy height (Table 3.7) and roughness properties (Table 3.8) within the model also appear to contribute to systematic uncertainties between modelled and observed R_a ($z - d$) which also depends on the stability parameter (z/L) and R_b (MRB; Table 3.3).

By nudging the UKCA model with meteorological ECMWF ERA-40 re-analysis data (Telford et al., 2008), the model showed a good capability of reproducing the diurnal cycle of the net incoming solar radiation. However, differences between modelled (for each surface type) surface temperature T_s and relative RH (grid average) against observed values were found particularly during daytime.

According to Telford et al., (2008), the dynamic variables (temperature, zonal wind u and meridional wind v) were adjusted towards ECMWF ERA-40 re-analysis data but

this process does not involve all model levels. This results in no nudging being applied above ~50 km and below the lowest levels constituting the boundary layer (~3 km), which might account for the discrepancy between modelled and observed T_s values. Model nudging was reported to produce a better representation of the atmosphere, reducing the bias of variables not directly adjusted such as vertical wind q ($\omega = dP/dt$) and improving the correlation in time of rain precipitation (Telford et al., 2008), which appear to be captured as shown in Figure 3.4 for the Mediterranean site of Castelporziano, although some differences still exist.

As shown in Table 3.6, this study also highlighted inconsistencies in the area of the surface taking part in the dry deposition process (both stomatal and non-stomatal pathways) per unit ground area (i.e. *LAI*). In the model the canopy stomatal conductance is modelled scaling the leaf-level stomatal conductance up to the canopy level assuming that the incident radiation attenuates through the canopy following the Beer's Law (Cox et al., 1998, 1999). However, Mercado et al. (2007, 2009) reported that this approach may lead to unrealistic diurnal cycle of photosynthesis and hence evapotranspiration. Hence, a different representation of vegetation within the model through *LAI* might also contribute to the discrepancies between modelled and observed G_s for O_3 as well as G_{ns} simulated with both WES and ZHG scheme as they also scale with *LAI*. Furthermore, this might also partly explain the large modelled *LE* flux (Figure 3.3) as the latent heat flux *LE* is made by a combination of transpiration and bare soil evaporation and their relative contributions depends on the density of the leaves (i.e. *LAI*) (Best et al., 2011).

The representation of the soil properties in MOSES 2.2 might represent another source of inconsistency with that observed in the field. MOSES 2.2 has three soil texture types (fine, medium and coarse) and the sand/silt/clay fractions were derived from 1° x 1° soil classes of Wilson and Henderson-Sellers (1985) then re-gridded to 3.75° x 2.5°. A considerable difference was found between modelled soil moisture content at the root zone and measured values as shown at the Castelporziano site (Figure 3.4). This site has a soil composition of 80% sand and 20% clay and a slightly more superficial root distribution (~1 m) compared to the model (3 m). Therefore, these inconsistencies might also contribute to the large differences between modelled and observed G_s which were found for that site. This is important

as properly modelling the soil water status and the influence of drought conditions on the stomatal function also relies upon the characteristics of the environment (i.e. soil texture and related capability of the soil to hold water, vegetation specific density and structure of the roots) being accurately represented within the model (Büker et al., 2012).

3.4.5 Analysis of the ozone deposition parameterization performances

The ability of MOSES2.2, driven with the climate model meteorology, to reproduce the measurement-derived stomatal conductance differs greatly between sites and seasons, for different reasons: performance was good for the coniferous forest at Hyytiälä in spring and reasonable for the Easter Bush grassland. By contrast, the model overestimated G_s greatly for the broadleaf forest at Castelporziano (both in spring and in summer), and also significantly for Hyytiälä in summer.

As discussed above, there is strong evidence to suggest that drought stress resulted in stomatal closure at the Italian site and that this is poorly represented in the model calculations. In addition, *RH* was greatly overestimated (and *VPD* underestimated) at Hyytiälä (probably due to the presence of lakes in the grid cell), with difference at Castelporziano in the opposite direction and possibly due to the dominance of non-forest vegetation.

By contrast, driving the ZHG non-stomatal ozone deposition routines with measured meteorology it was also possible to assess their structural correctness, within the error limits of the measurement-derived values of G_{ns}. The ZHG G_{ns} scheme performed well for Hyytiälä in summer (Figure 3.9c), but greatly overestimated measurement-derived values during spring (Figure 3.7c). At Castelporziano, G_{ns} values were well represented during spring (Figure 3.5c) and of the right magnitude during daytime in summer (Figure 3.2c), but the diurnal cycle was markedly different. This could, however, be due to the effect of measurements not having been corrected for storage effects. At the Easter Bush grassland site, moving to measured meteorology deteriorated the measurement/model comparison further, with the model underestimating the non-stomatal sink (Figure 3.11c).

Overall, the WES scheme performed better for G_{ns} than the ZHG scheme at Hyytiälä during spring. The ZHG scheme performed better than WES at Castelporziano during spring and Hyytiälä during summer, but only after it was driven with observed meteorology. At Castelporziano in summer, the ZHG scheme as driven with the modelled meteorology performed poorly and after switching to measured meteorology performance was of similar quality as the WES prediction, but both showed diurnal cycles that differed both with each other and the measurement derived estimate.

There are processes which are known to be lacking even in the ZHG scheme. For example, O_3 non-stomatal pathways which are yet not captured are: (i) thermal decomposition of O_3 on dry surfaces which increases as the temperature increases (Fowler et al, 2001, 2009; Cape et al., 2009; Coyle et al., 2009); (ii) O_3 aqueous chemistry occurring on the leaf cuticles (Fuentes et al., 1992, 1994; Altimir et al., 2006; Coyle, 2005,; Coyle et al., 2009); (iii) in-canopy O_3 chemistry reactions mediated by biogenic volatile organic compounds (bVOC) (Kurpius and Goldestein, 2003; Fares et al., 2009, 2010a, 2014; Gerosa et al., 2009); (iv) the additional O_3 sink due to reaction with NO emitted from canopy soil (Gerosa et al., 2009; Fumagalli et al., 2016). In addition, the presence of snow thawing on the leaves and on the soil below the canopy may represent a further O_3 chemical sink (Albert et al., 2002), which appears not be simulated by the ZHG scheme.

The lack of representativeness of the ZHG scheme for some sites and seasons may be also explained in terms of the approach used to derive the parameterizations. In fact, these were derived using measurements over five different vegetation canopies in the US (mixed forest, deciduous forest, corn, soybean and pasture) and correlating measured canopy resistance values with some local environmental factors (u_*, *LAI*, *RH*, leaf surface wetness, solar radiation) (Zhang et al.,2002b). Furthermore, Zhang et al., (2002b) pointed out that other potential dependencies on canopy structure, local in-canopy chemistry reactions and other environmental variables might be important but they were not measured in that study.

A multivariate analysis of G_{ns} against some environmental factors revealed that in Hyytiälä surface temperature T_s, *VPD* and monoterpene concentration were significant variables in explaining at least the seasonal variability of the O_3 non-

stomatal deposition (Rannik et al., 2012). Although some progress has been made in better understanding the potential drivers of the O_3 non-stomatal deposition (Kurpius and Goldestein, 2003; Coyle et al., 2009; Fowler et al., 2009; Fares et al., 2010a), a mechanistic representation of these processes in GCMs and CTMs still remains unresolved.

3.4.6 Should the ZHG scheme be used in place of the WES scheme?

The ZHG scheme, as the more dynamic and more mechanistic representation of the deposition process, ought to capture inter-site variability better than other approaches, which typically assign constant values to the non-stomatal resistances (Fowler et al., 2009). Therefore, in this study ZHG scheme was considered more suited to explore the effect of meteorology and, by extension, changing climate on the O_3 deposition sink.

The results of this study showed that the ZHG scheme may not provide a generic improvement of WES on a site-by-site basis because the site-specific input parameters cannot adequately be reproduced, and highlighted that accurately simulating the driving meteorology is fundamental to better represent the O_3 deposition using ZHG, with particular regards to the non-stomatal component, especially to forests. In addition, the results of this analysis indicate that ZHG may lead to an improved average O_3 deposition sink, with a more mechanistic partitioning of the total O_3 flux between its stomatal and non-stomatal components.

However, due to the variability in the results presented here, it was not possible to conclude whether ZHG could represent as an alternative to the WES scheme in UKCA.

More long-term measurements (detailed in in Section 5.2.1) are needed to provide a generic improvement of both WES and ZHG schemes in UKCA and to further assess both the approaches against observations, especially over vegetated rural areas in the NH and over tropical regions where the model showed the most significant changes in O_3 deposition as a result of the change of scheme (Chap. 2). An analysis of large amount of well-quality O_3 flux datasets (full seasonal cycle) and other parameters across different vegetation types (at mid-high latitudes in the NH and over tropical

regions) and climate conditions are fundamental to derive more mechanistic O_3 deposition parameterizations. In addition, a better understanding of the O_3 interactions with leaf surface films and the in-canopy O_3 chemistry interactions mediated by bVOC through field measurements and laboratory experiments is urgent to help developing the representation of the O_3 dry deposition in GCMs (better detailed in Section 5.3.1).

3.4.7 Recommendations

Based on these study results, the following recommendations are provided for future UKCA global O_3 dry deposition and surface modelling studies:

- Land cover specific u_* and explicit vegetation type heat flux H calculations should be included in the UKCA dry deposition simulations. Implementing a specific vegetation type H and assuming a logarithmic wind profile within the boundary layer, would allow u_* to be expressed as a function of the mean wind speed and the stability function Φ_m (z/L) (Bassin et al., 2004). Although the simultaneous calculation of u_* and Φ_m may require an iterative procedure as L is a function of u_* and Φ_m (Bassin et al., 2004), this approach should lead to a more realistic influence of u_* on the aerodynamic and quasi-laminar layer resistance terms as well as to a better representation of the O_3 non-stomatal deposition component (as shown for forested sites with the ZHG dry deposition scheme).

- The version of the model used for this study included a limited number of land cover types which added further uncertainty to the original Wesely (1989) and Zhang et al. (2003) models, first developed for a more detailed classification. A more recent version of the land surface model (JULES 3.2) incorporates 11 plant functional types (including distinction between deciduous and evergreen forest for temperate/tropical broad leaf forests and deciduous and evergreen for needle leaf forests). Therefore, this configuration should be used in the future O_3 dry deposition modelling studies. An equivalent land cover type classification is also highly recommended within UKCA.

- A comparison of the modelled canopy stomatal conductance for O_3 against observations revealed that the model tends to produce large values especially for forest vegetation sites. This might be related to the leaf level canopy conductance being scaled up to the canopy level assuming that the incident radiation attenuates through the canopy following the Beer Law (Cox et al., 1998, 1999). A multi-layer canopy photosynthesis approach with the two stream radiation model might represent a further improvement in the future O_3 dry deposition studies as this leads to a better representation of light response and diurnal cycles of canopy photosynthesis and to an improvement of stomatal and canopy conductance (Jogireddy et al., 2006; Mercado et al., 2007).

- In this study, inconsistencies were found in canopy height (h_c) and the leaf area index (*LAI*) between modelled and observed values. As these are environmental factors taken into account in both the stomatal and non-stomatal O_3 deposition, remote sensing data of both variables with a higher spatial and temporal resolution could be considered as input for the UKCA dry deposition modules. Improving the consistency of the modelled roughness length z_0 (vital for several related micrometeorological variables) with observations is also advisable.

- A considerable discrepancy between the modelled soil moisture content (*SMC*) at the root zone and the observed value in a Mediterranean site was found in this study. A thorough calculation of this parameter is fundamental as it affects the stomatal conductance aperture through the water stress factor β (Cox et al., 1999; Best et al., 2011). In the future, a more detailed assessment of the current capability of the land surface model MOSES 2.2 (JULES) to simulate *SMC* is desirable.

3.5 Conclusions

In this study, the performance of two widely used dry deposition parameterizations (WES and ZHG scheme) was assessed against measurements over temperate broadleaf and needle leaf forests and C3 grass/crop sites in Europe and two forested

sites in N. America. The implementations of both schemes were compared with observations focusing on the diurnal and seasonal variations of the O_3 dry deposition velocity terms and the partitioning of the O_3 deposition flux between stomatal and non-stomatal components. The emphasis of this analysis has been on characterizing inconsistencies in site meteorology caused by the low spatial model resolution, limitations due to the use of generic vegetation type properties and problems with the parameterizations of the dry deposition schemes. The main conclusions of this evaluation study can be summarized as follows:

- Both the WES and ZHG schemes capture well G_c diurnal variability, although differences were found between sites, season and time of the day. The larger discrepancies between modelled G_c (using the WES and the ZHG scheme) and observations were detected over the Holm Oak forest site of Castelporziano (MAE ~ 2.2 mm s^{-1}) and over the Pine plantation site of Blodgett Forest (MAE ~ 3.5 mm s^{-1}).
- This study tested the ability of the land surface model MOSES 2.2 to simulate the measurement-derived O_3 canopy stomatal conductance G_s with results that differ between sites and season. Performance was good for the coniferous forest at Hyytiälä in spring and reasonable for the Easter Bush grassland. By contrast, the model overestimated G_s greatly for the Mediterranean broadleaf forest at Castelporziano (both in spring by a factor of two (~ 4 mm s^{-1}) and in summer by a factor of four (~ 6 mm s^{-1}), and also significantly overestimated for the needleleaf forest at Hyytiälä (in summer by a factor of two e.g. ~ 3 mm s^{-1}). Discrepancies between modelled and observed soil moisture content at the root zone and vapour pressure deficit appear to be responsible for the inadequate stomatal closure simulated at Castelporziano and Hyytiälä respectively.
- The seasonal variations of the fractions of O_3 deposition occurring via stomatal and non-stomatal pathways simulated using the WES and ZHG schemes were compared to observations. The ZHG scheme increased the O_3 non-stomatal deposition by up to 60% over the coniferous forest site at Hyytiälä and over the grassland site at Easter Bush as much as of 62% on annual average compared to WES. Although differences were found between the two schemes in spring and

in summer, the fraction of the non-stomatal deposition simulated with ZHG for NL tree and C3 grass at Hyytiälä and Easter Bush is closer to observations (Fowler et al, 2001; Coyle, 2005, Rannik et al., 2012) than WES. By contrast, the modelled O_3 non-stomatal component at Castelporziano was always smaller (28% WES; 14% ZHG) than the stomatal fraction compared to observations (up to 70%) on annual average.

- Off-line sensitivity simulation tests were conducted on the O_3 non-stomatal deposition (G_{ns}) and its leaf cuticles (G_{cut}) and in-canopy+soil ($G_{inc.+s.}$) components simulated using the ZHG scheme. By driving the ZHG scheme with real environmental factors (*RH*, u_* and *LAI*), G_{ns} calculated with ZHG performed better for than WES at Castelporziano during spring and at Hyytiälä during summer. By contrast G_{ns} simulated with WES scheme performed better than ZHG scheme at Hyytiälä during spring. At the Easter Bush grassland site, moving to measured meteorology further deteriorated the comparison between modelled and observed G_{ns}, although large uncertainties in the observed G_c values exist. Overall, this analysis tested the ZHG O_3 non-stomatal parameterizations structural correctness. This work also highlighted that some processes such as thermal decomposition (Fowler et al., 2001, 2009; Coyle et al., 2009) as well as O_3 leaf aqueous chemistry mediated by BVOC (Fares et al., 2009; Rannik et al., 2012) constitute O_3 non-stomatal pathways not yet represented in the model, and neither is the additional O_3 chemical sink due to the reaction with NO (Gerosa et al., 2009).
- Inconsistencies between modelled and observed values of some key meteorological factors such as u_*, *RH*, *LE* and *H* fluxes were found. Discrepancies between model and observed vegetation properties such as *LAI*, canopy height (h_c) and roughness properties (z_0) were also detected. The different representation of u_*, z_0 and h_c within the model leads to systematic uncertainties between modelled and observed R_a (z-d) and R_b (Table 3.1).
- O_3 dry deposition velocities simulated using WES and ZHG scheme under identical meteorological conditions were compared over three different vegetation types mainly across Europe and two sites in the US. Overall, this

study highlighted that although both WES and ZHG schemes capture well diurnal variations of V_d, inconsistencies in the input parameters, non-specific vegetation types meteorological factors used in the dry deposition parameterizations constitute a significant source of uncertainties in the modelled V_d using both the schemes (Table 3.1).

- A comparison of the modelled surface O_3 concentration against observations both in the NH and SH revealed that the model performs well in the NH using both WES and ZHG schemes, capturing the observed surface O_3 cycle and the absolute values. With regards the NH monitoring sites considered for this study, ZHG leads to a reduction of the annual bias (up to -13.5% on average) compared to WES. However, WES performs better at the tropical site of Mauna Loa and at the high latitude site of Barrow. By contrast, the model performs less well in the SH sites considered here. In these sites, the seasonal cycle and absolute values of the observed surface O_3 are not well reproduced by the model, except at Syowa and the South Pole where the model performs well using both the schemes. Modelled surface O_3 in the SH sites considered for this study exhibited a larger bias using the ZHG scheme (60% on average) compared to WES scheme (47% on average). However, more work is needed in order to evaluate the model performance using both the schemes at the global scale.
- The ZHG scheme, providing a more dynamic and mechanistic representation of the O_3 dry deposition process, ought to capture inter-site variability better and more suited to explore the effect of meteorology and changing climate on surface O_3. This study represented a first attempt to evaluate O_3 dry deposition in UKCA model and the results presented here showed that ZHG scheme may provide an improved average O_3 deposition sink, with a more mechanistic partitioning of the total O_3 flux between its stomatal and non-stomatal components. Owing to the variability in the results, it was not possible to conclude whether ZHG could represent an alternative to WES scheme in UKCA. However, the results presented here provide a valid source of information to be used for further development of O_3 dry deposition representation in a GCM. Further evaluations are needed to better assess both the schemes using long term

datasets over different vegetation types (especially at mid-high NH latitudes and tropical regions) and climate conditions (as detailed in Section 5.3.1).

- Both schemes were originally developed using a small amount of datasets and by challenging it with a number of measurement sites provides a significant step forwards. A meta-analysis of a large number of long term well quality-assured O_3 flux datasets and other data (covering a full seasonal cycle) and detailed in Section 5.3.1 across different ecosystems and climate conditions may provide a generic improvement in both the deposition approaches.

  Improvements in the understanding of some of the O_3 deposition processes, such as O_3 interaction with water films and in-canopy O_3 chemistry reactions mediated by bVOC, through field observations and laboratory experiments (Section 5.3.1), are also urgently required to develop more mechanistic deposition parameterisations that work well across sites and seasons.

Chapter 4

The sensitivity of global ozone predictions to dry deposition schemes and their response to climate change

4.1 Introduction

Ozone (O_3) is formed in the troposphere in the presence of sunlight as a result of the reactions of nitrogen oxides (NO_x = NO_2 + NO), volatile organic compounds (VOCs), methane (CH_4) and carbon monoxide (CO) (Von Schneidemesser et al., 2015). Tropospheric O_3 is a dangerous secondary short-lived and chemically active air pollutant, causing serious damage to ecosystems and human health (Monks et al., 2015) and is also considered the third most important greenhouse gas contributing to radiative forcing of climate change (IPCC, 2013; Stevenson et al., 2013; Stevenson et al., 2006). Climate change and air pollution are linked environmental issues as changes in anthropogenic emissions are predicted to have an extensive range of effects on the processes governing the interactions between atmospheric composition and the biosphere (Fowler et al., 2009). There are multiple pathways by which climate change may have impacts on O_3 air quality (Fiore et al., 2012). Changes in meteorological factors (temperature, humidity, precipitation, cloud cover, boundary layer stability, etc.) influence the chemistry and the dry deposition sink (Vautard et al., 2005; Solberg et al., 2008; Andersson and Engardt, 2010), the natural emissions of O_3 precursors such as isoprene (Lathiere et al., 2005; Guenther et al., 2006) and

the stratosphere-troposphere O3 exchange, all of which have impacts on the tropospheric O_3 concentration (Monks et al, 2015; Von Schneidemesser et al., 2015). Changes in land use are predicted to occur in the future which may have a significant influence on the O_3 deposition processes to vegetation surfaces and on the biogenic VOC emissions (Jacob and Winer, 2009; Ganzeveld et al., 2010; Wu et al., 2012; Verbeke et al., 2015). So far global chemistry models have attempted to provide estimates of the impact of climate change on tropospheric O_3 focusing mainly on long-term O_3 precursor emission scenarios and atmospheric dynamics (Fowler et al., 2009). Despite some regional variability, a multi-model inter-comparison study points towards an increase in near-future O_3 concentrations as a consequence of global warming (Stevenson et al., 2006). Young et al. (2013) showed that the ACCMIP (Atmospheric Chemistry and Climate Model Inter-comparison Project) models were sensitive to changes in the climate change variables and emissions from RCP scenarios. However, differences in those sensitivities were found across the model predictions. Furthermore, Young et al. (2013) attribute differences in the predicted total annual O_3 dry deposition amounts with RCP 8.5 between the ACCMIP models to differences in the modelled surface O_3 distributions as well as the properties of the dry deposition schemes.

Among the variety of effects resulting from climate change, O_3 dry deposition processes are associated with large uncertainties (Fiore et al., 2012; Monks et al., 2015), with substantial implications for surface O_3 predictions, air quality policy and ecosystem effects. In particular, only a few studies have so far looked at the influence of climate change on the accumulation of O_3 dose to plants (Harmens et al., 2007; Fuhrer, 2009).

Therefore, improving the understanding of the mechanisms controlling the atmosphere-biosphere exchange of O_3 as a response to climate change is vital for both climate and air quality studies. The purpose of this study is to explore the effect of climate change induced by the increase in greenhouse gases (GHGs) with the RCP 8.5 scenario (CO_2 emissions increase up to 960 ppm by 2100 leading the global surface temperature to rise by about 5-6 °C by 2100) on the dry deposition sink and associated concentration changes across the troposphere, contrasting two different non-stomatal deposition parameterizations (WES and ZHG schemes; Chap. 2). To

isolate the role of the response of dry deposition to climate change as much as possible, the study contrasts the results of present-day climate runs with climate runs for 2100, whilst deliberately keeping anthropogenic emissions and land use / land cover constant between runs. This also includes the sea ice cover which was only modified for the climate model component, but not for the dry deposition calculations.

Section 4.2 introduces details of the simulation setups used for this study. Section 4.3.1 presents the O_3 deposition and surface O_3 as simulated at present day conditions using WES and ZHG schemes. In Section 4.3.2 the meteorological conditions modelled with RCP 8.5 are introduced. The overall effects of the climate change on O_3 dry deposition velocity, surface O_3 and O_3 dry deposition at the global scale are presented in Section 4.3.3. The sensitivities of O_3 changes to the two different dry deposition schemes as a result of climate change are described in Sections 4.4.4 and 4.4.5. In Section 4.7, the model results are analysed and the impacts of climate change on future O_3 air quality are discussed. Potential implications of these results on ecosystems effects are provided in Section 4.8. Conclusions are presented in Section 4.9.

4.2 Experimental design

4.2.1 Simulation setup

This study used the UKCA model in its atmosphere-only setup at N48L60 resolution (better described in Chap. 2) to perform a series of time-slice simulations. Each model integration lasted 10 years and was performed using the WES and the ZHG dry deposition schemes described in Chapters 2 and 3. Both present day simulations ($BASE_{WES}$ and $BASE_{ZHG}$) were year 2000 time integrations whereas the future climate (CC_{WES} and CC_{ZHG}) were 2095 time slice runs.

For the BASE simulations CO_2 and CH_4 mixing ratios were set to 370 ppm and 1765 ppb, respectively, whereas the other GHGs (N_2O and compounds containing halogens) were prescribed according to the RCP dataset for the year 2000

(Van Vuuren et al., 2011). The surface emissions used for the BASE simulations were decadal averages centred on the year 2000 based on the gridded dataset of Lamarque et al. (2010). Sea surface temperatures (SSTs) and sea-ice concentrations (SICs) were based on climatological (1998-2002) values taken from the Rayner et al. (2003) HadISST dataset. In the CC_{WES} and CC_{ZHG} model simulations, the climate was changed by altering the concentrations of GHG (CO_2, N_2O, hydrochlorofluorocarbons – HCFCs and chlorofluorocarbons – CFCs) in the radiation scheme (and hence the radiative forcing of the atmosphere) and by prescribing SSTs/SICs. Future climate GHGs are specified in both CC_{WES} and CC_{ZHG} according to the RCP 8.5 scenario (Riahi et al., 2011). SSTs/SICs are (2091-2100) averages which were taken from the coupled atmosphere ocean (HadGEM2-CC) model simulations (Martin et al., 2011). In both future climate integrations the CH_4 concentrations were kept fixed in the UKCA chemistry scheme at present day levels (= 1765 ppb) in order to isolate the effect of deposition under changed climate conditions on O_3 from that of changing chemistry.

The land cover and land use fields were not changed in all model simulations and are based on Sellers et al. (1996). Anthropogenic emissions and NO_x emissions from soil as well as biogenic emissions of VOCs were also kept constant for these simulations, and were taken from Lamarque et al. (2010).

4.2.2 Model outputs analysis

In this study the grid O_3 dry deposition velocity ($V_d = F(O_3)/[O_3]$) is derived from the total O_3 dry deposition flux, summing all the contributions across the boundary layer (as better described in Sec. 2.2.5, Chap. 2) and the surface O_3 concentration at the lowest model level (50 m). This approach allows the impacts of climate change on surface O_3 to be related to the changes in grid O_3 V_d.

To investigate how stomatal and non-stomatal O_3 deposition changes contribute to changes in grid O_3 V_d, specific model diagnostics were used to output O_3 V_d and canopy conductance terms (G_c, G_s, G_{ns}) simulated by the model for each vegetation type within the model grid using both the WES and the ZHG scheme (for both the present day and future climate simulations).

The changes in stomatal and non-stomatal O_3 dry deposition terms were averaged accounting for the fraction of each vegetation type in a model grid in order to quantify the impacts of climate change on global O_3 deposition to vegetated surfaces.

4.3 Results

4.3.1 Modelling present-day surface ozone and ozone dry deposition

Figure 4.1a, 4.1c and 4.1e present the decadal (1996-2005) average of O_3 grid dry deposition velocity, surface O_3 and the total annual O_3 dry deposition and as simulated by UKCA at present day conditions using the WES scheme. Figures 4.1b, 4.1d and 4.1f present the same O_3 fields but using the ZHG dry deposition scheme. The average ratios between the stomatal (G_s) and the total canopy conductance (G_c) modelled with WES and ZHG are introduced in Figures 4.1g-4.1h as a measure of the fraction of O_3 dry deposition that enters the stomata causing damage to plants.

As shown in Figure 4.1a, the WES scheme leads to large average V_d values over vegetated areas in South America, Central Europe and East-Asia (up to 0.4 cm s^{-1}) whereas the highest V_d values (up to 0.5 cm s^{-1}) modelled using the ZHG scheme (Figure 4.1b) are simulated across North Europe and over the Boreal forests. As a result of a more dynamic non-stomatal deposition component and the additional effect of stomatal blocking by leaf water, the ZHG scheme predicts larger deposition velocities than the WES scheme, by as much as +40% over boreal forests and reductions in O_3 V_d by up to -30% over tropical regions (see Chap. 2).

Surface O_3 reaches the highest values over East-Asia (Tibet), the Arabian Peninsula, the Sahara desert and western USA. Surface O_3 simulated with the ZHG scheme (Figure 4.1d) shows lower values (up to -20 %) than using WES over land at mid-latitude continental regions whereas higher values are calculated (up to +20%) over tropical regions and East-Asia at the annual average.

The highest O_3 dry deposition fluxes were simulated over eastern USA, C. Europe and E. Asia (up to 100 kg ha^{-1} yr^{-1}) with WES (Figure 4.1e). A larger fraction of O_3

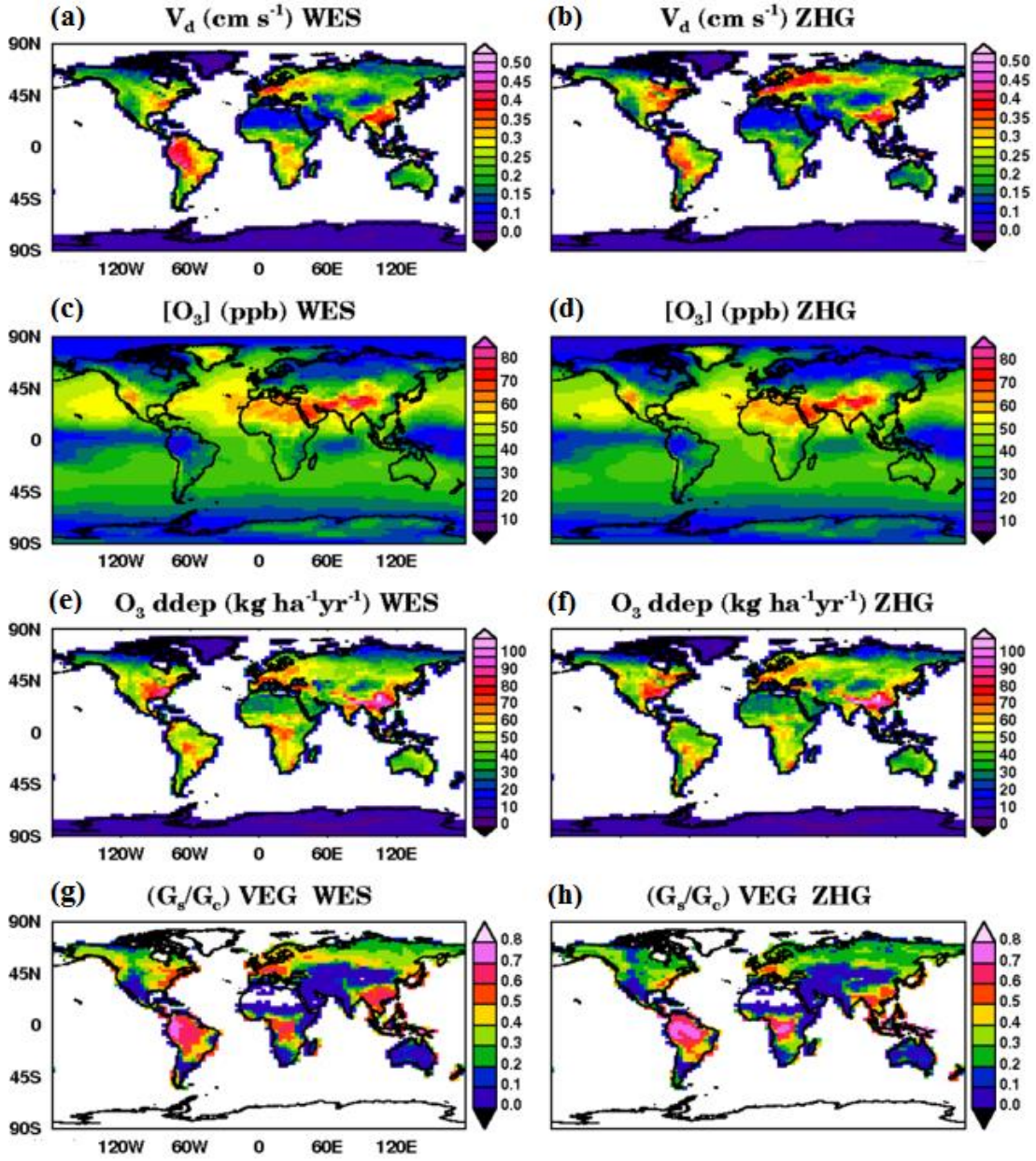

Figure 4.1. Decadal (1996-2005) mean absolute values of O_3 dry deposition velocity V_d (cm s^{-1}), surface O_3 concentration (ppb) and total annual O_3 dry deposition (kg $ha^{-1}yr^{-1}$) as modelled by UKCA using WES (**a-c-e**) and ZHG dry deposition schemes (**b-d-f**). The grid average (all vegetation types) ratio between stomatal and total canopy conductance as simulated with WES (**g**) and ZHG (**h)** at present day conditions. Simulated V_d and O_3 dry deposition values over the oceans with both WES and ZHG schemes were not shown.

is deposited with WES on average via the stomatal pathway (higher G_s/G_c values; Figure 4.1g) compared with ZHG (Figure 4.1h). By contrast, as shown in Figure 4.1f, ZHG simulates slightly less O_3 dry deposition (up to -10%) over tropical regions and more O_3 dry deposition over boreal forested areas and East-Asia (up to +15%) at the annual average. Compared with WES, a larger fraction of O_3 is deposited on average via non-stomatal pathways with ZHG (lower G_s/G_c; Figure 4.1h) across mid-high latitudes in the NH and E. Asia whereas more O_3 dry deposition is modelled with ZHG on average to stomatal pathways over tropical forests (higher G_s/G_c) compared to WES.

4.3.2 Changes of meteorological factors due to climate change

Figure 4.2 presents the absolute and relative differences of key meteorological factors to facilitate the interpretation of the processes responsible for regional and global changes in surface O_3 associated with climate change. Consistent with the rest of the study, these are the changes that would be expected if land cover and land use did not adjust to climate change. As a response to the RCP 8.5 scenario and the changes in the prescribed SST and SIC, the model exhibits a considerable increase in the surface temperature over land especially in NH with values by up to 10 °C at the northern high latitudes (Figure 4.2a). Figure 4.2b reveals an increase in the boundary layer height (BL_h) as a response to climate change across Eurasia and C. America (up to 150 m), over forested areas in Africa (up to 100 m) and South America (BL_h > 200 m). As shown in Figure 4.2c, considerable increases in the net (short wave) surface radiation occur over N. America and across Eurasia (up to 15 W m^{-2}) and over forested areas in South America and Central Africa (up to 10 to 15 W m^{-2}). Figure 4.2d shows irregular changes of friction velocity (u_*) occur over land in the NH (with more uniform decreases in N. America up to -0.025 cm s^{-1}) whereas large increases are predicted over Arctic regions (~ 0.016-0.018 cm s^{-1}) and over South America (up to 0.025 cm s^{-1}). Figure 4.2e shows changes in the relative humidity associated with climate change, revealing that decreases of *RH* occur across N. America and Europe (to -10 to -15%) and over the Amazon forest (up to -30%). By contrast, a considerable increase of *RH* is simulated over Northern Australia (up

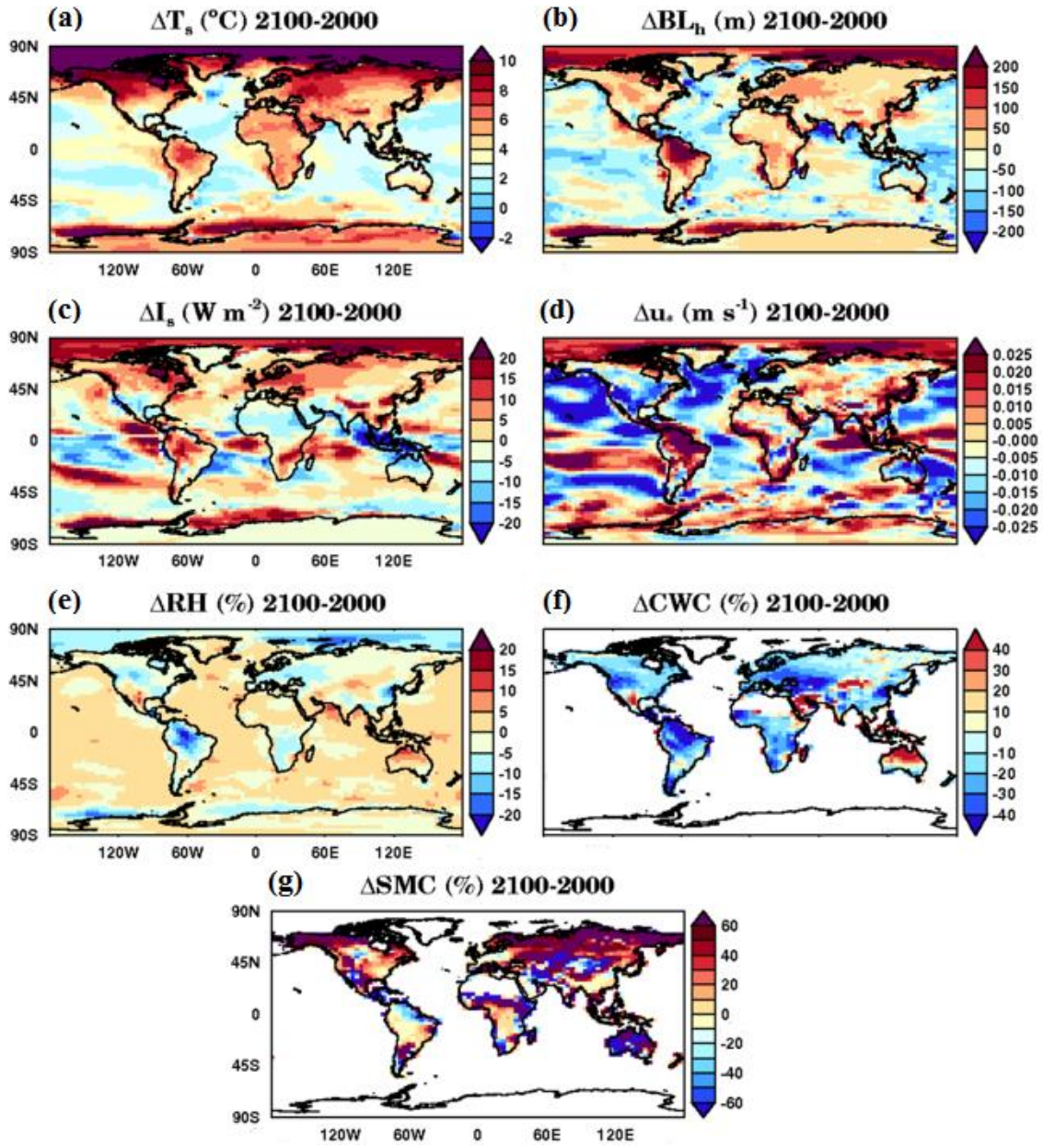

Figure 4.2. Absolute difference (decadal mean) between future climate and present day surface temperature T_s (ºC) (**a**), boundary layer height BL_h (m) (**b**), net short-wave surface radiation I_s (W m^{-2}) (**c**), friction velocity u_* (cm s^{-1}) (**d**) and relative humidity (in %) of humidity *RH* (**e**). Relative differences of grid average canopy water content *CWC* (**f**) and grid average soil moisture content at the root zone *SMC* (**g**) between future climate (RCP 8.5) and present day.

up to +15%). Significant changes of the average grid (all vegetation type) canopy water content (*CWC*) are predicted both in the NH and in the SH, especially over the Amazon forest (up to -30%) and N. Australia across S. Asia (up to +40%) (Figure 4.2f).

Finally, relevant changes in the average grid soil moisture (*SMC*) at the root zone are simulated between 2100s and present day (Figure 4.2g). More uniform increases in *SMC* are simulated over boreal regions and across Eurasia (up to 50%) as well as African equatorial regions and N. Australia (up to 65%) whereas significant decreases occur across Europe (up to -20%), E. Asia (-15%) and S. America (up to -30%).

4.3.3 Overview of climate impacts on O_3 fields

Figures 4.3a and 4.3b show the changes in O_3 dry deposition velocity between present day and 2100s predicted using the WES and the ZHG dry deposition schemes. Both the relative V_d changes with WES and ZHG are calculated using the values simulated under present day climate conditions. In both future climate and present day V_d simulations, the same anthropogenic emissions and land use scenario were used as a base (as described in Sec. 4.2.1). Overall, both schemes appear to respond to changing climate in a similar way, with deposition velocities to land decreasing in most areas. The largest V_d changes between 2000 and 2100 occur over heavily vegetated areas both in NH and SH (Figures 4.3a and 4.3b). In the NH the larger V_d decreases occur across N. America, Europe and E. Asia (up to -25%) whereas the strongest decrease is simulated over tropical regions in S. America and C. Africa (up to -40%). Both WES and ZHG show an increase of V_d over non-vegetated areas, including the polar regions (by as much as +15%), the Arabian peninsula as well as parts of India and .N. Australia.

Figure 4.3c shows the change in surface ozone due to 2000-2100 climate change, expressed as a percentage of the year 2000 values, for the WES scheme. Figure 4.3d is the equivalent for ZHG. For the 2100 climate with RCP 8.5 scenario, modelled surface O_3 using both WES and ZHG exhibits large increases in the NH at mid-high latitudes (up to 25%) and over S. America (up to 30%) and C. Africa (up to 20%).

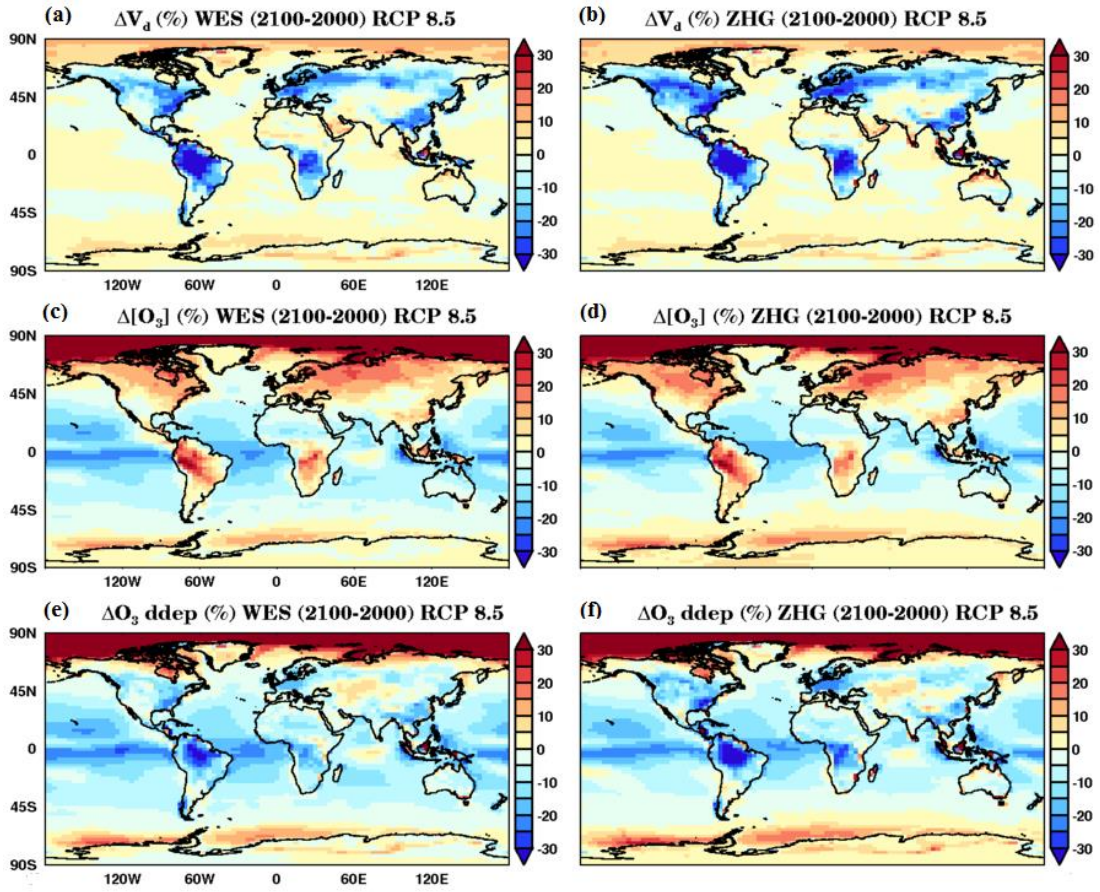

Figure 4.3. Decadal mean changes (% changes relative to 2000 values) of O_3 grid dry deposition velocity, surface O_3 concentration and total O_3 dry deposition between 2100s and present day induced by the RCP 8.5 scenario. O_3 field changes predicted by the model using the WES scheme (**a-c-e**) and the ZHG scheme (**b-d-f**).

This is consistent with decreases in the total modelled O_3 dry deposited on annual average over vegetated areas with both WES and ZHG, with the stronger changes predicted over the Amazon (up to -30%) and C. Africa (up to -20%) forests.

Despite a predicted increase in V_d for the Arctic, the model shows a strong increase in O_3 surface concentration at the northern high latitudes (Figure 4.3a-b).

4.3.4 Sensitivity of O_3 predictions to the dry deposition schemes

Figure 4.4a presents the differences between absolute changes in V_d simulated using ZHG compared to WES in response to climate change. Whilst the two schemes behave similarly (Figures 4.3a and 4.3b), the decrease of land V_d induced by climate change predicted is generally larger using ZHG than WES in areas dominated by tropical broadleaf forest, including tropical S. America (up to 0.038 cm s^{-1}), South Asia (up to 0.024 cm s^{-1}), and northern Australia (up to 0.012 cm s^{-1}). By contrast, ZHG predicts smaller changes in V_d than WES across N. America and Eurasia (up to -0.05 cm s^{-1}) (Figure 4.4a), considering that at present day conditions ZHG calculates larger V_d values than WES over those areas (Figures 4.1a-b). However, these areas are heavily influenced by how the model treats coniferous forests and C3 grassland, but also includes areas dominated by broadleaf forest.

Figure 4.3b shows the differences expressed in absolute 2100-2000 changes in surface O_3 modelled using ZHG compared to WES as a response to climate change. This reveals that the ZHG scheme leads to larger increases (or smaller decreases) in surface O_3 than WES, by as much as +3 ppb across N. America and of up to +1.5 ppb over E. Europe. Significant differences in surface O_3 are also predicted across India (up to 2 ppb), E. Asia (~1.5/2 ppb). Interestingly, an increase in surface O_3 by up to 2 ppb is simulated across all the SH when using ZHG compared to WES (relative to present day simulated values as shown Figures 4.1c and 4.1d).

Compared to WES, ZHG leads to different O_3 dry deposition predictions with less O_3 dry deposited across N. America (by up to -6 kg $ha^{-1}yr^{-1}$) and E. Europe (up to -8 kg $ha^{-1}yr^{-1}$) at the annual average (Figure 4.3c). By contrast, ZHG points toward more O_3 dry deposited across S.E. Asia (up to +6 kg $ha^{-1}yr^{-1}$) and N. Australia (up to +3 kg $ha^{-1}yr^{-1}$) than WES compared to present day estimates (Figures 4.1e-4.1f).

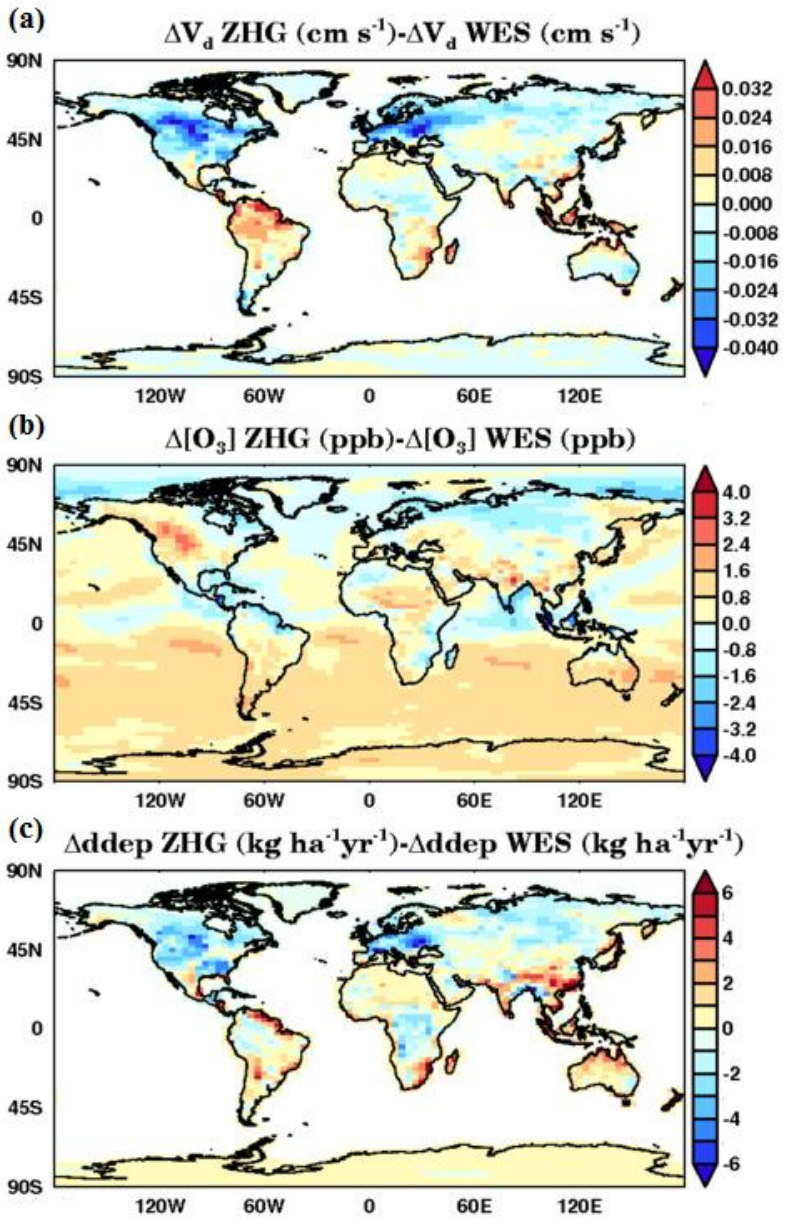

Figure 4.4. Decadal mean differences between predicted absolute changes (using WES and ZHG) of O_3 grid dry deposition velocity V_d (cm s^{-1}) (**a**), surface O_3 concentration (ppb) (**b**) and total annual O_3 dry deposition (kg ha^{-1} yr^{-1}) (**c**) between 2100s and present day as a response to climate change. V_d and O_3 dry deposition changes over the oceans are not shown.

4.3.5 Tropospheric O_3 and its sensitivity to dry deposition schemes

Simulated (2100-2000) changes in the zonal mean global distribution of tropospheric O_3 using WES and ZHG are presented in Figures 4.5a and 4.5b. As a response to climate change, modelled O_3 with both WES and ZHG exhibits a large increase throughout the tropical upper troposphere (up to 12 ppb) and in the NH subtropical upper troposphere (up to 8 ppb). A significant increase of O_3 (up to 8 ppb) is also simulated near the surface over the Arctic with both schemes.

By contrast, climate change reduces mean O_3 concentrations in the lower troposphere using WES and ZHG especially over tropical regions and over low mid-latitudes in the NH (by up to -4 ppb). Tropospheric changes of O_3 levels show regional differences with WES extending from the tropics to low mid-latitudes and ZHG decreases occurring more between the equator and low mid-latitudes. Figure 4.5c presents the differences between the absolute tropospheric O_3 (2100-2000) changes (ppb) simulated by UKCA using ZHG compared to WES. As a response to climate change, ZHG shows a larger increase of O_3 than WES in the southern hemisphere troposphere, with the largest differences simulated in the SH low latitudes (Figure 4.5c).

4.4 Influence of climate change on O_3 dry deposition components

4.4.1 Stomatal dry deposition

The average grid stomatal conductance for G_s (O_3) changes (weighted by the fraction of each vegetation type within the model grids) was investigated to isolate the impact of the climate change. The effect of climate change on G_s as simulated with the WES the ZHG schemes is presented in Figures 4.6a and 4.6b. Modelled G_s using both WES and ZHG exhibits increases over boreal forested regions (up to 10%) and Russian Arctic regions (up to 15%), and decreases across C. USA and C. Asia (up to 15%). Changes in G_s are also simulated across S. Asia and Australia with increases

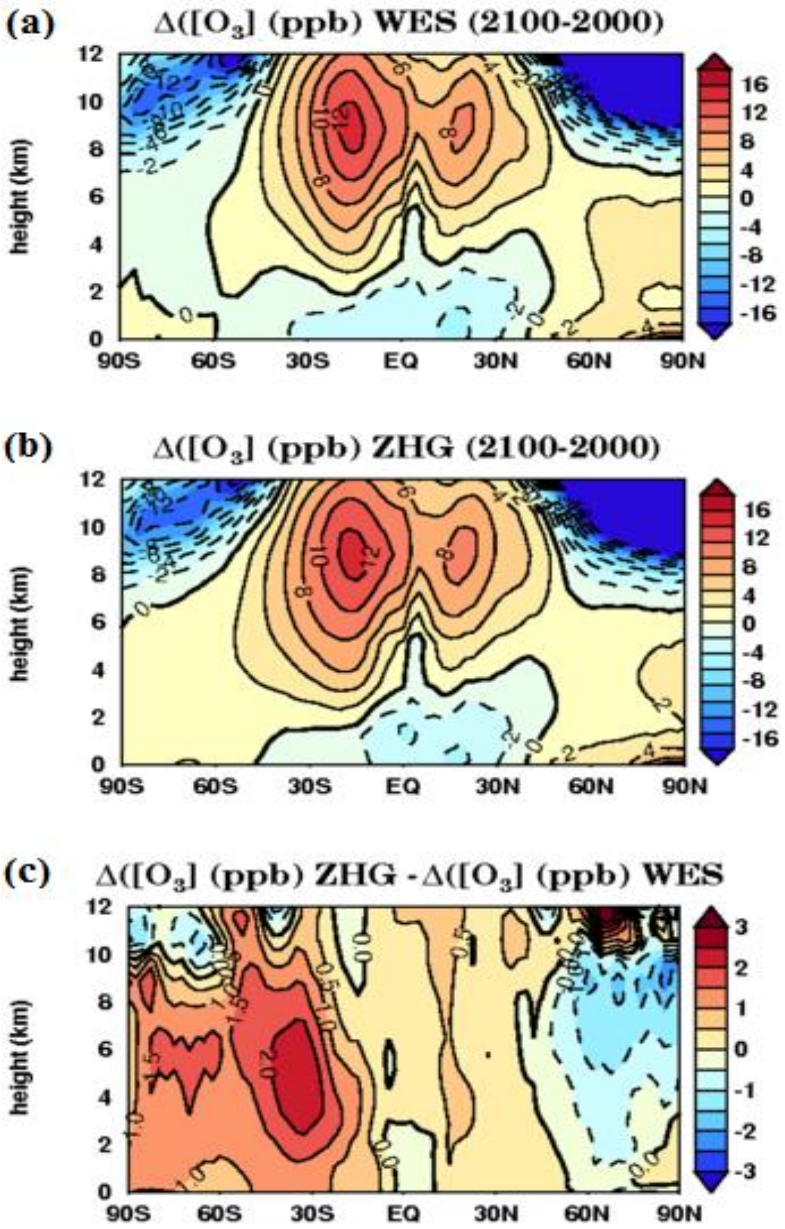

Figure 4.5. Changes in zonal O_3 (decadal) mean (ppb) between 2000s and 2100s due to climate change with WES (**a**) and ZHG (**b**) schemes. The absolute differences (ppb) in zonal O_3 changes between 2100 and 2000 as a result of the change of scheme (from WES to ZHG) are shown in (**c**).

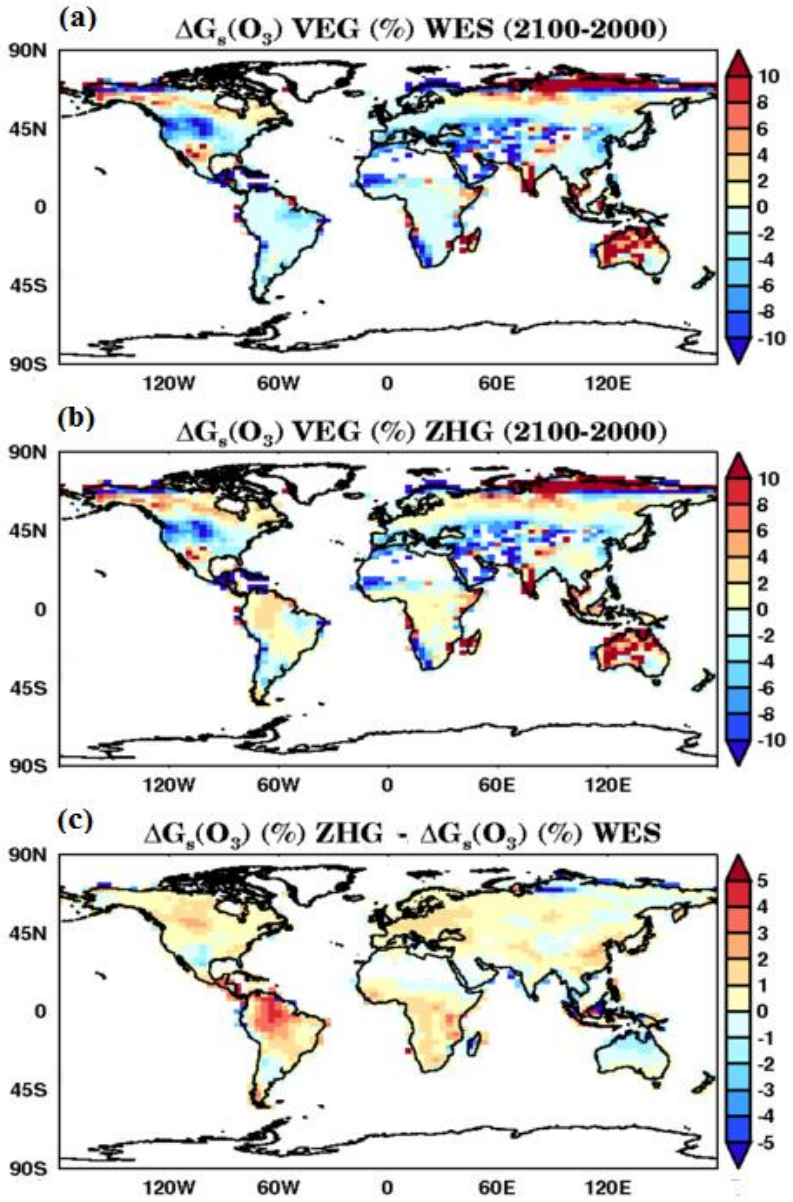

Figure 4.6. Decadal mean changes (% relative values) of average grid (all vegetation types) canopy stomatal conductance for $G_s(O_3)$ as simulated with the WES (**a**) and ZHG (**b)** between present and 2100s as a response to climate change**.** Relative difference (%) between G_s changes predicted with ZHG compared to WES (**c)**.

and Russian Arctic regions (up to 15%), and decreases across C. USA and C. Asia (up to 15%). Changes in G_s are also simulated across S. Asia and Australia with up

to +10% on average. Figure 4.6c implies that in response to climate change, the overall future G_s changes predicted by ZHG are biased towards larger values as compared with WES. The UKCA implementations of the two schemes share the same stomatal conductance scheme, with the only exception that additional stomatal blocking by leaf water is implemented in the ZHG scheme. Thus, red areas in Figure 4.6c indicate stomatal blocking is going to be reduced and blue areas where stomatal blocking may become more important, at the annual average.

4.4.2 Non-stomatal deposition

Figures 4.7a and 4.7b present the average grid (all vegetation types) non-stomatal conductance (G_{ns}) to changing climate as modelled with WES and ZHG. In the WES parameterisation only the soil resistance shows a dependence on meteorology and therefore simulated G_{ns} using WES exhibits only small variations across land, with the most significant decreases occurring over tropical regions (-5% to -10%) and moderate increases shown across the NH (up to +5%). By contrast, modelled G_{ns} using ZHG show a highly spatially variable response to changing climate conditions compared to WES and appear more regionally distributed than WES (Figure 4.7b). ZHG leads to decreases of G_{ns} across N. America (up to -30%), Europe (up to -20%) and E. Asia (up to -30%). Differently, O_3 non-stomatal deposition changes simulated with ZHG over tropical regions are more variable (-30% to +30%) than WES, with positive values calculated along coastal areas and negative changes simulated inland.

4.4.3 Changes in the O_3 dry deposition partitioning

Figures 4.8a and 4.8b show the changes due to climate (2100-2000) in average grid (all vegetation type) ratio (G_s/G_c) between the canopy stomatal and non-stomatal O_3 dry deposition, i.e. the fraction of the deposited flux that enters the stomata. The G_s/G_c values are relative to the year 2000 (Figures 4.1g and 4.1h). This shows how the partitioning of the O_3 dry deposition flux modelled with WES and ZHG varies globally as a response to climate change. As a consequence of the changes in the

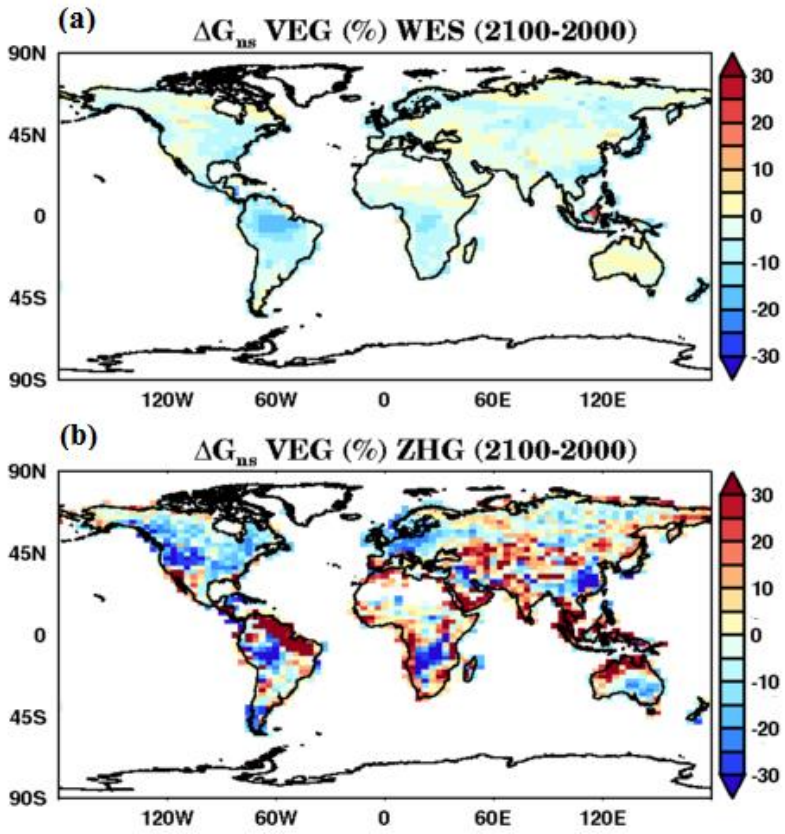

Figure 4.7. Decadal mean changes (% relative values) of average grid (all vegetation types) non-stomatal conductance for G_{ns} as simulated with the WES (**a**) and ZHG (**b)** between present and 2100s as a response to climate change**.**

stomatal and non-stomatal deposition induced by climate change, WES points to a general increase of the stomatal fraction (G_s/G_c) (up to +15%) between present and 2100s. By contrast, ZHG exhibits a latitudinal gradient of G_s/G_c changes, with significant increases occurring in the NH especially across N. America, Europe and E. Asia (up to +30%). ZHG leads to contrasting changes of G_s/G_c with particular regards of the tropical regions. The most significant changes in the partitioning of the O_3 deposition flux are simulated with ZHG more inland in S. America and S. Africa (up to +30%) and S. Australia (up to +20%) whereas decreases in the G_s/G_c are predicted over coastal areas and as well in S. Asia (up to -30%).

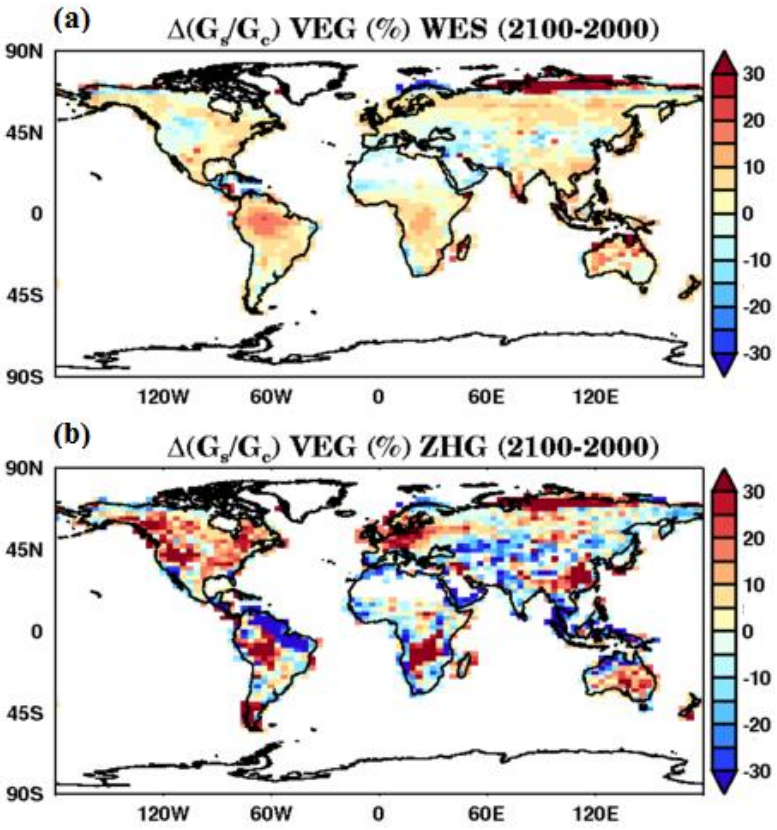

Figure 4.8. Decadal mean changes (% relative values) of the ratio between average grid (all vegetation types) canopy stomatal conductance for O_3 (G_s) and average grid (all vegetation types) canopy conductance (G_c) as simulated with the WES (**a**) and ZHG (**b)** between present day and 2100s**.**

4.5 Discussion

4.5.1 Overall influence of climate change alone on O_3 dry deposition

Earlier studies highlighted that changes in meteorology associated with climate change may have significant impacts on O_3 dry deposition leading to large increases in surface O_3 at the regional scale (Solberg et al., 2008; Andersson and Engardt, 2010; Vieno et al., 2010). In this study, the impacts of climate change predicted on

the basis of the RCP 8.5 scenario on O_3 dry deposition processes were investigated at the global scale. The approach specifically ignored associated changes in land-use, represented by a strong expansion in the agricultural field that are projected to occur especially in developing countries due to increasing population and economic growth (Riahi et al. 2011). In addition, natural vegetation would also be expected to adapt significantly under this more extreme climate scenario as indicated, e.g., in response to the large change expected in *SMC* as shown in Figure 4.2g.

A considerable increase of the emissions of methane (CH_4) is also projected with RCP 8.5 (Riahi et al. 2011), which would enhance ozone production. However, in this study CH_4 emissions were maintained at present day values to isolate the influence of changing climate conditions on surface O_3 and O_3 dry deposition. Overall, the results presented in this study point toward a significant reduction in O_3 dry deposition velocity over vegetated areas predicted with both WES and ZHG (Table 4.1). V_d reduces considerably as a response to climate change over the tropical S. America (up to -24%) whereas in the NH the most significant decreases in V_d are simulated across Eurasia (up to -10%) and N. America (up to -17%). Whilst the two schemes behave similarly, the decrease in land V_d is generally larger in ZHG. Modelled V_d changes with ZHG shows a latitudinal gradient, with less decreases predicted in the NH and more increases over tropical regions compared to WES (Figure 4.4a). ZHG leads to an increase in V_d (up to 10%) in S. Asia and N. Australia as response to climate change. By contrast, Verbeke et al. (2015) found a large impact of climate change with RCP 8.5 on O_3 V_d over land with a latitudinal gradient and large changes as much as of +50% occurring especially during winter across Eurasia whereas smaller changes were detected over tropical regions. Verbeke et al. (2015) also stated that the influence of land cover-change on O_3 V_d was more heterogeneous compared to climate change only.

4.5.2 Role of the turbulent transport

Analysis of the change in the individual components of the dry deposition schemes (Table 4.2) sheds light on the drivers that are responsible for the overall decrease in

Table 4.1. Decadal mean of present day (**P)** and future climate (**F**) surface O_3 concentrations (ppb), total annual O_3 dry deposition (kg ha^{-1} yr^{-1}) and dry deposition velocity V_d (cm s^{-1}) averaged over homogenous regions, over land and globally simulated using WES and ZHG. 'Δ_{CLIM}' indicate the decadal mean changes (in %) of the above O_3 fields predicted using WES and ZHG schemes as a response to climate change over homogenous regions, over land and globally.

	[O_3]						**O_3 ddep**						**V_d**					
	WES			**ZHG**			**WES**			**ZHG**			**WES**			**ZHG**		
	P	**F**	**Δ_{CLIM}**	**P**	**F**	**Δ_{CLIM}**	**P**	**F**	**Δ_{CLIM}**	**P**	**F**	**Δ_{CLIM}**	**P**	**F**	**Δ_{CLIM}**	**P**	**F**	**Δ_{CLIM}**
	(ppb)		**(%)**	**(ppb)**		**(%)**	**(kg ha^{-1} yr^{-1})**		**(%)**	**(kg ha^{-1} yr^{-1})**		**(%)**	**(cm s^{-1})**		**(%)**	**(cm s^{-1})**		**(%)**
Global	35.6	35.8	0.6	34.9	35.5	1.7	17.2	16.4	-4.7	16.7	15.9	-4.8	0.078	0.074	-5.1	0.078	0.073	-6.4
Land	35.5	36.7	3.4	34.7	36.2	4.3	27.1	25.6	-5.5	26.2	24.6	-6.1	0.126	0.115	-8.7	0.125	0.113	-9.6
Eurasia	39	41	5.1	36	39	8.3	42	41	-2.4	41.7	39.6	-5.0	0.25	0.23	-8.0	0.33	0.30	-9.1
Europe	38	41	7.9	35	38	8.6	44.5	42	-5.6	44	40	-9.1	0.32	0.28	-12.5	0.40	0.35	-12.5
N. America	38	41.5	9.2	35	39	11.4	43.8	40.2	-8.2	45.5	4	-12.1	0.25	0.22	-12.0	0.28	0.23	-17.9
Tropical S. America	30.8	33	7.1	33	35	6.1	48.3	39	-19.3	44	35.5	-19.3	0.36	0.28	-22.2	0.30	0.23	-23.3
Tropical Africa	36.5	38	4.1	39	41	5.1	42.3	37.6	-11.1	38	33.3	-12.4	0.28	0.25	-10.7	0.25	0.22	-12.0
S. Asia	34	33	-2.9	36	35	-2.8	29.6	28	-5.4	24.6	25	1.6	0.172	0.167	-2.9	0.153	0.17	11.1
E. Asia	50	53	6.0	49	51	4.1	58.3	52.5	-9.9	56.4	51.9	-8.0	0.41	0.37	-9.8	0.45	0.41	-8.9
N. Australia	36	33	-8.3	38	35	-7.9	29.8	28.9	-3.0	26.2	27.5	5.0	0.25	0.26	4.0	0.20	0.24	20.0
S. Australia	38.5	38	-1.3	39	40	2.6	35.9	34.7	-3.3	33.9	33.4	-1.5	0.190	0.189	-0.5	0.170	0.168	-1.2
Antarctica	29.9	30.1	0.7	29.4	30.6	4.1	5.45	5.53	1.5	5.4	5.6	3.7	0.035	0.036	2.9	0.035	0.036	2.9

Table 4.2. Decadal relative mean changes (in %) of grid average (all vegetation types) O_3 stomatal conductance (G_s), cuticular conductance (G_{cut}), in-canopy+soil conductance ($G_{inc.+s.}$), total non-stomatal conductance (G_{ns}) and the sum of aerodynamic (R_a) and boundary layer resistance (R_b) simulated using WES and ZHG between 2000s and 2100s as a response to climate change.

Δ_{CLIM}	G_s (%)		G_{cut} (%)		G_{inc+s} (%)		G_{ns} (%)		G_s/G_c (%)		(R_a+R_b) (%)
	WES	**ZHG**	**WES**	**ZHG**	**WES**	**ZHG**	**WES**	**ZHG**	**WES**	**ZHG**	**WES/ZHG**
Eurasia	-3	-2	0.0	-2	-4	6	-4	3	2	-1.7	-24
Europe	-4	-2	0.0	-10	-4	9	-4	-6	1.5	6	-12
N. America	-5	-3	0.0	-15	-5	-4	-5	-11	3	14	-4
Trop. S. America	-3	2	0.0	-16	-14	8	-14	-11	16	10	-27
Trop. Africa	-4	3	0.0	-8	-4	7	-4	-6	8	2	-8
S. Asia	9	8	0.0	12	-2	-10	-2	10	10	-3	-10
E. Asia	-6	2	0.0	-8	-4	5	-4	-4	1.5	10	2
N. Australia	18	16	0.0	15	0.5	14	0.5	19	20	-10	-14
S. Australia	3	2	0.0	-3	-0.5	-1	-0.5	-2	-4	-8	2

V_d. Turbulence appears to increase everywhere except E. Asia and S Australia, resulting in reduced resistances of $R_a + R_b$ (Chap. 2). Whilst in some cases this change is further exacerbated by increases in G_s and G_{ns} (e.g. ZHG in S. Asia, N. Australia) resulting in increases in V_d (Table 4.1), more often the increase in turbulence is more than compensated by decreases particularly in G_{ns}, resulting in an overall decrease in V_d. In the future climate modelled with RCP 8.5, a considerable increase in surface temperature especially at mid-high latitudes (Figure 4.2a) and a rise in the boundary layer heights (BL_h) especially over tropical forested areas are predicted (Figure 4.2b). In the NH, this indicates that changes in the turbulent transport might occur in response to climate change, leading to less intense effective boundary layer mixing (Solberg et al, 2008; Andersson et al., 2010). In contrast, the larger increase in BL_h over tropical regions especially over S. America is likely to be associated with an increase in wind speed, as the rise in friction velocity over that area suggests (Figure 4.2d). An increase in heat fluxes relative to moist input to the boundary layer especially over tropical forests might also result in an increase of the BL_h (Ganzeveld et al., 2010).

4.5.3 Changes in the O_3 stomatal uptake

This study showed that average changes in O_3 stomatal deposition (all the vegetation types) (Table 4.2) slightly contributed to changes in V_d. Overall, the O_3 canopy stomatal conductance (G_s) simulated with WES generally responds to climate change with larger decreases than ZHG such as over the USA (up to -10%) and increases (up to 8%) over boreal forested areas. Modelled G_s with MOSES 2.2 are sensitive to changes in radiation, canopy temperature, canopy humidity deficit and soil moisture availability (Cox et al., 1999). G_s decreases are related to changes in canopy humidity regimes (Figures 4.2e and 4.2f) and increases in surface temperature (Figure 4.2a). In contrast, increases of G_s can be attributed to the enhanced soil moisture availability simulated across the mid-high NH latitudes, S. Asia and N. Australia. This might represent a response to the increase in rain precipitation predicted with RCP 8.5 at mid-high latitudes (IPPC, 2013) and not shown in this study. Overall, the relative small changes in canopy stomatal conductance simulated

with both the schemes may also be attributed to the direct effect of CO_2 on photosynthesis which saturates when high concentrations are reached (Cox et al., 2001; Cox et al., 2004). By contrast, modelled G_s with ZHG exhibit larger changes than WES especially over tropical regions (up to +5% over the Amazon forest). This indicates that the stomatal blocking effect modelled with ZHG (Zhang et al., 2003 and described in more detail in Chap. 2) will become less important in the future. This shows that changes in G_s over tropical regions might occur due to changing canopy moisture regimes induced by climate change.

4.5.4 Changes in O_3 non-stomatal deposition

In this study, the effect of climate change on the dry deposition sink of O_3 was quantified using contrasting (WES and ZHG) non-stomatal deposition parameterizations. As summarized in Table 4.2, this study shows that changes in V_d are dominated by changes in the modelled O_3 non-stomatal deposition between future climate and present day conditions. The decreases in the non-stomatal deposition modelled with WES are mostly associated with changes in the deposition onto in-canopy pathways and the soils beneath the canopies as the deposition resistances to leaf cuticles in the WES scheme do not change with meteorological conditions. The simulated differences in the non-stomatal deposition simulated with WES are associated with changes in the soil moisture availability as the model generally sets the soil resistance to R_{soil} = 200 s m^{-1} for dry soils whereas R_{soil} = 500 s m^{-1} when the soil is wet (Massman et al., 2004 and better described in Chap.2, Sec. 2.2.4.3). By contrast, the results of this study show that the non-stomatal deposition modelled with ZHG responds to changing climate conditions more regionally (Table 4.2). In the NH, the deposition onto leaf cuticles strongly decreases with ZHG and this appears to be mainly driven by changes in the turbulent transport as indicated by the differences in u_* (Figure 4.2d). ZHG deposition onto in-canopy and soils (G_{inc+s}) generally increases in the NH (as a consequence of the strong influence of u_* in the ZHG R_{ac} parameterization) whereas decreases over C. America, S. Asia and N. Australia where an increase in the soil moisture content is predicted. Over Europe, the role of increasing turbulence as a main drivers seems

confirmed by the correlation between the changes in the total non-stomatal conductance G_{ns} and the changes in u_* (r^2 = 0.7). Sensitivity tests on the non-stomatal deposition G_{ns}, using observed environmental factors over European forested sites, support this interpretation (Chap. 3).

By contrast, in the SH the non-stomatal deposition changes simulated with ZHG are more spatially variable. The influence of increasing turbulence on non-stomatal deposition is still substantial along coastal areas and inland across the SH (e.g. S. America, C. Africa and S. Asia). However, the overall small correlations between changes in G_{ns} and changes in u_*, *RH* respectively simulated over S. Asia (r^2 = 0.45; r^2 = 0.42) and N. Australia (r^2 = 0.49; r^2 = 0.34), indicate a rather complicated response of the total non-stomatal deposition simulated with ZHG over S. Asian tropical forests.

The influence of changing canopy moisture regimes on the O_3 dry deposition sink has been widely documented (Fuentes et al., 1992; Altimir et al., 2006; Coyle et al., 2009). This study results highlight the impact of future climate conditions on the O_3 dry deposition via changes in the non-stomatal components.

4.6 Sensitivity of future O_3 air quality to dry deposition schemes

4.6.1 Surface ozone

In recent years, modelling studies looked at the impacts of climate change on global ozone, considering the effects of changes in atmospheric chemical composition (Brasseur et al., 2006; Stevenson et al., 2006; Morgestern et al., 2013; Young et al., 2013; Banerjee et al., 2014), bVOC and land use (Ganzeveld et al., 2010; Wu et al., 2012; Squire et al., 2014; Verbeke et al., 2015). Despite regional discrepancies, the prevailing outcome is represented by an increase in global ozone as a result of climate change (Monks et al., 2015).

This study isolates the effects of climate change on surface O_3 that are mediated through changes in the dry deposition, whilst keeping anthropogenic emissions and land cover constant. Overall, the changes in surface O_3 induced by climate-only with

RCP 8.5 are mostly positive over land, with differences between WES and ZHG at the regional scale (Table 4.1). The largest modelled increases in surface O_3 occur in the NH (up to 12% in N. America and up to 11% in Europe) and in the tropical regions (up to 9% over the tropical S. America). Significant increases are also predicted over Arctic regions (up to 30%) and over Antarctica (up to 5% with ZHG). By contrast, O_3 changes over the oceans are predominately negative with both WES and ZHG.

Climate change effects, via deposition, increase surface O_3 over areas mainly covered by vegetation. However, the changes in surface O_3 can only be partly attributed to a reduction in dry deposition. This is because other factors also contribute to surface O_3 changes as a result of climate change. It is well known that in polluted regions high surface O_3 strongly correlates with temperature (Fiore et al., 2012; Jacob et al., 2009). By contrast, in remote regions typically associated with low-NO_x levels, climate change can enhance O_3 destruction due to higher water vapour abundance (Johnson et al., 1999; Jacob and Winner, 2009). In particular, this occurs over the oceans and remote areas such as over tropical regions. Here more water vapour means more O_3 destruction via the reactions $O_3 + h\nu \rightarrow O_2 + O(^1D)$ and $O(^1D) + H_2O \rightarrow 2OH$ (Von Schneidemesser et al., 2015).

This study shows that modelled surface O_3 changes induced by climate change are sensitive to different dry deposition parameterizations. Modelled O_3 dry deposition over land with ZHG responds to climate change more dynamically than WES, generally leading to larger decreases in the NH and increases in the SH. These are mainly due to differences in the O_3 non-stomatal deposition driven by changes in atmospheric turbulence, canopy surface wetness and canopy moisture. Using ZHG, the predicted surface O_3 changes are larger than WES especially over the USA (up to +3 ppb), S. Asia (up to +2.4 ppb) and E. Asia (up to +1.8 ppb) on average. Differences in surface O_3 predictions are also simulated across Europe between WES and ZHG (Figure 4.4b), with the latter leading to smaller changes in the N. Europe (up to -2.4 ppb) and larger values over the Iberian peninsula and France (up + 1.6 ppb).

The large increases in surface O_3 over the Polar regions may be due to greater export from the surrounding continents (due to less deposition over land). This might also

be associated with intensifying stratosphere-troposphere exchange as a response to an increase in GHGs concentrations (Hauglustaine et al., 2005; Butchart et al., 2006; Zeng et al., 2008). However, in order to better quantify these effects, more investigations are needed.

Anderson and Engardt (2010) report an increase in modelled surface O_3 of up 5 ppb by 2050 as a response to climate change over Europe, pointing out that 60% of this change can be attributed to reduced dry deposition. Solberg et al. (2008) emphasize the link between the reduction of dry deposition and the increase in surface O_3 as a consequence of the heat wave that occurred in the summer 2003.

To summarize, these study results point towards an increase in surface O_3 as a result of global warming (Stevenson et al., 2006). Dry deposition constitutes one of the key uncertainties regarding the effects of a changing climate on the future O_3 concentrations (Jacob et al., 2009; Fiore et al., 2012; Monks et al., 2015). This study emphasizes that the changes in meteorological factors owing to climate change further affect surface O_3 through deposition.

The results presented here show that changes in O_3 dry deposition through stomatal and non-stomatal pathways might reduce or exacerbate the effects of changes in meteorological factors on future O_3 production, that is defined as "climate penalty" (Wu et al., 2008). Model results show that this effect is more important over the USA, Europe and E. Asia where ZHG exhibits larger changes in O_3 deposition, compared to WES. This would have relevant consequences for human health considering that significant increases in surface O_3, driven by changes in meteorological factors, are predicted to occur as a response to climate change over those areas (Bloomer et al., 2009; Langner et al., 2012; Colette et al., 2013; Wang et al., 2013; Pfister et al., 2014).

The global O_3 increase due to changes in dry deposition in response to climate found here is smaller than many presented in the literature, but the effect for individual regions can be significant (Table 4.1). It should be pointed out, however, that these simulations do not include the effect of responses in vegetation cover and composition to climate change, which will influence the terrestrial ozone sink further.

4.6.2 Tropospheric ozone

The sensitivity of future tropospheric O_3 to the dry deposition scheme was also explored in this study. Both zonal mean changes of O_3 predicted with WES and ZHG as a response to climate change show that enhanced O_3 production dominates in the tropical troposphere (Figures 4.5a-b). Strengthening lightning NO_x production in the free troposphere and intensifying deep convection occurring in the tropical upper and middle troposphere due to climate change, are responsible for the large increases in O_3 production (Doherty et al., 2005; Zeng et al., 2008).

Interestingly, the ZHG scheme exhibits a larger increase in the southern hemisphere tropospheric O_3 due to climate change compared to WES (Figure 4.5c). Less O_3 dry deposited especially over tropical S. America and tropical Africa, simulated by ZHG, may partly explain that effect. Over these tropical regions, the model predicts an increase in temperature with associated changes in canopy humidity and soil moisture content. Changes in BL heights predicted in this study, especially over the Amazon forest, may also be important as they determine the exchange volume of the compounds interacting with O_3 (Ganzeveld et al, 2010). Changes in these climate parameters might occur in a future climate over the Amazon, Southern Africa and southern Europe, leading to enhanced O_3 destruction over those regions (Cox et al., 2004). These results show that the lower deposition rates predicted with ZHG lead to an increase in long-range transport of O_3, partly explaining the increase in surface O_3 and O_3 deposition shown in this study over Antarctica (Table 4.1).

To summarize, the results of this study highlight a strong sensitivity of SH tropospheric O_3 to changes in dry deposition over vegetated tropical regions as a response to climate change. These model simulation results are based on a present day land use scenario. However, large land use changes are likely to occur in the future leading to large changes in surface O_3 (Squire et al., 2014) and O_3 deposition (Ganzeveld et al, 2010; Wu et al., 2012; Verbeke et al., 2015). The results presented here show that a better understanding of the effects of climate change on O_3 dry deposition processes, has substantial implications for future climate as O_3 is the third most important greenhouse gas (Stevenson et al., 2006, 2013), and for air quality policy (Monks et al., 2015)

4.7 Impact of climate change on future ecosystems

This study represents a first attempt to investigate the influence of climate change on the O_3 dry deposition flux partitioning. Model results indicate that generally using WES, more O_3 might be deposited globally through stomata as a response to climate change, especially over tropical forests where the increase of G_s/G_c appears larger compared to present day (Figure 4.8a). By contrast, ZHG leads to contrasting changes of G_s/G_c compared to present day, showing more regionally distributed variations (Figure 4.8b). In the NH, the larger G_s/G_c changes are simulated with ZHG over W. America, C. Europe and E. Asia (up to 30%). This indicates that in the ZHG non-stomatal deposition G_{ns} decreases more than the stomatal component G_s as a response to climate change compared to WES. Therefore, due to the reported correlation between stomatal conductance and O_3 damage to plants (Reich and Amundson, 1985), these results might have potentially important implications for future O_3 damage assessments using ZHG as more O_3 is predicted to be deposited through stomatal pathways in a future climate. By contrast, the ZHG G_s/G_c appears to respond more regionally in the SH due to changing meteorological conditions (u_*, *CWC*, *RH*, *SMC*). This indicates that climate change might lead to some counteracting effects especially over tropical coastal areas and across S. Asia. However, part of the G_s/G_c changes might also be explained as compensating effects.

At present day, metrics for O_3 damage risk assessment based on accumulated O_3 dose above a phytotoxic threshold Y ($AF_{st}Y$) (Karlsson et al., 2004), assume that the majority of O_3 deposits through stomata and the non-stomatal sinks are supposed to be constant (Touvinen et al., 2009; Emberson et al., 2013). Touvinen et al. (2009) report that the dose index $AF_{st}Y$ can be sensitive to varying non-stomatal conductance sinks, with increasing G_{ns} values generally leading to less O_3 damage. Harmens et al. (2007) report that climate change might lead to a reduction of O_3 dose for winter wheat over Europe. However, only the impact of climate change on the stomatal flux was considered in that study.

To summarize, the results of this study show that the climate change might have a strong influence on the O_3 deposition flux partitioning if using the ZHG non-stomatal

parameterizations, with significant implications for present day and future ecosystems damage studies. However, more work is needed in order to investigate the effects of climate change on the stomatal flux and to better quantify the effect of future climate conditions on the phytotoxic O_3 dose.

4.8 Conclusions

Atmospheric concentrations of surface O_3 are strongly influenced by dry deposition processes to the biosphere. Deposition processes are sensitive to turbulence, temperature and relative humidity. However, how dry deposition may respond to climate change still remains very uncertain, with implications both for air quality (e.g. human health) and ecosystem effects (e.g. crop yields). Therefore, improving the understanding of the interactions between the climate and O_3 dry deposition processes is crucial.

This study represents a first attempt to isolate the sensitivity of future global O_3 predictions to the climate change with RCP 8.5 scenario, contrasting two different deposition schemes (WES and ZHG) with particular regards of the non-stomatal deposition component. Overall, the results of this study point toward a general reduction of O_3 V_d over vegetated areas as a response to climate change (by up to -24% over S. America, -17% over N. America and -10% over Europe). Whilst the two schemes behave similarly, the decrease in land V_d induced by climate change is generally larger in ZHG. Modelled V_d changes with ZHG exhibit a latitudinal gradient, with less decreases predicted in the NH and more increases over tropical regions compared to WES. By contrast, Verbeke et al. (2015) found that as a response to climate change alone, the strongest increase of V_d occurs in the NH whereas the smaller changes are predicted over tropical regions. The regional differences in V_d changes simulated with WES and ZHG were attributed to the different responses of the stomatal and non-stomatal deposition to climate change (Table 4.2). Overall, model results show that an increase in turbulence constitutes the main driver of the changes in V_d. In ZHG, increases in turbulent aerodynamic and boundary quasi-laminar components (both WES and ZHG) are more than

compensated by decreases in the non-stomatal deposition. By contrast, in WES the overall decreases in V_d are more driven by a combination of decreases in G_s and G_{ns}. The results of this study show that the changes in surface O_3 induced by climate change-only with RCP 8.5 are mostly positive over land, with differences between WES and ZHG on a regional scale (Table 4.1). Climate change effects, via deposition, increase surface O_3 over areas mainly covered by vegetation (up to 12% in N. America, up to 11% in Europe and as much as 9% over tropical regions). Significant increases were also found over Arctic regions (by up to 30%) with both the schemes and over Antarctica (up to 5%) with ZHG. Although other factors may contribute to O_3 changes as a response to global warming (Jacob and Winer, 2009; Fiore et al, 2012), this study highlights that modelled surface O_3 changes induced by climate change are sensitive to different dry deposition parameterizations. Using ZHG, the predicted surface O_3 changes are larger than WES especially over the US (up to +3 ppb), S. Asia (up to +2.4 ppb) and E. Asia (up to +1.8 ppb) on average. Overall, the results of the study emphasise that changes in meteorological factors influence surface O_3 via deposition in a future climate. This means that changes in deposition might exacerbate the effect of future changes in meteorological factors on O_3 production (Wu et al., 2008). Model results indicate that this effect is important over USA, Europe and E. Asia, where ZHG exhibits larger differences in deposition compared to WES as a result of changing climate.

The increase of surface O_3 over Arctic and Antarctic regions highlights the strong effect of O_3 deposition on the long-range O_3 transport, with implications for future climate (Doherty et al., 2013).

Finally, the influence of climate change of the O_3 dry deposition flux partitioning was investigated in this study. The larger G_s/G_c changes simulated with ZHG over N. America, C. Europe and E. Asia (up to 30%) indicate that more O_3 is predicted to deposit through stomatal pathways compared to WES as a response to climate change. These results might have potentially important implications for present and future O_3 damage assessment studies (Touvinen et al., 2009; Emberson et al., 2013). However, more work is needed to better quantify the impacts of climate change on the O_3 stomatal flux and their related effects on the phytotoxic O_3 dose.

Chapter 5
Conclusions

The sophisticated United Kingdom Chemistry Aerosol model (UKCA) has been used to study the ozone dry deposition processes at the global scale, with a view to improve the understanding of the interactions between O_3 air quality and climate change. This study is the first to revise the current UKCA dry deposition scheme which is based on a simplification of the parameterizations suggested by Wesely (1989) (here called WES scheme). Some errors in the existing implementation of the UKCA dry deposition parameterizations were identified and corrected, quantifying their effects on modelled O_3 and detailed in Chapter 2. An alternative non-stomatal deposition approach along with the effect of the blocking of stomata, based on a simplified version of the Zhang et al. (2003) parameterizations (here called ZHG scheme), has been successfully incorporated in the UKCA model. The sensitivities of the modelled O_3 deposition and surface O_3 concentrations to the different deposition approaches were thoroughly investigated in this study (Chapter 2 and Chapter 3).

Secondly, this thesis has compared the performance of both schemes with measurements, focussing on the diurnal and seasonal variations of the dry deposition velocity terms and the partitioning of O_3 fluxes between stomatal and non-stomatal sinks. This study is the first to investigate the UKCA dry deposition scheme in detail and identify the difficulties in comparing modelled and measured O_3 V_d due to low model spatial resolution and incomplete representation of sub-grid variations in surface (vegetation) specific characteristics and the driving meteorological variables. Furthermore, off-line sensitivity tests conducted on the modelled non-stomatal

deposition component using the ZHG scheme, showed the importance of modelling some key environmental factors accurately (e.g. friction velocity, relative humidity, leaf area index).

A comparison of the modelled surface O_3 concentrations with observations, from a range of monitoring sites in the NH and SH, has been presented in this thesis (Sections 3.4.2.1 and 3.4.2.2). This allowed, for the first time, an examination of the sensitivity of the modelled surface O_3 with UKCA to different dry deposition approaches at present day conditions and to compare their performances against observations. This analysis showed that the observed surface O_3 seasonal cycle and the absolute concentration values are simulated well using both WES and ZHG schemes across the NH sites used for this study. For these sites, ZHG generally leads to a reduction of the relative annual bias, although the correlation with measured values is slightly deteriorated compared to WES (Table 3.4). By contrast, both the schemes fail to capture the observed surface O_3 seasonal cycle and absolute O_3 concentration values across the SH sites used for this study, with ZHG exhibiting a larger annual bias than WES (Table 3.5).

Overall, this work represents a first significant step forward in understanding of both WES and ZHG dry deposition approaches in UKCA. The results of this study showed that the ZHG scheme may lead to an improved average O_3 deposition sink, with a more mechanistic partitioning of the total O_3 between its stomatal and non-stomatal components. However, due to the variability in the results and the limited amount of O_3 datasets considered here, it is not possible to conclude whether ZHG should replace or not the WES scheme in UKCA.

Neither WES nor ZHG provide a fully mechanistic representation of O_3 deposition in UKCA and obtaining improvements in both the approaches still remains challenging. Long term measurements with high temporal resolution, covering the full seasonal cycles (especially over vegetated areas at mid-high latitudes in the NH and over tropical regions) as detailed in Section 5.2.1, are urgently needed to provide a generic improvement of both the WES and ZHG approaches as well as to further assess both the schemes across different vegetation types and climate conditions.

A meta-analysis of a large number of well quality-assured datasets and an improvement in the understanding of non-stomatal processes such the interaction of

O_3 with leaf water films and in-canopy O_3 chemistry sinks mediated by bVOC (Section 5.2.1), are urgently required to develop more mechanistic O_3 deposition parameterizations which works well across sites and seasons to be used for future UKCA O_3 deposition studies.

The sensitivity of global ozone predictions to dry deposition schemes and their response to climate change (induced by the increases in GHGs with RCP 8.5 scenario) has been investigated using UKCA. By contrasting two different deposition schemes (WES and ZHG) with quite different treatment of the non-stomatal component, allowed an identification of the key differences in the response of global O_3 deposition and global surface O_3 to climate change. The influence of climate change on the O_3 dry deposition flux partitioning was also investigated in this study.

To conclude, the results of this thesis work emphasize that the representation of the O_3 dry deposition processes in a global climate-chemistry model does matter and different approaches can lead to contrasting O_3 simulation results, with potential implications for both climate and air quality studies under present day and future climate conditions. Therefore, to help reducing the uncertainties in modelling surface O_3 and O_3 deposition, further investigations and developments of dry deposition schemes should remain a priority for GCM modellers.

In response to the research questions proposed in Section 1.9, a summary of the most significant findings is presented hereafter.

5.1 Summary of key findings

I. The current UKCA dry deposition scheme has been revised and the sensitivity of O_3 deposition and surface O_3 to a mechanistic non-stomatal deposition approach has been tested at the global scale.

(a) The current UKCA dry deposition scheme, based on a simplified version of the Wesely (1989) parameterizations, has been thoroughly investigated and described (Sections 2.2.4-2.2.5). Incorrect values for stomatal conductance of water vapour and the lack of the in-canopy aerodynamic resistance for some of the dry deposited chemical species, constituted the two main problems which were identified and corrected in the UKCA dry deposition scheme (WES scheme) (Sections 2.2.6.1-2.2.6.2).

(b) The impacts of model corrections on simulated O_3 were investigated and quantified (Sec. 2.3.1). As a result of the model amendments, the O_3 stomatal uptake decreased and the non-stomatal deposition increased over vegetated areas globally; this led to a reduction of the O_3 dry deposition velocity over land, particularly over Eurasia, N. America and Central Africa with changes by as much as -50%. This was associated with a decrease in O_3 deposition over land up to -30%. As a consequence of all the model changes, an increase in intercontinental O_3 transport from Asia and N. America to the Arctic was found due to reduced O_3 deposition over land. Overall, the total annual global dry deposition reduced by -150 $Tg(O_3)$ yr^{-1} (-13%) and this led to a small increase of the O_3 life time (+0.7 days; +3.4%).

(c) The implementation of a more mechanistic non-stomatal deposition approach and the effect of blocking of stomata (ZHG scheme) led to significant changes of the modelled annual mean distribution of surface O_3, V_d and O_3 dry deposition flux using UKCA (Sec. 2.3.2). V_d considerably increased in the NH across Eurasia and N. America as much as +40% and decreased over tropical regions (up to -30%) owing to differences in the modelled the stomatal and non-stomatal deposition using ZHG compared to WES (Sections 2.3.2.2-2.3.2.3). This led to a

decrease of O_3 deposition up to -20% over the same areas and an increase of as much as +20% over tropical regions and E. Asia.

(d) Differences in surface O_3 concentration were found using ZHG compared to WES, with a decrease up to -20% over most land surfaces in the NH, due to the increased dry deposition, and an increase of up to 20% over tropical areas and E. Asia (Sec. 2.3.2.1) as a result of decreases in dry deposition. The change of scheme also led to hemispheric differences in O_3 concentrations throughout the troposphere. ZHG showed larger values over the tropical lower troposphere (up to +16%) and the Arctic (up to 10%) whereas more uniform and smaller values (up to -4%) were simulated with ZHG over the NH mid-latitudes compared to WES (Sec. 2.3.2.1).

II. The WES and ZHG dry deposition schemes and modelled surface O_3 have been compared with observations focusing on their diurnal/seasonal variations. Subsequently, the sources of uncertanty of the UKCA modelled O_3 dry deposition velocity terms using both the schemes have been investigated.

(a) A comparison of modelled O_3 V_d using the WES and the ZHG schemes over three different vegetation types (Broadleaf and Needleleaf forests, C3 grass and crop) across Europe and USA revealed that overall UKCA captures the diurnal variations of V_d quite well. However, substantial differences between modelled and observed aerodynamic, boundary layer and canopy resistance terms were identified, many of which were due to the measured values being provided by land cover variables that did not match the values for the large grid square values in the model (Sec. 3.4.1). Thus, inconsistencies in the input parameters, non-specific vegetation type meteorological factors used in the dry deposition parameterizations constitute the main source of uncertainties in the modelled V_d using both the schemes (Table 3.1).

(b) Discrepancies between modelled and observed values of key meteorological factors such as u_*, *RH*, *LE* and *H* fluxes were found (Sec. 3.4.1). Due to inconsistencies between modelled and observed *SMC* at the root zone and *VPD*, modelled canopy stomatal conductance for O_3 (G_s) was greatly overestimated for

the Mediterranean broadleaf forest at Castelporziano both in spring and in summer (~ 6 mm s^{-1}) and also significantly for the needleleaf forest in summer (~ 3 mm s^{-1}).

Differences between model and observed vegetation properties such as *LAI*, canopy height (h_c) and roughness properties (z_0) were also detected (Tables 3.6-3.7-3.8). Inconsistencies in the representation of u_*, z_0 and h_c leads to systematic uncertainties between model and observed aerodynamic R_a (z-d) and boundary layer R_b resistances (Table 3.1).

(c) ZHG scheme increased the O_3 non-stomatal deposition by to 60% over the coniferous forest site of Hyytiälä and over the grassland site at Easter Bush by as much as of 62% on annual average compared to WES. The fraction of non-stomata deposition simulated with ZHG for NL tree and C3 grass at Hyytiälä and Easter Bush is closer to observations than WES (Fowler et al., 2001; Coyle, 2005; Rannik et al., 2012). By contrast, the modelled non-stomatal deposition was always smaller (28% with WES and 14% with ZHG) than observations (up to 70%) on annual average (Gerosa et al., 2009).

(d) The very limited land cover types implemented in MOSES 2.2 and UKCA constitute a first key uncertainty in simulating O_3 deposition (both Wesely (1989) and Zhang et al. (2003) parameterizations were formulated for a more detailed land cover classification). The low spatial resolution and the fact that certain meteorological parameters are only simulated at the grid cell level, increases the level of uncertainty further. The model dynamical variables were adjusted towards ECMWF ERA-40 re-analysis data. However, this study showed that differences between modelled and observed meteorological factors still exist, partly attributed to the aggregation of vegetation and land cover properties.

(e) Off-line sensitivities tests were conducted on the O_3 non-stomatal conductance (G_{ns}) driving the ZHG scheme with observed *RH*, u_* and *LAI* (Sections 3.3.4-3.4.1). Using these real environmental factors, modelled G_{ns} with ZHG performed better than WES at Castelporziano in spring and at Hyytiälä in summer. By contrast WES led to a better agreement of modelled G_{ns} than ZHG

at Hyytiälä. Overall, this study tested the structural correctness of the ZHG O_3 non-stomatal parameterizations, revealing that the following three non-stomatal deposition pathways may be not yet represented in the model: (i) O_3 thermal decomposition occurring on vegetated surfaces (Coyle et al., 2009; Fowler et al., 2001, 2009); (ii) O_3 leaf aqueous chemistry mediated by BVOC (Fares et al., 2009; Rannik et al., 2012); (iii) the additional in-canopy O_3 chemical sink due to the reactions with NO (Gerosa et al., 2009).

(f) Overall, modelled surface O_3 concentrations compares well with observations in the NH using both WES and ZHG scheme, reproducing the observed O_3 seasonal cycle and the absolute values (Sec. 3.4.2.1). With regards to the monitoring sites considered in this study, ZHG leads to a reduction of the relative annual bias (-13.5%) on average compared to WES. By contrast, the model performs less well in the SH sites considered here (Sec. 3.4.2.2). Overall, in the SH the model failed to capture the seasonal and absolute values, apart of the Syowa and the South Pole sites where UKCA performs well using both the schemes. Modelled surface O_3 using ZHG exhibited a larger annual bias using the ZHG scheme (60% on average) compared to WES (47% on average).

(g) UKCA modelled O_3 concentrations are very sensitive to the change of dry deposition (Section 2.3.2.1). ZHG scheme led to a hemispheric difference of O_3 concentrations, with larger values (up to 16%) over the tropical troposphere and more uniform and smaller changes (up to -4%) throughout the NH mid-latitudes compared to WES. By contrast, ZHG leads to an increase in O_3 concentration (up to 10%) in the Arctic lower troposphere.

III. UKCA has been used to explore the sensitivity of future O_3 predictions to different dry deposition schemes and their response to changing climate conditions with the RCP 8.5 scenario.

(a) As a result of climate change induced by the increase in GHGs only under the RCP 8.5 scenario (under the same anthropogenic emissions and land use scenario), modelled O_3 V_d largely decreases especially over heavily vegetated

surface areas both in the NH (up to -25% across N. America, Europe and E. Asia) and in the SH (up to -35% in S. America and C. Africa) (Sec. 4.3.3). Both WES and ZHG show an increase of V_d over non-vegetated areas including the polar regions (by up to 15%), the Arabian peninsula as well as parts of India and N. Australia. Model results showed that changes in surface O_3 predicted as a response to climate with RCP 8.5 are mostly positive over land (up to 25% over mid-latitudes in the NH, 30% over S. America and 20% over C. Africa). Regional differences were found between modelled changes in surface O_3 with the WES and the ZHG schemes (Table 4.1). A strong increase in surface O_3 concentrations (up to 30%) at the northern high latitudes was predicted using both WES and ZHG schemes (Sec. 4.3.3). Such changes would have important consequences for human health, with large increases in effects in the major developed countries.

(b) Whilst the WES and ZHG behave similarly, the decrease in V_d induced by climate change is generally larger in ZHG, with less decreases in the NH and more increases over tropical regions predicted with ZHG compared to WES (Sec. 4.3.4). The different responses of the stomatal and non-stomatal deposition to climate change simulated with WES and ZHG explain the regional differences in V_d changes (Table 4.2).

(c) Model results showed that an increase in turbulence constitutes the main driver of the changes in V_d. As a result of a general increase in turbulence (except of E. Asia and S. Australia), $R_a + R_b$ generally decrease (Table 4.2). In some cases this change is further exacerbated by increases in G_s and G_{ns} (e.g. E. Asia and N. Australia), resulting in increases in V_d. More often, the increase in turbulence is more than compensated by decreases in G_{ns} using ZHG, resulting in a decrease in V_d. By contrast, the decreases in G_s and the changes in G_{ns} simulated with WES, associated with changes in the soil moisture availability, generally led to a reduction of V_d.

(d) Although other factors contribute to O_3 changes as a response to global warming (Jacob and Winer, 2009; Fiore et al., 2012), this study results showed that modelled surface O_3 induced by climate change are sensitive to different dry

deposition parameterizations. Using ZHG, the predicted surface O_3 changes are larger than WES especially over the US (up to 3 ppb), S. Asia (up to 2.4 ppb) and E. Asia (up to 1.8 ppb) on average (Sec. 4.3.4). This means that changes in deposition might exacerbate the "climate penalty" (Wu et al., 2008) on future O_3 production. Model results indicate that this effect might be more important over USA, Europe and E. Asia, where ZHG exhibits larger changes in O_3 deposition compared to WES as a response to climate change (Sec. 4.3.4).

(e) The influence of climate change on the O_3 dry deposition flux has been investigated (Sec. 4.7). Model results indicate that generally using WES, more O_3 might be generally deposited through stomata especially over tropical forests as a response to climate change. By contrast, ZHG showed more regionally distributed variations in the ratio G_s/G_c, with the larger changes simulated over W. America, C. Europe and E. Asia. This indicates that over these areas, ZHG leads to increase of O_3 deposited through stomatal pathways compared to WES as a response to climate change. In the SH, the regional responses of the G_s/G_c simulated with ZHG indicate that climate change may lead to some counteracting effects especially over tropical coastal areas and across S. Asia due to changing meteorological conditions (u_*, *CWC*, *RH* and *SMC*). These results might have potential implications for present day and future O_3 damage assessment studies. However, more work is needed to better quantify the effect of climate on the stomata flux and the effect of future climate on the phyto-toxic O_3 dose.

5.2 Future work

5.2.1 Observations needed to further evaluate and improve the UKCA dry deposition scheme

The WES and ZHG parametrizations for ozone were originally developed using measurements over a limited amount of vegetation canopies (mainly in N. America) and other surface types (Wesely, 1989; Zhang et al., 2002a,b, 2003). Therefore, both the approaches cannot be considered fully mechanistic as they were derived under restricted meteorological and environmental conditions.

Further evaluations are needed using large number of observations covering long time periods across different ecosystems and climate conditions. This may help developing more mechanistic parameterizations that work well for different vegetation types and seasons as well as to better understanding both the WES and ZHG schemes in UKCA.

The measurements described below are recommended over broadleaf and needle evergreen/deciduous forests in the NH (particularly at mid-high latitudes), over tropical forested areas, over grassland (and crops) and moorland across Eurasia, East and South Asia.

a) Long term well-quality assured O_3 flux measurements with eddy-covariance (EC) technique and high temporal resolution (hourly) from both above and below the canopy (Altimir et al., 2006; Gerosa et al., 2009; Fares et al., 2014) covering the full seasonal cycle. Long term measurements of O_3 concentration using chemiluminescence from both above and below the canopy (Fares et al., 2014) and possibly at multiple canopy levels.

b) Hourly shoot-scale measurements of O_3 flux using the enclosure technique are also desirable to provide an estimate of the O_3 deposition for broadleaf and needleleaf forests at the leaf scale (Altimir et al., 2006).

c) Hourly micro-meteorological measurements of turbulent fluxes of CO_2, H_2O, sensible heat and latent heat fluxes and energy exchange between the canopy environment and the atmosphere are recommended using EC method

(Fares et al., 2014). Measuring standard meteorological conditions (ambient and leaf surface temperature, ambient relative humidity, rainfall, wind direction, turbulence) with sensors at multiple canopy levels is also advisable (Schallhart et al., 2016).

d) More accurate measurements of solar radiation and leaf surface wetness at multiple canopy levels are recommended to better characterize the effect of stomata blocked by water films forming on the leaves after rain or dew events (Zhang et al., 2002a).

e) To better characterize and parameterize the O_3 non-stomatal deposition to vegetation canopies, the following long term (hourly) measurements are recommended: (i) chemical composition analysis of the leaf surface aqueous solutions (Poitier et al., 2015), possibly at multiple canopy levels; (ii) bVOC fluxes and concentrations using proton-transfer-reaction mass Spectrometer (PTR-MS) at several heights within the canopy and at the bottom (Acton et al., 2016; Schallhart et al., 2016)

f) More laboratory (chamber) experiments are desirable to help characterizing the chemical composition of aqueous solutions on leaves and to better understand how different chemical/biological/physical properties may affect the O_3 (non-stomatal) deposition to plant surfaces and other non-vegetated materials (Fuentes et al., 1994; Cape et al., 2009; GrØntoft et al., 2004; Jud et al, 2016).

g) Hourly long term observations of NO and NO_2 flux using EC are also desirable as these may help to better quantify the O_3 storage inside the canopy and to model its related effect on the O_3 non-stomatal deposition (Gerosa et al., 2009; Fumagalli et al., 2016). Hourly in-canopy concentration measurements of NO_x, CO_2 at different canopy heights using chemiluminescence are also advisable (Schallhart et al., 2016).

h) Hourly long term measurements of the net leaf photosynthesis rate (A_l), internal and leaf surface CO_2 partial pressure, soil moisture content and soil temperature (Marzuoli et al., 2016) at different depths would allow a more sensible assessment of the H_2O (and O_3) stomatal conductance used in UKCA (detailed in Chap.2).

5.2.2 Model simulations and developments

In Chap. 2 some errors in the UKCA deposition parameterizations were introduced and the effects of their corrections on simulated O_3 were presented. In particular, this study investigated and quantified the impacts of the changes in canopy stomatal conductance for water vapour and the in-canopy aerodynamic resistance on modelled O_3 V_d, surface O_3 concentrations and O_3 deposition, showing that these effects were significant. However, the effects of these model corrections on surface NO_2/PANs (here called NO_w) and NO_w deposition remains to be better quantified. O_3 production and chemical removal are sensitive to NO_x concentrations (Royal Society, 2008). In particular, the difference between the model outputs of a simulation in which the corrections are applied to NO_2 and PAN species only whilst the original deposition parameterizations are used for O_3, would allow an investigation of the effects of changes in NO_w on the O_3 production or chemical loss. A better analysis of these effects in future UKCA studies is also important for the climate interactions between O_3 and N (Royal Society, 2008; Simpson et al., 2014; Mills et al., 2016).

Results presented in Chapter 3 provided potential source of improvements of modelled O_3 V_d in UKCA. Implementing a more land specific representation of u_* in UKCA should lead to a more realistic influence of turbulence on the aerodynamic and quasi-laminar boundary resistance components. This should also provide a better representation of the O_3 non-stomatal deposition (G_{ns}), as shown with the sensitivity tests conducted on G_{ns} simulated using the ZHG scheme. Chapter 3 showed that, discrepancies between specific vegetated and non-vegetated properties associated with a poor land cover representation and low model resolution, represent other sources of uncertainties. Therefore, the use of a more developed land cover type (as done in JULES 3.2) would be beneficial in future UKCA O_3 deposition and surface O_3 studies.

A multi-layer canopy photosynthesis approach with two stream canopy photosynthetic active (PAR) radiation interception model (calculating upward and downward scattered direct and diffuse beam radiation components for each of 10 canopy layers) might also lead to a further improvement as study results indicate that this approach leads to a better representation of the light response and diurnal cycle

of the canopy photosynthesis and the canopy stomatal conductance (Jogireddy et al., 2006; Mercado et al., 2007; Clark et al., 2011).

Jogeriddy et al. (2006) also pointed out that assessing and better calibrating some tuneable parameters associated with the leaf photosynthesis approach used in MOSES 2.2 (JULES), is crucial to improve the canopy light interception. Therefore, a more explicit investigation and characterization of these parameters for each vegetation type is highly recommended in future UKCA O_3 studies.

Chapter 3 also revealed discrepancies between some key specific modelled vegetation type properties (*LAI*, h_c, z_0) and observations. For *LAI*, the use of higher resolution (e.g. remote sensing *LAI* data) is highly advisable. Chapter 3 highlighted the need of a more detailed assessment of the capability of MOSES 2.2 (JULES) to simulate *SMC,* due to its crucial role in regulating the stomatal conductance aperture through the water stress factor β (Cox et al., 1999; Best et al., 2011).

Finally, Chapter 4 showed that the potential influence of climate change, induced by the increases of GHGs only with RCP 8.5, on global O_3 deposition and global tropospheric O_3 concentrations may be significant. However, other modelling studies indicate that changes in future land use (Ganzeveld et al., 2010; Wu et al., 2012; Squire et al., 2014; Verbeke et al., 2015), anthropogenic and isoprene emissions (Squire et al., 2014) may have relevant effects on future O_3 and O_3 deposition.

The sensitivity of modelled tropospheric O_3 and O_3 deposition using different dry deposition schemes to these climate change related effects with RCP 8.5 scenario remains unexplored. A set of model integrations would allow an investigation of the combined and separated impacts of these changes on future O_3 and O_3 deposition, and further exploring the sensitivity of UKCA modelled O_3 predictions to different dry deposition approaches.

This study also investigated the influence of climate change on the O_3 flux partitioning, showing that ZHG scheme leads to larger changes of the ratio between stomatal and the total canopy conductance (G_s/G_c) compared to WES. However, the impacts of climate change on the O_3 stomatal flux and the phyto-toxic O_3 need to be better investigated and quantified.

Bibliography

Acton,W. J. F., Schallhart, S., Langford, B., Valach, A., Rantala, P., Fares, S., Carriero, G., Tillmann, R., Tomlinson, S. J., Dragosits, U., Gianelle, D., Hewitt, C. N., and Nemitz, E.: Canopyscale flux measurements and bottom-up emission estimates of volatile organic compounds from a mixed oak and hornbeam forest in northern Italy, Atmos. Chem. Phys., 16, 7149–7170, 2016.

Andersson, C. and Engardt, M.: European ozone in a future climate: Importance of changes in dry deposition and isoprene emissions, J. Geophys. Res.-Atmos., 115, D02303, doi:10.1029/2008jd011690, 2010.

Abraham, L., Archibald, A.T., Bellouin, N., Boucher, O., Braesicke, P., Bushell, A., Carslaw, K., Collins, B., Dalvi, M., Emmerson, K., Folberth, G., Haywood, J., Johnson, C., Kipling, Z., Macintyre, H., Mann, G., Telford, P., Merikanto, J., Morgenstern, O., O'Connor, F., Ordonez, C., Osprey, S., Pringle, K., Pyle, J., Rae, J., Reddington, Savage, S., Spracklen, D., Stier, P. and West, R.: Unified Model Documentation Paper No. 84: United Kingdom Chemistry and Aerosol (UKCA) Technical Description MetUM Version 8.2, available on www.UKCA.ac.uk/wiki/index.php/Documentation, 1-70, 2012.

Ainsworth, E.A., Yendrek, C.R., Sitch, S., Collins, W.J., and Emberson, L.: The effects of tropospheric ozone on net primary productivity and implications for climate change, Annu. Rev. Plant Biol., 63: 637-661, 2012.

Albert, M. R., Grannas, A. M., Bottenheim, J., Shepson, P. B., and Perron, F. E.: Processes and properties of snow-air transfer in the high Arctic with application to intersticial ozone at Alert, Canada, Atmos. Environ., 36, 2379–2787, 2002.

Altimir, N., Kolari, P., Tuovinen, J.-P., Vesala, T., Bäck, J., Suni, T., Kulmala, M., and Hari, P.: Foliage surface ozone deposition: a role for surface moisture?, Biogeosciences, 3, 209–228, 2006.

Ashmore, M.: Assessing the Future Global Impacts of Ozone on Vegetation, Plant Cell Environ., 28, 949–964, 2005.

Ashmore, M., Emberson, L., Karlsson, P. E., and Pleijel, H.: New Directions: A new generation of ozone critical levels for the protection of vegetation in Europe, Atmos. Environ., 38, 2213–2214, 2004.

Atkinson, R.: Atmospheric chemistry of VOCs and NOx, Atmos. Environ., 34, 2063– 2101, 2000.

Banerjee, A., Archibald, A. T., Maycock, A. C., Telford, P., Abraham, N. L., Yang, X., Braesicke, P., and Pyle, J. A.: Lightning NOx, a key chemistry–climate interaction: impacts of future climate change and consequences for tropospheric oxidising capacity, Atmos. Chem. Phys., 14, 9871–9881, 2014.

Bassin, S., Calanca, P., Weidinger, T., Gerosa, G., and Fuhrer, J., Modelling seasonal ozone fluxes to grassland and wheat: Model improvement, testing, and application, Atmos. Environ., 38, 2349–2359, 2004.

Bates, D. V.: Ambient ozone and mortality, Epidemiology, 16, 427–429, 2005.

Bentley, D., Deposition Studies, Met Office, January 2014.

Best, M. J., Pryor, M., Clark, D. B., Rooney, G. G., Essery, R .L. H., Ménard, C.B., Edwards, J.M., Hendry, M.A., Porson, A., Gedney, N., Mercado, L.M., Sitch, S., Blyth, E., Boucher, O., Cox, P.M., Grimmond, C.S.B., and Harding, R.J.: The Joint UK Land Environment Simulator (JULES), model description – Part 1: Energy and water fluxes, Geosci. Model Dev., 4, 677– 699, 2011.

Bloomer, B. J., Stehr, J.W., Piety, C. A., Salawitch, R. J., and Dickerson, R. R.: Observed relationships of ozone air pollution with temperature and emissions, Geophys. Res. Lett., 36, L09803, doi:10.1029/2009gl037308, 2009.

Brasseur, G. P., Schultz, M. G., Granier, C., Saunois, M., Diehl, T., Botzet, M., Roeckner, E., and Walters, S.: Impact of climate change on the future chemical composition of the global troposphere, J. Clim., 19, 3932–3951, 2006.

Brook, J., Zhang, L., Franco, D., and Padro, J.: Description and evaluation of a model of deposition velocities for routine estimates of air pollutant dry deposition over North America, Part I: Model development, Atmos. Environ., 33, 5037–5052, 1999.

Brueniger, C., Oswald R., Kesselmeier, J., Meixner, F.X, The dynamic chamber method: trace gas exchange fluxes (NO, NO_2, O_3) between plants and the atmospherein the laboratory and in the field, Atmos. Meas. Tech., 5, 955-989, 2012.

Brutsaert, W., Evaporation into the Atmosphere, Kluwer Academic, Norwell, Mass., 1973.

Büker, P., Morrissey, T., Briolat, A., Falk, R., Simpson, D., Touvinen, J.P., Alonso, R., Barth, , Baumgarten, S., Grulke, N., Karlsson, P.E., King, J., Lagergren, F., Matyssek, R., Nunn, A., Ogaya, R., Peñuelas, J., Rhea, L., Schaub, M., Uddling, J., Werner, W., and Emberson, L.D.: DO_3SE modelling of soil moisture to determine ozone flux to forest trees, Atmos. Chem. Phys., 12, 5537-5562, 2012.

Butchart, N., Scaife, A. A., Bourqui, M., et al.: Simulations of anthropogenic change in the strength of the Brewer-Dobson circulation, Clim. Dynam., 27, 727–741, 2006.

Cape, J.N., Hamilton, R., Heal, M.R.: Reactive uptake of ozone at simulated leaf surfaces: implications for ‘non-stomatal’ ozone deposition, Atmos. Environ., 43, 1116–1123, 2009.

Cieslik, S.: Ozone uptake at various surface types: a comparison between dose and exposure, Atmos. Environ., 38, 2409-2420, 2004.

Clark, D. B., Mercado, L. M., Sitch, S., Jonem C. D., Gedneym N.: The Joint UK Land Environment Simulator (JULES), model description – Part 2: Carbon fluxes and vegetation dynamics, Geosci. Model Dev., 4, 701– 722, 2011.

Colette, A., Bessagnet, B., Vautard, R., Szopa, S., Rao, S., Schucht, S., Klimont, Z., Menut, L., Clain, G., Meleux, F., Curci, G., and Rouïl, L.: European atmosphere

in 2050, a regional air quality and climate perspective under CMIP5 scenarios, Atmos. Chem. Phys., 13, 7451–7471, 2013.

Collatz, G.J., Ribas-Carbo, M., and Berry, J.A.: A coupled photosynthesis-stomatal conductance model for leaves for C4 plants. Australian Journal of Plant Physiol., 19, 519 – 538, 1992.

Collatz, G.J., Ball, J.T., Grivet, C. and Berry, J.A. : Physiological and environmental regulation of stomatal conductance, photosynthesis and transpiration: a model that includes a laminar boundary layer, Agricult. Forest Meteorol., 54, 107 – 136, 1991.

Cooper, O. R., Parrish, D. D., Ziemke, J., Balashov, N. V., Cupeiro, M., Galbally, I. E., Gilge, S., Horowitz, L., Jensen, N. R., Lamarque, J. F., Naik, V., Oltmans, S. J., Schwab, J., Shindell, D. T., Thompson, A. M., Thouret, V., Wang, Y., and Zbinden, R. M.: Global distribution and trends of tropospheric ozone: An observation-based review, Elem. Sci. Anth., 2, 000029, doi:10.12952/journal.elementa.000029, 2014.

Coyle, M., Nemitz, E., Storeton-West, R., Fowler, D., and Cape, J. N.: Measurements of ozone deposition to a potato canopy, Agricul. Forest Meteor., 149 (3-4). 655-666., 2009.

Coyle, M., Fowler, D., Nemitz, E., Philips, G., Storeton-West, R., Thomas, and Field, R.: Measurements of the ozone flux to vegetation. In: Ozone Umbrella: Effects of Ground-level Ozone on (Upland) Vegetation in the UK. Centre of Ecology and Hydrology, UK, pp. 68–104. CEH C02158 Report No. AS 06/02, 2006.

Coyle, M.. The Gaseous Exchange of Ozone at Terrestrial Surfaces: Non-stomatal Deposition to Grassland, School of Geosciences, Faculty of Science and Engineering, PhD thesis. The University of Edinburgh, Edinburgh, 270 pp, 2005.

Cox, P. M., Betts., R. A. , Collins, M., Harris, P. P., Huntingford, C., and Jones, C. D.: Amazonian forest dieback under climate-carbon cycle projections for the 21st century, Theor. Appl. Climatol. 78, 137–156, 2004.

Cox, P. M., Betts, R. A., Jones, C. D., Spall, S. A., and Totterdell, I. J.: Modelling vegetation and the carbon cycle as interactive elements of the climate system. In: Pearce R (ed) Meteorology at the millennium. Academic Press, pp 259–279, 2001.

Cox, P. M., Betts, R. A., Bunton, C. B., Essery, R. L. H., Rowntree, P. R.: Smith J., The impact of new land surface physics on the GCM simulation of climate and climate sensitivity, Climate Dynamics, 15, 183 – 203, 1999.

Cox, P.M., Huntingford, C., Harding, R.J.: A canopy conductance and photosynthesis model for use in a GCM land surface scheme, Journal of Hydrology, 212-213, 79-94, 1998.

Crutzen, P. J.: Photochemical reactions initiated by and influencing ozone in the unpolluted troposphere, Tellus, 26, 47–57, 1973.

Doherty, R. M., Wild, O., Shindell, D. T., Zeng, G., MacKenzie, I. A., Collins, W. J., Fiore, A. M., Stevenson, D. S., Dentener, F. J., Schultz, M. G., Hess, P., Derwent, R. G., and Keating, T. J.: Impacts of climate change on surface ozone and intercontinental ozone pollution: A multi-model study, J. Geophys. Res.-Atmos., 118, 3744–3763, 2013.

Doherty, R. M., Stevenson, D. S., Collins, W. J., and Sanderson, M. G.: Influence of convective transport on tropospheric ozone and its precursors in a chemistry-climate model, Atmos. Chem. Phys., 5, 3205–3218, 2005.

Dupont, S. and Patton, E. G.: Momentum and scalar transport within a vegetation canopy following atmospheric stability and seasonal canopy changes: the CHATS experiment, Atmos. Chem. Phys., 12, 5913–5935, 2012.

Dyer, A. J. and Hicks, B. B.: Flux-gradient relationships in the constant flux layer. Quarterly Journal of the Royal Meteorological Society, 96(410), 715–721. ISSN 1477-870X.doi:10.1002/qj.49709641012., 1970.

Duyzer, J., Weststrate, H., Walton, S.: Exchange of ozone and nitrogen oxides between the atmosphere and coniferous forest. Journal Water, Air, & Soil Pollution 85 (4), 2065–2070. Springer, Netherlands, 1995.

Emberson, L.D., Kitwiroon, N., Beevers, S., Büker, P., and Cinderby, S.: Scorched Earth: how will changes in the strength of the vegetation sink to ozone deposition affect human health and ecosystems?, Atmos. Chem. Phys., 13, 6741-6755, 2013.

Emberson, L. D., Ashmore, M. R., Cambridge, H. M., Simpson, D., and Tuovinen, J.-P.: Modelling stomatal ozone flux across Europe, Environ. Poll., 109, 403–413, 2000a.

Emberson, L.D., Simpson, D., Tuovinen, J.-P., and Ashmore, M.R.: Cambridge, H.M.: Towards a model of ozone deposition and stomatal uptake over Europe. EMEP/ MSC-W Note 6/2000b. Norwegian Meteorological Institute, Oslo, 2000, www.emep.int/reports/dnmi note 6 2000.pdf,.

Erisman, J.W., Vanpul, A., Wyers, P., 1994. Parameterization of surface-resistance for the quantification of atmospheric deposition of acidifying pollutants and ozone. Atmos. Environ., 28, 2595–2607.

Essery, R. L. H., Best, M. J., Betts, R. A., Cox, P. M., and Taylor, C. M.: Explicit representation of subgrid heterogeneity in a GCM land surface scheme, J. Hydromet., 4, 530–543, 2003.

Essery, R. L., Best M. and Cox, P. L.: MOSES 2.2 technical documentation. Hadley Centre Tech. Note 30, Met Office, Bracknell, United Kingdom, 30 pp., 2001.

Fares, S., Savi, F., Muller, J., Matteucci, G. and Paoletti, E.: Simultaneous measurements of above and below canopy ozone fluxeshelp partitioning ozone deposition between its various sinks in a Mediterranean Oak Forest, Agric. For. Meteorol., 198-199, 181-191, 2014.

Fares, S., Matteucci, G., Mugnozza, G. S., Morani, A., Calfapietra, C., Salavatori, E., Fusaro, L., Manes F., and Loreto, F.: Testing of models of stomatal ozone fluxes

with field measurements in a mixed Mediterranean forest, Atmos. Environ., 67, 242–251, 2013.

Fares, S., McKay, M., Holzinger, R., Goldstein, A.H.: Ozone fluxes in a Pinus ponderosa ecosystem are dominated by non-stomatal processes: evidence from long-term continuous measurements. Agric. For. Meteorol., 150,420–431, 2010a.

Fares, S., Goldstein, A., Loreto, F.: Determinants of ozone fluxes and metrics for ozone risk assessment in plants. J. Exp. Bot., 61:629–33, 2010b.

Fares, S., Mereu, S., Scarascia Mugnozza, G., Vitale, M., Manes, F., Frattoni, M., Ciccioli, P., Gerosa, G. and Loreto, F.: The ACCENT-VOCBAS field campaign on biosphere-atmosphere interactions in a Mediterranean ecosystem of Castelporziano (Rome): site characteristics, climatic and meteorological conditions, and eco-physiology of vegetation, Biogeosciences, 6, 1043–1058, 2009.

Finkelstein, P.L., Ellestad, T.G., Clarke, J. F., Meyers, T. D., Schwede, D. B., Hebert, E. O. and Neal, J.A.: Ozone and sulfur dioxide dry deposition to forests: Observations and model evaluation, Geophys. Res. Lett.,105, 15.365-15.377, 2000.

Fiore, A. M., Naik, V., Spracklen, D. V., Steiner, A., Unger, N., Prather, M., Bergmann, D., Cameron-Smith, P. J., Cionni, I., Collins, W. J., Dalsoren, S., Eyring, V., Folberth, G. A., Ginoux, P., Horowitz, L. W., Josse, B., Lamarque, J.-F., MacKenzie, I. A., Nagashima, T., O'Connor, F. M., Righi, M., Rumbold, S. T., Shindell, D. T., Skeie, R. B., Sudo, K., Szopa, S., Takemura, T., and Zeng, G.: Global air quality and climate, Chem. Soc. Rev., 41, 6663–6683, 2012.

Fiore, A. M., Dentener, F. J., Wild, O., Cuvelier, C., Schultz, M. G., Hess, P., Textor, C., Schulz, M., Doherty, R. M., Horowitz, L. W., MacKenzie, I. A., Sanderson, M. G., Shindell, D. T., Stevenson, D. S., Szopa, S., Van Dingenen, R., Zeng, G., Atherton, C., Bergmann, D., Bey, I., Carmichael, G., Collins, W. J., Duncan, B. N., Faluvegi, G., Folberth, G., Gauss, M., Gong, S., Hauglustaine, D., Holloway, T., Isaksen, I. S. A., Jacob, D. J., Jonson, J. E., Kaminski, J. W., Keating, T. J., Lupu, A., Marmer, E., Montanaro, V., Park, R. J., Pitari, G., Pringle, K. J., Pyle, J. A., Schroeder, S., Vivanco, M. G., Wind, P., Wojcik, G., Wu, S., and Zuber, A.: Multimodel estimates of intercontinental source-receptor relationships for ozone pollution, J. Geophys. Res.-Atmos., 114, D04301, doi:10.1029/2008jd010816, 2009.

Flechard, C.R., Nemitz, E., Smith, R.I., Fowler, D., Vermeulen, A.T., Bleeker, A., Erisman, J.W., Simpson, D., Zhang, L., Tang, Y.S., and Sutton, M.A.: Dry deposition of reactive nitrogen to European ecosystems: a comparison of inferential models across the NitroEurope network, Atmos. Chem. Phys., 11, 2703-2728, 2011.

Fowler, D., Pilegaard, K., Sutton, M. A., Ambus, P., Raivonen, M., Duyzer, J., Simpson, D., Fagerli, H., Fuzzi, S., Schjoerring, J. K., Granier, C., Neftel, A., Isaksen, I. S. A., Laj, P., Maione, M., Monks, P. S., Burkhardt, J., Daemmgen, U., Neirynck, J., Personne, E., Wichink-Kruit, R., Butterbach-Bahl, K.,

Flechard, C., Tuovinen, J. P., Coyle, M., Gerosa, G., Loubet, B., Altimir, N., Gruenhage, L., Ammann, C., Cieslik, S., Paoletti, E., Mikkelsen, T. N., Ro-Poulsen, H., Cellier, P., Cape, J. N., Horvath, L., Loreto, F., Niinemets, U., Palmer, P. I., Rinne, J., Misztal, P., Nemitz, E., Nilsson, D., Pryor, S., Gallagher, M. W., Vesala, T., Skiba, U., Brueggemann, N., Zechmeister-Boltenstern, S., Williams, J., O'Dowd, C., Facchini, M. C., de Leeuw, G., Flossman, A., Chaumerliac, N., and Erisman, J.W.: Atmospheric composition change: Ecosystems-Atmosphere interactions, Atmos. Environ., 43, 5193–5267, 2009.

Fowler. D., Flechard. C., Cape. J.N., Storeton-West, R.L, and Coyle,M.: Measurements of ozone deposition to vegetation quantifying the flux, the stomatal and non-stomatal components, Water Air Soil Pollut., 130, 63-74, 2001.

Fuentes, J. D., Den Hartog, G., Neumann, H. H., and Gillespie, T. J.: Measurements and modelling of ozone deposition to wet foliage, in: Air pollutants and the leaf cuticle, edited by: Percy, K. E., Cape, J. N., Jagels, R., and Simpson C. J., NATO, ASI Series G, 36, p. 239–253, 1994.

Fuentes, J. D., Gillespie, T. J., Den Hartog, G., Neumann, H. H.: Ozone deposition onto a decicuous forest during dry and wet conditions, Agric. For. Meteorol., 62, 1-18, 1992.

Fuhrer, J.: Ozone risk for crops and pastures in present and future climates, Naturwissenschaften, 96, 173–194, 2009.

Fumagalli, I., Gruening, C., Marzuoli, R., Cieslik, S. and Gerosa, G.: Long-term measurements of NO_x and O_3 soil fluxes in a temperate deciduous forest, Agric. For. Meteorol., 228-229, 205-2016, 2016.

Ganzeveld, L., Amman C. and Loubet, B., Modelling Atmosphere-Biosphere Exchange of Ozone and Nitrogen Oxides, in, Review and Integration of Biosphere-Atmosphere Modelling of Reactive Trace Gases and Volatile Aerosols, Massad, R.S. and Loubet, B., Editors, pp. 235, Springer, France, 2015.

Ganzeveld, L., Bouwman, L., Stehfest, E., Vuuren, D. P. V., Eickhout, B., and Lelieveld, J.: Impact of future land use and landcover changes on atmospheric chemistry-climate interactions, J. Geophys. Res., 115, D23301, doi:10.1029/2010JD014041, 2010.

Ganzeveld L.N., Lelieveld, J., Dentener, F.J., Krol, M.C., and Roelofs, G.-J.: Atmosphere-biosphere trace gas exchanges simulated with a single-column model, J. Geophys. Res, 107, 4297, 2002.

Ganzeveld, L. and Lelieveld, J.: Dry deposition parameterization in a chemistry general-circulation model and its influence on the distribution of reactive trace gases, J. Geophys. Res., 100, 20999–21012, 1995.

Garland, J. A.: The dry deposition of sulphur dioxide to land and water surfaces., Proceedings of the Royal Society of London A, 354, 245-268, 1977.

Garland, J.A.: Dry deposition of SO2 and other gases. In: Atmosphere-Surface Exchange of Particulate and Gaseous Pollutants (1974). CONF-740921, Technical Information Center, Office of Public Affairs, Energy Research and

Development Administration, US Department of Commerce, Springfield, VA, pp. 212–227, 1976.

Garratt, J. R., and B. B. Hicks: Momentum, heat and water vapour transfer to and from natural and artificial surfaces, Q. J. R. Meteorol. Soc., 99, 680-687, 1973.

Gerosa, G., Finco, A., Mereu, S., Vitale, M., Manes, F., and Denti, A. B.: Comparison of seasonal variations of ozone exposure and fluxes in a Mediterranean Holm oak forest between the exceptionally dry 2003 and the following year, Environ. Pollut., 157, 1737–1744, , 2009.

Gerosa, G., Vitale., M., Finco, A., Manes, F., Ballarin Denti, A., and Cieslik S.: Ozone uptake by an evergreen Mediterranean forest (Quercus ilex). I. Micrometeorological flux measurements and flux partitioning. Atmos. Environ, 39, 3255–3266, 2005.

Gerosa, G., Marzuoli, R., Cieslik, S., and Ballarin-Denti, A.: Stomatal ozone uptake by barley in Italy. Effective exposure as a possible link between concentration- and flux-based approaches, Atmos. Environ., 38, 2421–2432, 2004.

Gerosa, G., Cieslik, S., and Ballarin-Denti, A.: Micrometeorological determination of time-integrated stomatal ozone fluxes over wheat: a case study in Northern Italy, Atmos. Environ., 37 (6), 777–788, 2003.

Giannakopoulos, C.: Three dimensional modelling of the concentration and deposition of tropospheric trace gases, Ph.D. thesis, University of Cambridge, UK, 1998.

Grantz, D. A., Zhang , X. J., Massman, W. J., Delany, A. C., and Pederson, J. R., Ozone deposition to a cotton (Gossypium hirsutum L.) field: stomatal and surface wetness effects during the California Ozone Deposition Experiment, Agric. For. Meteorol., 85, 19-31, 1997.

GrØntoft, T., Henriksen, J. F., and Seip, H. M.: The humidity dependence of ozone deposition onto a variety of building surfaces, Atmos. Environ., 38, 59–68, 2004.

Guenther, A., Karl, T., Harley, P., Wiedinmyer, C., Palmer, P. I., Geron, C.: Estimates of global terrestrial isoprene emissions using MEGAN (Model of Emissions of Gases and Aerosols from Nature, Atmos. Chem. Phys., 6, 3181-3192, 2006.

Güsten, H., Heinrich, G., Monnich, E., Sprung, D., Weppner, J., Ramadan, A., Ezz El-din, M.R.M., Ahmed, D.M., Hassan, G.K.Y.: On-line measurements of ozone surface fluxes: Part II. Surface-level ozone fluxes onto the Sahara desert. Atmos. Environ., 30, 911–918, 1996.

Hardacre, C., Wild, O., and Emberson, L.: An evaluation of ozone dry deposition in global scale chemistry climate models, Atmos. Chem. Phys., 15, 6419–6436, 2015.

Harmens, H., Mills, G., Emberson, L. D., and Ashmore, M. R.: Implications of climate change for the stomatal flux of ozone: a case study for winter wheat, Environ. Pollut., 146, 763–770, 2007.

Hauglustaine, D.A., Lathiere, J., Szopa, S., and Folberth, G.A.: Future tropospheric ozone simulated with a climate-chemistry-biosphere model, Geophys. Res. Lett. 32, L24807, 2005.

Hewitt, H. T., Copsey, D., Culverwell, I. D., Harris, C. M., Hill, R. S. R., Keen, A. B., McLaren, A. J., and Hunke, E. C.: Design and implementation of the infrastructure of HadGEM3: the nextgeneration Met Office climate modelling system, Geosci. Model Dev., 4, 223-253, 2011.

Hogg, A., Uddling, J., Ellsworth, D., Carroll, M.A., Pressley, S., Lamb, B., and Vogel, C.: Stomatal and non-stomatal fluxes of ozone to a northern mixed hardwood forest, Tellus B 59, 514–525, 2007.

Hirdman, D., Burkhart, J. F., Sodemann, H., Eckhardt, S., Jefferson, A., Quinn, P. K., Sharma, S., Ström, J., and Stohl, A.: Longterm trends of black carbon and sulphate aerosol in the Arctic: changes in atmospheric transport and source region emissions, Atmos. Chem. Phys., 10, 9351–9368, 2010.

IPCC: Climate Change 2013 – The Physical Science Basis, Cambridge University Press, Cambridge, 1552 pp., 2013.

Isaksen, I. S. A., Granier, C., Myhre, G., Berntsen, T. K., Dalsoren, S. B., Gauss, M., Klimont, Z., Benestad, R., Bousquet, P., Collins, W., Cox, T., Eyring, V., Fowler, D., Fuzzi, S., Jockel, P., Laj, P., Lohmann, U., Maione, M., Monks, P., Prevot, A. S. H., Raes, F., Richter, A., Rognerud, B., Schulz, M., Shindell, D., Stevenson, D. S., Storelvmo, T., Wang, W. C., van Weele, M., Wild, M., and Wuebbles, D.: Atmospheric composition change: Climate-Chemistry interactions, Atmos. Environ., 43, 5138–5192, 2009.

Jacob, D. J. and Winner, D. A.: Effect of climate change on air quality, Atmos. Environ., 43, 51–63, 2009.

Jacobs, A. E. G., Van Boxel, J.H., and R. M. M. El-Kilani, R. M.: Night time free convection characteristics within a plant canopy, Bound. Layer Meteor., 71, 375-391, 1994.

James, S. A., Smith, W.K., and Vogelmann, T.C.: Ontogenetic differences in mesophyll structure and chlorophyll distribution in eucalyptus globulus ssp. globulus (myrtaceae), Am. J. Bot., 86, 198-207, 1999.

Janssen, L.H.J.M., and Romer, F.G.: The frequency and duration of dew occurrence over a year. Tellus 43B, 408-419, 1991.

Jogireddy, V., Cox, P. M., Huntingford, C., Harding, R. J., and Mercado, L. M.: An improved description of canopy light interception for use in a GCM land-surface scheme: calibration and testing against carbon fluxes at a coniferous forest, Hadley Centre Technical Note 63, Hadley Centre, Met Office, Exeter, UK, 2006.

Johnson, C.E., Collins, W.J., Stevenson, D.S., Derwent, R.G.: The relative roles of climate and emissions changes on future oxidant concentrations. J. Geophys. Res., 104, 631–18, 645, 1999.

Jud, W., Fischer, L., Canaval, E., Wohlfahrt, G., Tissier, A., and Hansel, A.: Plant surface reactions: an opportunistic ozone defence mechanism impacting atmospheric chemistry, Atmos. Chem. Phys., 16, 277–292, 2016.

Karlsson, P., Uddling, J., Braun, S., Broadmeadow, M., Elvira, S., Gimeno, B., Le Thiec, D., Oksanen, E., Vandermeiren, K., Wilkinson, M.L.E.: New critical levels for ozone effects on young trees based on AOT40 and simulated cumulative leaf uptake of ozone. Atmos. Environ., 38, 2283-2294, 2004.

Karlsoon P.E., Braun S., Broadmeadow M., Elvira S., Emberson, L., Gimeno, B.S., Thiec, D.L., Novak, N., Oksanen, E., Schaub, M., Uddling, J., and Wilkinson, M.: Risk assessments for forest trees: The performance of the ozone flux versus the AOT concepts, Environ. Pollut., 146: 608-616, 2007.

Keronen, P., Reissell, A., Rannik, Ü., Pohja, T., Siivola, E., Hiltunen, V., Hari, P., Kulmala, and Vesala, M. T.: Ozone flux measurements over a Scots pine forest using eddy-covariance method: performance evaluation and comparison with flux-profile method, Boreal Environmental Research, 8, 425-443, 2003.

Kurpius, M.R., Goldstein, A.H.: Gas-phase chemistry dominates O_3 loss to a forest, implying a source of aerosols and hydroxyl radicals to the atmosphere. Geophysical Research Letters 30, 1371, 2003.

Langner, J., Engardt, M., and Andersson, C.: European summer surface ozone 1990–2100, Atmos. Chem. Phys., 12, 10097–10105, 2012a.

Langner, J., Engardt, M., Baklanov, A., Christensen, J. H., Gauss, M., Geels, C., Hedegaard, G. B., Nuterman, R., Simpson, D., Soares, J., Sofiev, M., Wind, P., and Zakey, A.: A multi-model study of impacts of climate change on surface ozone in Europe, Atmos. Chem. Phys., 12, 10423–10440, 2012b.

Lamarque, J.-F., Bond, T. C., Eyring, V., Granier, C., Heil, A., Klimont, Z., Lee, D., Liousse, C., Mieville, A., Owen, B.,Schultz, M. G., Shindell, D., Smith, S. J., Stehfest, E., Van Aardenne, J., Cooper, O. R., Kainuma, M., Mahowald, N., Mc-Connell, J. R., Naik, V., Riahi, K., and van Vuuren, D. P.: Historical (1850–2000) gridded anthropogenic and biomass burning emissions of reactive gases and aerosols: methodology and application, Atmos. Chem. Phys., 10, 7017–7039, 2010.

Lamaud, E., Loubet, B., Irvine, M., Stella, P., Personne, E., and Cellier, P.: Partitioning of ozone deposition over a developed maize crop between stomatal and non-stomatal uptakes using eddy-covariance flux measurements and modeling, Agric. For. Meteorol., 149, 1385–1396, 2009.

Lathiere, J., Hauglustaine, D. A., De Noblet-Ducoudre, N., Krinner, G., Folberth, G. A : Past and future changes in biogenic volatile organic compound emissions simulated with a global dynamic vegetation model. Geophys. Res. Lett., 32, L20818, 2005.

Lelieveld, J. and Dentener, F. J.: What controls tropospheric ozone?, J. Geophys. Res.-Atmos., 105, 3531–3551, 2000.

Liu, S. C., D. Kley, M. McFarland, J. D. Mahlman, and H. Levy (1980): On the origin of tropospheric ozone, J. Geophys. Res., 85, 7546–7552.

Magnani, F., Leonardi, S., Tognetti,R., Grace, J. and Borghetti, M.: Modeling the surface conductance of a broad-leaf canopy: effects of partial decoupling from the atmosphere, Plant, Cell and Environment, 21, 867-879, 1998.

Martin, G.M., Bellouin, N., Collins, W.J., Culverwell, W.J., Halloran, P.R., Hardiman, S.C., Hinton, T.J., Jones, C.D., McDonald, R.E., McLaren, A.J., O'Connor, F.M., Roberts, M.J., Rodriguez, J.M., Woodward, S., Best, M.J., Brooks,M.E., Brown, M.R., Butchart, N., Dearden, C., Derbyshire, S. H., Dharssi, I., Doutriaux-Boucher, M., Edwards, J.M., Falloon, P.D., Gedney, N., Gray, L.J., Hewitt, H.T., Hobson, M., Huddleston, M.R., Hughes, J., Ineson, S., Ingram, W.J., James, P.M., Johns, T.C., Johnson, C.E., Jones, A., Jones, C.P., Joshi,M.M., Keen, A.B., Liddicoat, S., Lock, A.P., Maidens, A.V., Manners, J.C., Milton, S.F., Rae, J.G.L., Ridley, J.K, Sellar, A., Senior, C.A., Totterdell, I.J., Verhoef, A., Vidale, P.L., and Wiltshire, A.: The HadGEM2 family of Met Office Unified Model climate configurations, Geosci. Model Dev., 4, 723–757, 2011.

Marzuoli, R., Finco, A., Chiesa, M., and Gerosa G., A dose response relationship for marketable yield reduction of two lettuce (*lactuca sativa L.*) cultivars exposed to tropospheric ozone in Southern Europe, Environ. Sci. Pollut. Res., DOI 10.1007/s11356-016-8224-6, 2016.

Massman, W.J.: Toward an ozone standard to protect vegetation based on effective dose: a review of deposition resistances and a possible metric, Atmos. Environ., 38, 2323–2337, 2004.

McLinden, C. A., Olsen, S. C., Hannegan, B., Wild, O., Prather, M. J., and Sundet, J.: Stratospheric ozone in 3-D models: A simple chemistry and the cross-tropopause flux, J. Geophys. Res.- Atmos., 105, 14653–14665, 2000.

Meszaros, R., Horvath, L., Weidinger, T., Neftel, A., Nemitz, E., Dammgen, U., Cellier,P., and Loubet, B.: Measurement and modelling ozone fluxes over a cut andfertilized grassland. Biogeosciences 6, 1987–1999, 2009.

Mercado, L. M., Bellouin, N., Sitch, S., Boucher, O., Huntingford, C., Wild, M., and Cox, P. M.: Impact of changes in diffuse radiation on the global land carbon sink, Nature, 458, 1014–1018, 2009.

Mercado, L. M., Huntingford, C., Gash, J. H. C., Cox, P. M., and Jogireddy, V.: Improving the representation of radiation interception and photosynthesis for climate model applications, Tellus B, 59, 553–565, 2007.

Miao, J.-F., Chen, D., and Wyser, K.: Modelling subgrid scale dry deposition velocity of O_3 over the Swedish west coast with MM5-PX model, Atmos. Environ., 40, 415–429, 2006.

Mikkelsen, T. N., Ro-Poulsen, H., Hovmad, M. F., Jensen, N. O., Pilegaard, K., and Egelov, A. H.: Five-year measurements of ozone fluxes to a Danish Norway spruce canopy, Atmos. Environ., 38, 2361–2371, 2004.

Mills, G., Harmens, H., Wagg, S., Sharps, K., Hayes, F., Fowler, D., Sutton, M. and Davies, B.: Ozone impacts on vegetation in a nitrogen enriched and changing climate, Environ. Pollut., 208, 898-908, 2016.

Mills, G., Mapping critical levels for vegetation. In: UBA (Ed.), UNECE Convention on Long-range Transboundary Air Pollution. Manual on Methodologies and Criteria for Mapping Critical Loads and Levels and Air Pollution Effects, Risks

and Trends, 2004. Constantly updated version available at www.oekodata.com/icpmapping/.

Monin A. S. and A. M. Obukhov: Basic laws of turbulent mixing in the surface layer of the atmosphere. Contrib. Geophys. Inst. Acad. Sci. USSR, 151:163–187, 1954.

Monks, P. S., Archibald, A. T., Colette, A., Cooper, O., Coyle, M., Derwent, R., Fowler, D., Granier, C., Law, K. S., Stevenson, D. S., Tarasova, O., Thouret, V., von Schneidemesser, E., Sommariva, R., Wild, O., Williams, M. L.: Tropospheric ozone and its precursors from the urban to the global scale from air quality to short-lived climate forcer. Atmos. Chem. Phys., 15, 8889–8973, 2015.

Monteith, J.L., Unsworth, M.H.: Principles of Environmental Physics, Academic Press, 2007.

Monteith, J.L. and Unsworth, M.H.: Principles of Environmental physics, Edward Arnold, London, 290 pp., 1990.

Monteith J. L.: Evaporation and surface temperature, Quarterly Journal of the Royal Meteorological Society, 107, 1–27, 1981.

Morgestern, O., Zeng, G., Abraham, L., Telford, P.J., Braesicke, P., Pyle, J.A., Hardiman, S.C., O'Connor, F.M. and Johnson, C.: Impacts of climate change, ozone recovery, and increasing methane on surface ozone and tropospheric oxidizing capacity, J. Geophys. Res.- Atmos., 118, 1028-1041, 2013.

Munger, J. W., Wofsy, S. C., Bakwin, P. S., Fan, S. M., Goulden, M. L., Daube, B. C., Goldstein, A. H., Moore, K. E., and Fitzjarrald, D. R.: Atmospheric deposition of reactive nitrogen oxides and ozone in a temperate deciduous forest and a subarctic woodland .1. Measurements and mechanisms, J. Geophys. Res. -Atmos., 101, 12639–12657, doi:10.1029/96JD00230, 1996.

Musselman, R.C., and Minnick, J.T: Nocturnal stomatal conductance and ambient air quality standards for ozone, Atmos. Environ., 34, 719-733, 2000.

Nemitz, E., Hargreaves, K. J., Neftel, A., Loubet, B., Cellier, P., Dorsey, J. R., Flynn, M., Hense, A.,Weidinger, T., Meszaros, R., Horvath, L., Dämmgen, U., Frühauf, C., Löpmeier, F. J. , Gallagher, M. W., and Sutton, M. A.: Intercomparison and assessment of turbulent and physiological exchange parameters of grassland, Biogeosciences, 6, 1445–1466, 2009.

Nopmongcol, U., Koo, B., Tai, E., Jung, J., Piyachaturawat, P., Emery, C., Yarwood, G., Pirovano, G., Mitsakou, C., and Kallos, G.: Modeling Europe with CAMx for the Air Quality Model Evaluation International Initiative (AQMII), Atmos. Environ., 53, 177-185, 2012.

O'Connor, F. M., Johnson, C. E., Morgenstern, O., Abraham, N. L., Braesicke, P., Dalvi, M., Folberth, G. A., Sanderson, M. G., Telford, P. J., Voulgarakis, A., Young, P. J., Zeng, G., Collins, W. J., and Pyle, J. A.: Evaluation of the new UKCA climatecomposition model – Part 2: The Troposphere, Geosci. Model Dev., 7, 41–91, 2014.

Olson, J. R., Crawford, J. H., Davis, D. D., Chen, G., Avery, M. A., Barrick, J. D. W., Sachse, G. W., Vay, S. A., Sandholm, S. T., Tan, D., Brune, W. H., Faloona,

I. C., Heikes, B. G., Shetter, R. E., Lefer, B. L., Singh, H. B., Talbot, R. W., and Blake, D. R.: Seasonal differences in the photochemistry of the South Pacific: A comparison of observations and model results from PEM-Tropics A and B, J. Geophys. Res., 106, 32749–32766, 2001.

Pacifico, F., Folberth, G.A., Sitch, S., Haywood, J.M., Rizzo, L.V., Malavelle, F.F., and Artaxo, P.: Biomass burning related ozone damage on vegetation over the Amazon forest: a model sensitivity study, Atmos. Chem. Phys., 15, 2791–2804, 2015.

Pfister, G. G., Walters, S., Lamarque, J. F., Fast, J., Barth, M. C., Wong, J., Done, J., Holland, G., and Bruyere, C. L.: Projections of future summertime ozone over the US, J. Geophys. Res.- Atmos., 119, 5559–5582, 2014.

Pio, C. A., Feliciano, M. S., Vermeulen, A. T., and Sousa, E. C.: Seasonal variability of ozone dry deposition under southern European climate conditions, Atmos. Environ., 34, 195–205, 2000.

Plake, D., Stella, P., Moravek, A., Mayer, J.-C., Ammann, C., Held, A., and Trebs, I.: Comparison of ozone deposition measured with the dynamic chamber and the eddy covariance method, Agric. For. Meteorol., 206, 97-112, 2015.

Pleijel, H., Danielsson, H., Emberson, L., Ashmore, M.R., and Mills, G.: Ozone risk assessment for agricultural crops in Europe: Further development of stomatal flux and flux-response relationships for European wheat and potato, Atmos. Environ., 41: 3022-3040, 2007.

Pleim, J. E., Xiu, A., Finkelstein, P. L., and Otte, T. L.: A coupled land-surface and dry deposition model and comparison to field measurements of surface heat, moisture, and ozone fluxes,Water Air Soil Pollut., 1, 243–252, 2001.

Pöschl, U., von Kuhlmann, R., Poisson, N., and Crutzen, P.: Development and intercomparison of condensed isoprene oxidation mechanisms for global atmospheric modelling, J. Atmos. Chem., 37, 29–52, 2000.

Potier, E., Ogée. J., Jouanguy, J., Lamaud, E., Stella, P., Personne, E., Durand, B., Mascher, N., Loubet, B.: Multilayer modelling of ozone fluxes on winter wheat reveals large deposition on wet senescing leaves, Agric. For. Meteorol., 211-212, 58-71, 2015.

Potier, E., Etude des mécanismes du depôét d'ozone sur la végétation: mise en évidence d'un puits chimique surles feuilles mouillées en période de sénescence, Études de l'environnement, PhD Thesis, Université Pierre et Marie Curie, Paris, 144 pp, 2014.

Rannik, Ü, Altimir, N., Mammarella, I., Bäck, J., Rinne, J., Ruuskanen, T.M., Hari, P., Vesala, T. and Kulmala, M.: Ozone deposition into a boreal forest over a decade of observations: evaluating deposition partitioning and driving variables, Atmos. Chem. Phys., 12, 12165–12182, 2012.

Rayner, N., Parker, D., Horton, E., Folland, C., Alexander, L., Rowell, D.P., Kent, E.C. and Kaplan, A.: Global analyses of sea surface temperature, sea ice, and night marine air temperature since the late nineteenth century, J. Geophys. Res., 108, 4407, 2003.

Reich, P. B. and Amundson, R. G.: Ambient levels of ozone reduce net photosynthesis in tree and crop species, Science, 230, 566– 570, 1985.

Riahi, K., Rao, S., Krey, V., Cho, C., Chirkov, V., Fischer, G., Kindermann, G., Nakicenovic, N., and Rafaj, P.: RCP 8.5 – A scenario of comparatively high greenhouse gas emissions, Clim. Change, 109, 33-57, 2011.

Royal Society: Ground-level ozone in the 21st century: future trends, impacts and policy implications, London, 2008.

Rummel, U., Ammann, C., Kirkman, G.A.: Seasonal variation of ozone deposition to a tropical rain forest in southwest Amazonia, Atmos. Chem. Phys., 7, 7399–7450, 2007.

Sanderson, M., Collins, W., Johnson, C., and Derwent, R.: Present and future acid deposition to ecosystems: the effect of climate change, Atmos. Environ., 40, 1275–1283, 2006,

Sanderson, M. G., Collins,W. J., Hemming, D. L., and Betts, R. A.: Stomatal conductance changes due to increasing carbon dioxide levels: projected impact on surface ozone levels, Tellus B, 59, 404–411, 2007.

Schallhart, S., Rantala, P., Nemitz, E., Taipale, D., Tillmann, R., Mentel, T.F., Loubet, B., Gerosa, G., Finco, A., Rinne, J., and Ruuskanen, T. R.: Characterization of total ecosystem-scale biogenic VOC exchange at a Mediterranean oak–hornbeam forest, Atmos. Chem. Phys., 16, 7171–7194, 2016.

Seinfeld, J. and Pandis, S.: Atmospheric Chemistry and Physics: From Air Pollution to Climate Change, John Wiley & Sons, Hoboken, New Jersey, USA, 2nd Edn., 2006.

Sellers, P. J., Los, S. O., Tucker, C. J., Justice, C. O., Dazlich, D. A., Collatz, G. J., , and Randall, D. A. : A revised land surface parameterization (SiB2) for atmospheric GCMs. Part II: The generation of global fields of terrestrial biophysical parameters from satellite data. J. Climate, 9**,** 706–737, 1996.

Sellers, P. J., Berry, J. A., Collatz, G. J., Field, C. B., and Hall, F. G.: Canopy Reflectance, Photosynthesis, and Transpiration III, A Reanalysis Using Improved Leaf Models and a New Canopy Integration Scheme, Remote Sens. Environ., 42, 187–216, 1992.

Shindell, D., Kuylenstierna, J. C. I., Vignati, E., van Dingenen, R., Amann, M., Klimont, Z., Anenberg, S. C., Muller, N., Janssens-Maenhout, G., Raes, F., Schwartz, J., Faluvegi, G., Pozzoli, L., Kupiainen, K., Höglund-Isaksson, L., Emberson, L., Streets, D., Ramanathan, V., Hicks, K., Oanh, N. T. K., Milly, G., Williams, M., Demkine, V., and Fowler, D.: Simultaneously Mitigating Near-Term Climate Change and Improving Human Health and Food Security, Science, 335, 183–189, doi:10.1126/science.1210026, 2012.

Shindell, D., Schulz, M., Ming, Y., Takemura, T., Faluvegi, G., and Ramaswamy, V.: Spatial scales of climate response to inhomogeneous radiative forcing, J. Geophys. Res.-Atmos., 115, D19110, doi:10.1029/2010jd014108, 2010.

Sillman, S.: The relation between ozone, NO_x and hydrocarbons in urban and polluted rural environments. Atmos. Environ. 1999, 33, 1821.

Simpson, D., Arneth, A., Mills, G., Solberg, S., and Uddling, J.: Ozone - the persistent menace: interactions with the N cycle and climate change, Curr. Opinion Environ. Sustain., 9–10, 919, 2014.

Simpson, D., Emberson, L., Ashmore, M., Tuovinen, J.: A comparison of two different approaches for mapping potential ozone damage to vegetation. a model study, Environ. Poll., 146, 715-725, 2007.

Smith. S. D.: Coefficients for sea surface wind stress, heat flux, and wind profiles as a function of wind speed and temperature, J. Geophys. Res.: Oceans, 93, 15467–15472, 1988.

Smith, R., Fowler, D., Sutton, M., Flechard, C., and Coyle, M.: Regional estimation of pollutant gas dry deposition in the UK: model description, sensitivity analyses and outputs, Atmos. Environ., 34, 3757–3777, 2000.

Sitch, S., Cox, P.M., Collins, W. J., and Huntingford, C.: Indirect radiative forcing of climate change through ozone effects on the land-carbon sink, Nature, 448, 791-794, 2007.

Solberg, S., Hov, Ø., Søvde, A., Isaksen, I. S. A., Coddeville, P., De Backer, H., Forster, C. , Orsolini, Y., and Uhse, K.: European surface ozone in the extreme summer 2003, J. Geophys. Res., 113, D07307, doi:10.1029/ 2007JD009098, 2008.

Squire, O. J., Archibald, A. T., Griffiths, P. T., Jenkin, M. E., Smith, D., and Pyle, J. A.: Influence of isoprene chemical mechanism on modelled changes in tropospheric ozone due to climate and land use over the 21st century, Atmos. Chem. Phys., 15, 5123–5143, 2015.

Stella, P., Personne, E., Loubet, B., Lamaud, E., Ceschia, E., Béziat, P., Bonnefond, J. M., Irvine, M., Keravec, P., Mascher, N., and Cellier, P.: Predicting and partitioning ozone fluxes to maize crops from sowing to harvest: the Surfatm-O3 model, Biogeosciences, 8, 2869–2886, 2011a.

Stella, P., Loubet, B., Lamaud, E., Laville, P., and Cellier, P.: Ozone deposition onto bare soil: A new parameterization, Agric. For. Meteorol., 151, 669–681, 2011b.

Stevenson, D. S., Young, P. J., Naik, V., Lamarque, J.-F., Shindell, D. T., Voulgarakis, A., Skeie, R. B., Dalsoren, S. B., Myhre, G., Berntsen, T. K., Folberth, G. A., Rumbold, S. T., Collins, W. J., MacKenzie, I. A., Doherty, R. M., Zeng, G., van Noije, T. P. C., Strunk, A., Bergmann, D., Cameron-Smith, P., Plummer, D. A., Strode, S. A., Horowitz, L., Lee, Y. H., Szopa, S., Sudo, K., Nagashima, T., Josse, B., Cionni, I., Righi, M., Eyring, V., Conley, A., Bowman, K. W., and Wild, O.: Tropospheric ozone changes, radiative forcing and attribution to emissions in the Atmospheric Chemistry and Climate Model Intercomparison Project (ACCMIP), Atmos. Chem. Phys., 13, 6, 3063–3085, 2013.

Stevenson, D. S., Dentener, F. J., Schultz, M. G., Ellingsen, K., van Noije, T. P. C., Wild, O., Zeng, G., Amann, M., Atherton, C. S., Bell, N., Bergmann, D. J., Bey, I., Butler, T., Cofala, J., Collins, W. J., Derwent, R. G., Doherty, R. M., Drevet, J., Eskes, H. J., Fiore, A. M., Gauss, M., Hauglustaine, D. A., Horowitz, L. W., Isaksen, I. S. A., Krol, M. C., Lamarque, J. F., Lawrence, M. G., Montanaro, V.,

Muller, J. F., Pitari, G., Prather, M. J., Pyle, J. A., Rast, S., Rodriguez, J. M., Sanderson, M. G., Savage, N. H., Shindell, D. T., Strahan, S. E., Sudo, K., and Szopa, S.: Multimodel ensemble simulations of present-day and near-future tropospheric ozone, J. Geophys. Res.-Atmos., 111, D08301, doi:10.1029/2005jd006338, 2006.

Sturm, N., Köstner, B., Hartung, W., Tenhunen, J.D.: Environmental and endogenous controls on leaf- and stand-level water conductance in a Scots pine plantation, Ann. Sci. For., 55, 237-253, 1998.

Telford, P. J., Braesicke, P., Morgenstern, O., and Pyle, J. A., Technical Note: Description and assessment of a nudged version of the new dynamics Unified Model, Atmos. Chem. Phys., 8, 1701–1712, 2008.

Tuovinen, J.-P., Emberson, L., and Simpson, D.: Modelling ozone fluxes to forests for risk assessment: status and prospects, Ann. For. Sci., 66, p. 401, 2009.

Tuovinen, J.-P., Simpson, D., Altimir, N.: Modelling the Stomatal and Nonstomatal Ozone Fluxes to Coniferous Forests in Northern Europe. EGU General Assembly, 14–18 April 2008, Vienna, Austria, Geophysical Research Abstracts, vol. 10. EGU2008-A-08272, 2008.

Tuovinen, J.P. , Ashmore, M.R., Emberson, L.D., Simpson, D.: Testing and improving the EMEP ozone deposition module, Atmos. Environ., 38, 2373-2385, 2004. UN-ECE, Mapping critical levels for vegetation. Manual on methodologies and criteria for modelling and mapping critical loads & levels and air pollution effects, risks and trends (2008 ed.), United Nations Economic Commission for Europe (UNECE) Convection on Long-range Transboundary Air Pollution, Geneva, 254p. (URL: http://www.icpmapping.org), 2004b.

Tuovinen, J.P., Simpson, D., Mikkelsen, T.N., Emberson, L.D., Ashmore, M.R., Aurela,, M., Cambridge, H., Hovmand, M., Jensen, N., Laurila, T., Pilegaard, K., Ro-Poulsen, H.: Comparisons of measured and modelled ozone deposition to forests in Northern Europe. Water, Air and Soil Pollution: Focus 1, 263–274, 2001.

Val-Martin, M., Heald, C. L., and Arnold, S. R.: Coupling dry deposition to vegetation phenology in the Community Earth System Model: Implications for the simulation of surface O_3, Geophys. Res. Lett., 41, 2988–2996, doi:10.1002/2014gl059651, 2014.

Van Vuuren, D., Edmonds, J., Kainuma, M., Riahi, K., Thomson, A., Hibbard, K., Hurtt, G., Kram, T., Krey, V., Lamarque, J.-F., Masui, T., Meinshausen, M., Nakicenovic, N., Smith, S., and Rose, S.: The representative concentration pathways: an overview, Climatic Change, 109, 5–31, 2011.

Vargas, R., Sonnentag, O., Abramowitz, G., Carrara, A., Chen, J.M., Ciais, P., Correia,A., Keenan, T.F., Kobayashi, H., Ourcival, J.-M., Papale, D., Pearson, D., Pereira,J.S., Piao, S., Rambal, S. and Baldocchi, D.D.: Drought influences the accuracy of simulated ecosystem fluxes: a model-data meta-analysis for Mediterranean oak woodlands, Ecosystems, 16, 749–764, 2013.

Vautard, R., Honore, C., Beekmann, M., and Rouil, L.: Simulation of ozone during August 2003 heat wave and emission control scenarios, Atmos. Environ., 39, 2957–2967, 2005.

Verbeke T., Lathière J., Szopa S., and de Noblet-Ducoudré N.: Impact of future land-cover changes on HNO_3 and O_3 surface dry deposition, Atmos. Chem. Phys., 15, 13555–13568, 2015.

Vieno, M., Dore, A. J., Stevenson, D. S., Doherty, R., Heal, M. R., Reis, S., Hallsworth, S., Tarrason, L.,Wind, P., Fowler, D., Simpson, D., and Sutton, M. A.: Modelling surface ozone during the 2003 heat-wave in the UK, Atmos. Chem. Phys., 10, 7963–7978, doi:10.5194/acp-10-7963-2010, 2010.

Von Schneidemesser, E., Monks, P. S., Allan, J. D., Bruhwiler, L., Forster, P., Fowler, D., Lauer, A., Morgan, W. T., Paasonen, P., Righi, M., Sindelarova, K., and Sutton, M. A.: Chemistry and the Linkages between Air Quality and Climate Change, Chem. Rev., 115, 3856–3897, 2015.

Walker, T. W., Jones, D. B. A., Parrington, M., Henze, D. K., Murray, L. T., Bottenheim, J. W., Anlauf, K, Worden, J. R., Bowman, K. W., Shim, C., Singh, K., Kopacz, M., Tarasick, D. W., Davies, J., von der Gathen, P., Thompson, A. M., and Carouge, C. C.: Impacts of mid latitude precursor emissions and local photochemistry on ozone abundances in the Arctic, J. Geophys. Res.: Atmos., 117, D01305, doi:10.1029/2011jd016370, 2012.

Wang, Y., Shen, L., Wu, S., Mickley, L., He, J., and Hao, J.: Sensitivity of surface ozone over China to 2000−2050 global changes of climate and emissions. Atmos. Environ., 75, 374-282, 2013.

Wesely M. L.: Parameterization of surface resistances to gaseous dry deposition in regional-scale numerical models, Atmos. Environ., 23, 1293–1304, 1989.

Wesely, M. L: Turbulent transport of ozone to surface common in the eastern United States. In Trace Atmospheric Constituents: Properties, Transformations, and Fates (edited by Schwartz S. E.), pp. 345-370. John Wiley, New York, 1983.

Wild, O.: Modelling the global tropospheric ozone budget: exploring the variability in current models, Atmos. Chem. Phys., 7, 2643–2660, 2007.

Wilson, M.F. and Henderson-Sellers, A.: A global archive of land cover and soils data for use in general circulation climate models., J. Climate, 5, 119-143, 1985.

Wu, Z., Wang, X., Chen, F., Turnipseed, A. A., Guenther, A. B., Niyogi, D., Charusombat, U., Xia, B., William Munger, J., and Alapaty, K.: Evaluating the calculated dry deposition velocities of reactive nitrogen oxides and ozone from two community models over a temperate deciduous forest, Atmos. Environ., 45, 2663–2674, 2011.

Wu, S., Mickley, L. J., Leibensperger, E. M., Jacob, D. J., Rind, D., and Streets, D. G.: Effects of 2000–2050 global change on ozone air quality in the United States, J. Geophys. Res.-Atmos., 113, D18312, doi:10.1029/2007JD009639, 2008.

Wu, S. L., Mickley, L. J., Jacob, D. J., Logan, J. A., Yantosca, R. M., and Rind, D.: Why are there large differences between models in global budgets of tropospheric ozone?, J. Geophys. Res.-Atmos., 112, D05302, doi:10.1029/2006jd007801, 2007.

Young, P. J., Archibald, A. T., Bowman, K. W., Lamarque, J.-F., Naik, V., Stevenson, D. S., Tilmes, S., Voulgarakis, A., Wild, O., Bergmann, D., Cameron-Smith, P., Cionni, I., Collins,W. J., Dalsøren, S. B., Doherty, R. M., Eyring, V., Faluvegi, G., Horowitz, L. W., Josse, B., Lee, Y. H., MacKenzie, I. A., Nagashima, T., Plummer, D. A., Righi, M., Rumbold, S. T., Skeie, R. B., Shindell, D. T., Strode, S. A., Sudo, K., Szopa, S., and Zeng, G.: Preindustrial to end 21st century projections of tropospheric ozone from the Atmospheric Chemistry and Climate Model Intercomparison Project (ACCMIP), Atmos. Chem. Phys., 13, 2063 - 2090, 2013.

Zeng, G., Pyle, J. A., and Young, P. J.: Impact of climate change on tropospheric ozone and its global budgets, Atmos. Chem. Phys., 8, 369–387, 2008.

Zhang, L., Brook, J.R., and Vet R.: A revised parameterization for gaseous dry deposition in air-quality models, Atmos. Chem. Phys., 3, 2067–2082, 2003.

Zhang, L., Moran, M., Makar, P., Brook, J., and Gong, S.: Modelling Gaseous Dry Deposition in AURAMS A Unified Regional Air-quality Modelling System, Atmos. Environ., 36, 537–560, 2002a.

Zhang, L., Brook, J., and Vet, R.: On Ozone dry deposition with emphasis on non-stomatal uptake and wet canopies, Atmos. Environ., 36, 4787–4799, 2002b.